Karlsruhe Institute of Technology

Faculty of Electrical Engineering

Carina Mieth, B.Sc.

Observability of Multi-Carrier Energy Distribution Networks and Optimal Sensor Placement

Master's Thesis 904

Institute of Control Systems
Chair: Prof. Dr. Sören Hohmann

Chair: Prof. Dr. Dorothea Wagner
Institute of Theoretical Informatics

Karlsruhe Institute of Technology

Institute of Control Systems
Institute of Theoretical Informatics

Master's Thesis 904

Observability of Multi-Carrier Energy Distribution Networks and Optimal Sensor Placement

The transition of passive single carrier distribution networks to active multimodal energy distribution networks (MEDNs) is strongly related to the need of a more intense system monitoring. In consequence, distribution service operators are challenged to place additional sensors in order to ensure a safe operation of the system. For electric power systems the sensor placement problem has been well studied. However, no method is recognized which can be directly applied to MEDNs as they reveal new structural characteristics arising from the cross-domain conversion of energy.

This thesis addresses the sensor placement problem for MEDNs. The aim is to find the cheapest sensor configuration which ensures observability for a given network. In the first part of this work, an observability criterion for MEDNs has to be derived. Afterwards, the sensor placement problem is to be formulated as a constrained optimization problem, where the objective function is given by the costs of the sensor placement. The optimization is to be illustrated in a realistic setting for a subnetwork of the MEDN of Karlsruhe, Germany.

(Prof. Dr. Dorothea Wagner) (Prof. Dr. Sören Hohmann)

Student	:	Carina Mieth, B.Sc.
Supervisors	:	Franziska Wegner, M.Sc. and Martin Pfeifer, M.Sc.
Date of hand out	:	28-Nov-2016
Date of hand in	:	07-June-2017

I hereby declare that I wrote my Master's Thesis on my own and that I have followed the regulations relating to good scientific practice of the Karlsruhe Institute of Technology (KIT) in its latest form. I did not use any unacknowledged sources or means and I marked all references I used literally or by content.

Karlsruhe, 07-June-2017

Carina Mieth, B.Sc.

Abstract

In the energy supply, passive single-carrier energy distribution grids (such as in electricity distribution, natural gas, district heat) are changing towards active multi-carrier energy distribution networks (MEDNs). Key factors explaining this transition are the increased role of renewable energies and decentralized microgeneration (e.g. combined heat and power units). A multi-carrier perspective is advantageous, as synergies of the different energies can be taken into account, e.g. storing excessive electric energy in the gas network. In order to ensure the safe and efficient operation of MEDNs, operational variables need to be either measurable or calculable. This leads to the question of observability for MEDNs, where the system must be observable in order to calculate all important operation variables. As today's sensor placement is done by rules of thumb, it is generally not the optimal placement.

In this work, the approach of a graph-theoretical modeling of MEDNs and the computing of a cost-efficient optimal sensor placement ensures that the MEDN is observable. The derivation of the MEDN graph and the mixed-integer linear program (MILP) for the sensor placement will be illustrated in a case study for a subnetwork of the MEDN of Karlsruhe, Germany.

Kurzfassung

Aufgrund des steigenden Anteils an Erneuerbaren Energien in der heutigen Stromversorgung und der daraus resultierenden Dezentralisierung wandeln sich die passiven Ein-Domänen-Energieverteilnetze (Strom, Erdgas, Fernwärme) hin zu einem aktiven Multi-Domänen-Energieverteilnetz (MDE). Die Multi-Domänen Betrachtung ist vorteilhaft, da Synergien der verschiedenen Energien berücksichtigt werden können, wie z.B. die Speicherung überschüssiger elektrischer Energie im Gasnetz. Um einen effizienten und sicheren Betrieb von MDEen garantieren zu können, müssen alle wichtigen Betriebsgrößen mess- oder berechenbar sein. Dies führt zum Begriff der Beobachtbarkeit, da in einem beobachtbaren MDE alle Größen mess- oder berechenbar sind. Da die heutige Sensor-Platzierung nach Faustregeln erfolgt, ist es in der Regel nicht die optimale Platzierung.

In dieser Arbeit wird das Problem der optimalen Sensorplatzierung als gemischtganzzahliges Optimierungsproblem formuliert, welches durch Nebenbedingungen sicherstellt, dass das MDE beobachtbar ist. Der Ansatz wird anschließend in einer Fallstudie für ein Karlsruher Teilnetz untersucht.

Contents

List of Figures

List of Tables

Abbreviations and Symbols

Abbreviations

CHP	combined heat and power, page 1
FDI	fault detection and isolation, page 14
G2H	gas-to-heat, page 66
G2P	gas-to-power, page 66
GDN	gas distribution network, page 15
GNA	generalized nodal analysis, page 3
HDN	heat distribution network, page 15
LP	linear programming, page 61
LSS	linear structured system, page 12
MEDN	multi-carrier energy distribution network, page 1
MILP	mixed integer linear programming, page 55
MIMO	multiple-inputs multiple-outputs, page 31
MIQCP	mixed integer quadratically constrained programming, page 61
MIQP	mixed integer quadratic programming, page 61
MOP	maximum operating pressure, page 20
P2G	power-to-gas, page 1
P2H	power-to-heat, page 1
PMU	phasor measurement unit, page 15
QCP	quadratic constrained programming, page 61
QP	quadratic programming, page 61
RES	renewable energy sources, page 1
RMSE	root-mean-square error, page 15

SF6 sulphur hexafluoride, page 75

SISO single-input single-ouput, page 30

w.r.t. with respect to, page 58

Calligraphic and Other Symbols

$\mathcal{D}$ network data, page 53

$\mathcal{M}$ measurement data, page 53

$\mathcal{T}^\star$ reduced graph of inner vertices, page 49

$\mathcal{N}$ network matrix of the MEDN, page 51

$\mathcal{G}$ conductance matrix, page 22

$\mathcal{T}$ graph of MEDN, page 5

Indices, Exponents and Operator Names

χ index for energy carrier, page 21

el index for the electric energy carrier, page 40

g index for the gas energy carrier, page 40

h index for the heat energy carrier, page 40

i index for a row, page 8

j index for a column, page 8

Latin Letters

$c(a)$ capacity of arc a, page 19

G conductance, page 8

I current, page 21

n number of system states, page 7

n_C number of converters, page 42

n_V number of inner vertices, page 41

p number of inputs, page 7

q number of outputs, page 7

r number of linear independent rows, page 8

R^{el} resistance of an electric conductor, page 21

Matrices and Vectors

Sets

Units

Chapter 1

Introduction

Today's energy supply is undergoing major changes. In Germany, environmental policy favors a higher share of renewable energy sources (RES) in their electric energy supply. As a consequence, the balance between supply and demand is impeded by the volatility of RES. This creates the necessity of storing excessive electric energy during periods of low consumption for a release in periods of high demand. The idea of converting energy from one form to another was brought up as huge amounts of electric energy cannot be stored cheaply [IIP08].

Traditionally, the energy networks for the different energy carriers like heat, electricity and gas were sharply separated from each other. Now, the increasing number of power converters establish a coupling between the corresponding networks such that these energy carriers cannot be regarded independently anymore [GA07]. This coupling is a possible cornerstone for large-scale energy storage, as it takes advantage of the synergy effects of the different energy carriers. This coupled network type is hardly investigated and will be referred to as *multi-carrier energy distribution network* (MEDN).

Definition 1.1. A multi-carrier energy distribution network (MEDN) aggregates single-carrier energy distribution networks, which are coupled via energy converters, into one integrated network concept.

The scheme of a MEDN is outlined in Figure 1.1. The MEDN is composed of three energy distribution networks for electricity, gas and heat and contains Power-to-X-converters such as Power-to-Gas (P2G), Power-to-Heat (P2H) and combined heat and power (CHP) units. Energy converters connect different energy carriers by the exchange of energy between one network and another.

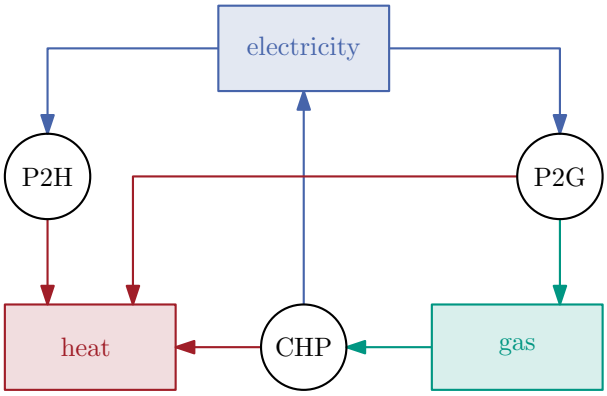

Figure 1.1: Coupling of the three different energy carriers electricity, gas and heat by the energy converters P2H, P2G and CHP, forming a scheme of a multi-carrier energy distribution network (MEDN).

In general, network operators have incomplete knowledge of the load distribution in their networks [KK15], which is due to financial and operational reasons [CLW+16]. On one hand, it would be too expensive to measure every quantity in the network [FBL+15] and on the other hand, telecommunications are only available at few network stations (the different monitoring infrastructures will be presented in Section 4.4). However, the knowledge of the system's state becomes more and more important, because the enhanced coupling between different energy networks leads to unknown and unpredictable behavior. For example, a higher share in RES can cause bidirectional energy flows which could violate voltage or pressure limits, respectively. In the worst case, this can lead to outages or the destruction of network components, if these violations are not detected. That lacking possibility to control MEDNs in a way that guarantees a secure operation as well as bad converter efficiencies are the main reasons why the lightly coupled single energy carrier networks are not operated as a MEDN, yet.

For future operation of MEDNs, *state estimation* for this new type of system class has great potential for an economical reasonable monitoring of MEDNs. State estimation is only possible if the underlying network is observable. Then, desired network quantities can be determined only by the knowledge of the available measurement data. The advantage of this approach are substantial savings, since only the necessary measures for a safe network operation must be measured. In general, network observability depends on the actual *sensor placement* in the network. The strategic positioning of specific sensors to favorable places in the network is the key to a successful state estimation and has influence on convergence and accuracy of future estimation algorithms [KD11]. However, today's sensor placement is typically carried out by following rules of thumb based on expert knowledge.

The benefit of a multi-carrier perspective in comparison to the previous single-carrier perspective is that synergies can be taken into account. With a MEDN approach it will be possible to use sensors in one domain for the estimation of measures in another. This can be used for cost savings or a higher failure safety. Moreover, one cannot say that an optimal operation for each single network guarantees the optimal operation for the whole MEDN.

Many different energy carriers can be included into a MEDN modeling approach, and consequently even more types of energy converters for the energy conversion between them. For this thesis, the most common energy carriers electricity, gas and heat were considered. The modeling approach is capable of describing the energy conversion between each energy carrier. Thus, CHP units, P2G, P2H and other converter can be easily integrated into the MEDN network model. The work in this thesis aims at answering the following key questions:

1. *Which* quantities should be measured to ensure observability for the MEDN and *how many* sensors are needed for this?
2. *What* sensor types should be used and *where* should they be placed to guarantee cost optimal placement for the greenfield approach? And in case of an existing sensor placement, how can it be completed reasonably?

The contribution of this thesis is the graph-theoretical modeling approach for MEDNs in Section 5.4 for which the generalized nodal analysis (GNA) was derived in Section 5.5. The GNA yields a system of equations describing the MEDN by only one network matrix $\mathcal{N}$ for which an observability criterion based on the rank of $\mathcal{N}$ is presented in Section 5.6. Furthermore, a sensor placement problem is stated in Section 5.7 that minimizes the overall sensor costs and ensures observability. This approach answers the aforementioned questions 1. and 2. and was successfully tested on a subnetwork of the MEDN of Karlsruhe in Chapter 6.

The necessary preliminaries for this thesis are presented next in Chapter 2. In Chapter 3 the related work on observability and sensor placement is outlined. Chapter 4 explains the system-theoretical and energy-technical fundamentals for the MEDN modeling approach in Chapter 5. Last but not least, the case study for a MEDN of Karlsruhe is given in Chapter 6. Unfortunately, the corresponding network plans and data are not available in this online version.

Chapter 2

Preliminaries

This chapter intends to provide a common basis, as the readership comes from different disciplines. For those, who are not familiar with graph theory, Section 2.1 gives a short overview on different graphs as well as their descriptions. A huge area in computer science is the theory of NP-completeness where a short overview is given in Section 2.2. Control engineers often use the state space model for describing dynamic systems which is defined in Section 2.3. Since there is no common nomenclature in computer science and electrical engineering, we introduce a nomenclature in Section 2.4 that will be used in this thesis. At the end of this chapter, there is a glossary that briefly explains the respective terms of both disciplines.

2.1 Graph Theory

A directed graph $\mathcal{T} = (V, A)$ consists of a vertex set V and an arc set A. An arc is a directed edge [Die06, p.2]. Two vertices u and v are called *adjacent* or *neighbor* if they are connected by an arc $a = (u, v)$ [Die06, p.3]. Two edges a_1 and a_2 are called *incident* if they share a common vertex w. The number of vertices $|V|$ is the cardinality of V and the number of arcs $|A|$ the cardinality of A.

The degree of a vertex $d(v)$ denotes the number of in- and outgoing edges at a vertex v [Die06, p.5]. In directed graphs, the degree of a vertex $d(v)$ can be split up in a part $d^-(v)$ that accounts for all incoming and a complementary part $d^+(v)$ that accounts for all outgoing edges, respectively.

Assume a flow $f(u, v)$ between vertex u and vertex v for which $f(u, v) \neq 0$. Regarding vertex v, the flow $f(u, v)$ can either have a positive sign (incoming flow) or negative sign (outgoing flow). The incoming flow can be denoted by $f^-(u, v)$, if $f(u, v) > 0$. By analogy, an outgoing flow $f(u, v) < 0$ can be written as $f^+(u, v)$. Note that the superscripted $+$ or $-$ is based on the definition of the degree of a vertex and can be against the physical flow direction as well.

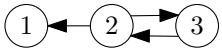

Figure 2.1: Example of a directed graph having three vertices and arcs, respectively. Vertex 2 and 3 are strongly connected by two arcs ($a_1 = (2, 3)$, $a_2 = (3, 2)$), whereas vertex 2 is only connected by an arc $a = (2, 1)$ to vertex 1.

Possible encoding schemes for graphs according to [GJ79, p.10] are illustrated using the example in Figure 2.1. The last two are most important for this thesis.

- *vertex and edge lists:*
  $V(1)V(2)V(3)(V(2)V(1))(V(2)V(3))(V(3)V(2))$, where $V(1)$, $V(2)$ and $V(3)$ are the three vertices and $(V(2)V(1))$, $(V(2)V(3))$ and $(V(3)V(2))$ are the three arcs of the graph in Figure 2.1.
- *neighbor lists:*
  $()(V(1)V(3))(V(2))$, where the adjacent vertices are given in parentheses for each vertex of the graph.
- *adjacency matrix rows:*
  $000/101/010$, where each vertex v is described by a row which contains $|\mathcal{T}|$ numbers. The i-th element of the number sequence in a row is 1, if there is an arc leaving v to vertex i or 0, if there is no arc.
- *incidence matrix rows:*
  $-100/11-1/0-11$, where each vertex v is described by a row which contains $||\mathcal{T}||$ numbers. The i-th element of the number sequence in a row is 1, if the arc i is leaving v, -1 if the arc i is pointing to v or 0, if there is no arc.

2.2 Theory of NP-Completeness

The theory of NP-completeness is used to prove that a problem is "just as hard as other problems that are widely recognized as being difficult" [GJ79, p.3]. Such hard problems are called inherently intractable if no polynomial time algorithm for their solution exists. How fast an algorithm works, can be stated using a time complexity function. Therefore the following definition is needed:

Definition 2.1. A function $f(n)$ is in $O(g(n))$, if a constant bound c can be found such that $| f(n) | \leq c \cdot | g(n) |$ for all values of $n \geq 0$.

A polynomial time algorithm has $O(p(n))$ running time, where p is some polynomial function, like for example $n, n^2, n^3, \ldots, n^k$ with $k \in \mathbb{N}$ and n is the input length. By contrast an exponential time algorithm can only, if at all, be bounded with more complex functions like $n^{\log n}$ or $2^n, \ldots, k^n$, where n is part of the exponent. There exists

a class of problems, called NP-complete problems, for which polynomial algorithms have not been found yet, because it is widely assumed that $\mathsf{P} \neq \mathsf{NP}$ (Millennium Prize Problem). For a new problem, it can be proved that it is intractable too, if it can be reduced to a known NP-complete problem [Kar72].

2.3 State Space Representation

The continuous–time linear time–invariant state space model of a dynamical system consist of the state space differential Equation 2.1 and the output Equation 2.2 [Foe13, pp. 243ff.],

$$\dot{\mathbf{x}}(t) = \mathbf{A}\mathbf{x}(t) + \mathbf{B}\mathbf{u}(t), \tag{2.1}$$

$$\mathbf{y}(t) = \mathbf{C}\mathbf{x}(t) + \mathbf{D}\mathbf{u}(t), \tag{2.2}$$

where t is the time, $\mathbf{x} \in \mathbb{R}^n$ is the state vector, $\mathbf{u} \in \mathbb{R}^p$ is the input vector, $\mathbf{y} \in \mathbb{R}^q$ is the output vector, $\mathbf{A} \in \mathbb{R}^{n \times n}$ is called the system matrix, $\mathbf{B} \in \mathbb{R}^{n \times p}$ is called the input matrix, $\mathbf{C} \in \mathbb{R}^{q \times n}$ is called the output matrix, $\mathbf{D} \in \mathbb{R}^{q \times p}$ is called the feed-through matrix, $n \in \mathbb{N}$ denotes the number of system states, $p \in \mathbb{N}$ denotes the number of elements in the input vector and $q \in \mathbb{N}$ denotes the number of elements in the output vector. The so-called observability matrix $\mathbf{Q}_B = [\mathbf{C}, \mathbf{CA}, \ldots, \mathbf{CA}^{n-1}]^\intercal \in \mathbb{R}^{nq \times n}$ for state space systems will be needed for the Kalman-Criterion 4.1 in Section 4.1.

In Section 3.1, a modification of the Rosenbrock system matrix $\mathbf{P}(s)$ is used. For the derivation of $\mathbf{P}(s)$, the state space model is transformed with the Laplace transformation,

$$s\mathbf{X}(s) - \mathbf{x}_0 = \mathbf{A}\mathbf{X}(s) + \mathbf{B}\mathbf{U}(s) \tag{2.3}$$

$$\mathbf{Y}(s) = \mathbf{C}\mathbf{X}(s) + \mathbf{D}\mathbf{U}(s), \tag{2.4}$$

where $\mathbf{x}_0$ is the initial system state, s the complex variable in the Laplace transformation domain and $\mathbf{X}(s)$, $\mathbf{Y}(s)$ and $\mathbf{U}(s)$ are the Laplace transforms of $\mathbf{x}(t)$, $\mathbf{y}(t)$

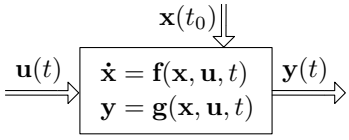

Figure 2.2: Continuous state space model of a dynamical system in style of Föllinger [Foe13], where $\mathbf{u}$ is the input to the system, $\mathbf{x}(t_0)$ the system's initial state and $\mathbf{y}(t)$ the system's output.

and $\mathbf{u}(t)$, respectively. When Equation 2.3 is solved for $\mathbf{X}(s)$, the two Equations 2.3 and 2.4 can be written in matrix notation,

$$\begin{bmatrix} s\mathbf{1} - \mathbf{A} & -\mathbf{B} \\ \mathbf{C} & \mathbf{D} \end{bmatrix} \begin{bmatrix} \mathbf{X}(s) \\ \mathbf{U}(s) \end{bmatrix} = \begin{bmatrix} -\mathbf{x}_0 \\ \mathbf{Y}(s) \end{bmatrix}, \tag{2.5}$$

where the Rosenbrock system matrix $\mathbf{P}(s)$[Foe13, p. 284] is the matrix on the left and the sub-matrix $\mathbf{1}$ in $\mathbf{P}(s)$ denotes the identity matrix of corresponding size.

2.4 Nomenclature

N.1 Vectors $\mathbf{a}$ and matrices $\mathbf{A}$ have bold characters. The former ones are written with small letters, whereas the latter ones are written with capital letters. Elements of a matrix are written with subscripts, for example: $A_{i,j}$. The rows and columns are denoted by i and j, respectively.

N.2 An edge e is described by the pair (u, v) or (v, u) of its adjacent vertices u and v. An arc a is designated by the ordered pair (u, v), if the arc points from u to v or by (v, u), if the arc points from v to u.

N.3 The notation $f(u, v)$ means that the flow f flows from vertex u to v. The same holds for resistance $R(u, v)$ or conductances $G(u, v)$ which are located on edges (u, v) between the vertices u and v.

N.4 The derivative by time can be briefly written with a point on the specific variable. An example is the derivate of distance which equals velocity $v = \frac{\text{distance } x}{\text{time } t} = \dot{x}$.

N.5 The small letter s is the complex variable in the Laplace transformation domain.

N.6 Superscript letters always specify the respective energy carrier type χ, for example $\mathcal{T}^{el}$ is a graph representing the electric network. To refer to the gas or heat network, the letters g or h are used instead.

N.7 The cardinality $|S|$ of a set S returns the number of elements of that set. The cardinality $|\mathcal{T}|$ of a graph $\mathcal{T}$ returns the number of vertices and $||\mathcal{T}||$ returns the number of edges, respectively.

N.8 The rank of a matrix $\mathbf{A}$ is given by $\text{rk}(\mathbf{A}) = r \in \mathbb{N}$ and denotes the number of linear independent rows r and is equal to the number of linear independent columns.

2.5 Glossary

This glossary presents a list of definitions for some remaining terms, where we think, that a brief explanation is sufficient.

G.1 *State Estimation:* calculation of the system's state only by the knowledge of some output variables

G.2 *Estimation Error:* the error that is made by calculating the system's state with incomplete data

G.3 *System's State:* set of variables which are unambiguously describing the system

G.4 *System vs. Network:* (here) a static system is called network whereas a dynamic system is shortly called system

G.5 *Traveling Salesman Problem:* find the shortest tour between different cities without visiting a city twice

G.6 A *directed graph* is a special graph whose edges have an associated direction, pointing from an initial vertex to a terminal vertex [Die06, p.28].

G.7 In a *complete graph* every vertex is connected with an arc to every other vertex [Die06, p.3]. The number of arcs n_A in a directed graph can be calculated using the number of vertices n_V [WL98].

$$n_A = 2 \cdot \binom{n_V}{2} \tag{2.6}$$

G.8 A *planar* graph is a graph that can be embedded in a plane [Die06, p.96].

Chapter 3

Related Work

This chapter provides an overview of previous results and outlines the gap in research by showing that almost all existing observability criteria and sensor placement strategies are not suitable for multi-carrier energy distribution networks (MEDNs). Section 3.1 presents recent research on observability criteria for energy networks followed by an illustration of different sensor placement strategies in Section 3.2.

3.1 Research on Observability

Up to now, there is no observability criterion available for MEDNs. This is due to the fact that there is no generally accepted mathematical model for this type of system class. So far, the only modeling approach is the energy hub concept [GA05a, GA07]. It combines optimal power flow and the economical dispatch problem (see Section 5.1). Power flow calculation for an electric network of $n_{V,el}$ vertices needs in general $n_M = n_{V,el}$ measurements to determine all $2n_{V,el}$ network states (all complex nodal voltages)[Cra12, p.419]. A lot of work is done concerning the topological optimization of energy hubs [GA06], but not in terms of their observability. The coupling matrix, which is part of the transfer function of such a hub, could basically be converted into a minimal state-space model. Then, the familiar observability criterion 4.1 from Section 4.1 could be applied. Since the system's in- and outputs are power flows, this approach is unsuitable for MEDNs (this is explained in more detail in Section 5.1).

Electric power system's static-state estimation was introduced by Schweppe et al. in 1970 [SW70]. Further work was done by Monticelli and Fu [Mon99] on solving the state estimation with weighted least squares methods. They defined observability for the electric power grid as follows:

Criterion 3.1. [MW85b] An electrical power system is observable only if the state estimation can be solved unambiguously.

Thus, the network is not observable, if the state estimation problem has more than one solution. They also developed an algorithm [MW85a, p.164] which is able to identify observable islands with unobservable interconnections. An observable island is a connected part of the network in which all branch flows can be calculated using the available measurements. Their algorithm starts by initializing one island for each bus in the network. Then, an arbitrary branch with a meter is chosen and it is checked whether the incident vertices belong to different islands. In case they do, the two islands are merged. This procedure continues until all flow measurements have been processed. After this, all flows inside one island are observable and the flows on branches connecting different observable island are unobservable. To make the whole network observable, Monticelli and Fu propose to place sensors on the unobservable interconnections.

Since the above mentioned definition of observability was practice-oriented for an electric power system, the next one will be motivated from a system theory's point of view. The regarded system class is called linear structured systems (LSSs) and is structurally related to the well-known state space model (see Section 2.3)

$$\Sigma : \begin{cases} \dot{\mathbf{x}}(t) = \mathbf{A}\mathbf{x}(t) + \mathbf{B}\mathbf{u}(t), \\ \mathbf{y}(t) = \mathbf{C}\mathbf{x}(t) + \mathbf{D}\mathbf{u}(t), \end{cases} \tag{3.1}$$

where Σ denotes the LSS, $\mathbf{A} \in \{0, *\}^{n \times n}$ the system matrix, $\mathbf{B} \in \{0, *\}^{n \times p}$ the input matrix, $\mathbf{C} \in \{0, *\}^{q \times n}$ the output matrix and $\mathbf{D} \in \{0, *\}^{q \times p}$ the feed-through matrix. The difference between the state space model and a LSS becomes obvious in the definition of their matrices. For LSS, only the zero (0) or non-zero ($*$) entries of $\mathbf{A}, \mathbf{B}, \mathbf{C}$ and $\mathbf{D}$ are known, whereas for the state space model the real values need to be specified (Equations 2.1 and 2.2).

For LSS, there exists a theory of strong structural controllability and observability which provides a criterion for the so-called generic observability [RHS14], where the term *generic* implies that the whole information on the system in the matrices $\mathbf{A}, \mathbf{B}, \mathbf{C}$ and $\mathbf{D}$ is structural. The non-zero entries (h is the number of non-zero entries) can be parameterized by scalar real parameters λ_i with $i = 1, \ldots, h$ forming the parameter vector $\Lambda = (\lambda_1, \ldots, \lambda_h)^T \in \mathbb{R}^h$ [BHM07]. The parameterized structured system Σ_Λ in Equation 3.2 results from the unparameterized system Σ in Equation 3.1 by inserting the λ_i and can be written as follows:

$$\Sigma_\Lambda : \begin{cases} \dot{\mathbf{x}}(t) = \mathbf{A}^\lambda\mathbf{x}(t) + \mathbf{B}^\lambda\mathbf{u}(t) \\ \mathbf{y}(t) = \mathbf{C}^\lambda\mathbf{x}(t) + \mathbf{D}^\lambda\mathbf{u}(t) \end{cases} \tag{3.2}$$

For the system Σ_Λ, a matrix $\mathbf{P}_\Lambda(s)$ similar to the Rosenbrock system matrix (see Equation 2.5) can be stated

$$\mathbf{P}_\Lambda(s) = \begin{pmatrix} \mathbf{A}^\lambda - s\mathbf{I}_n & \mathbf{B}^\lambda \\ \mathbf{C}^\lambda & \mathbf{D}^\lambda \end{pmatrix}, \tag{3.3}$$

which can then be used for the following observability Criterion 3.2:

Criterion 3.2. [BHM07] A structured system Σ_Λ is generically state and input observable if and only if:

$$g\_\text{rank}(\mathbf{P}(s)) = n + g\_\text{rank}\begin{pmatrix} \mathbf{B}^\lambda \\ \mathbf{D}^\lambda \end{pmatrix} = n + q \qquad \forall s \in \mathbb{C}, \tag{3.4}$$

where $g_$rank is the so-called generic rank of a matrix. The main characteristic of $g_$rank is that $g\_\text{rank}(\mathbf{P}(s)) = r$ with a $r \in \mathbb{N}$ for all $s \in \mathbb{C}$ meaning that for almost all parameter values $\lambda \in \mathbb{R}^h$, $\text{rk}(\mathbf{P}(s)) = r$ for all $s \in \mathbb{C}$.

A great advantage of LSSs is the possibility to graphically represent them using directed graphs [RHS14]. Boukhobza et al. as well as Alem and Benazzouz used the graphic representation for stating observability criteria for the associated graph. Nevertheless, this approach only provides structural information. According to Baldwin et al. [BMBA93] numerical observability implies structural observability, but not the converse. Therfore an algebraic description of the network is needed for the state estimation of MEDNs.

3.2 Sensor Placement

In practice, sensor placement has always been done by using rules of thumb. Kouzelis and Katsavounis [KK15] propose to place sensors in the electric grid at the substation (part (a) in Figure 3.1), mid- (part (b) in Figure 3.1) and end-point (part (c) in Figure 3.1) of the feeder as well as at sensitive loads (part (d) in Figure 3.1) . For the sensor allocation to these strategic network points, the mid-point of the feeder and the sensitive loads must be identified first. This is solved by an optimization problem combined with clustering technologies. In Figure 3.1, this approach is illustrated for an exemplary electric network. The blue lines mark the sensor positions according to Kouzelis and Katsavounis.

Most sensor placement strategies in literature are oriented towards a structural analysis and not towards an algebraic analysis. Hence, the term generic observability for LSSs often appears in this context. Khan and Doostmohammadian [KD11] present two lemmas for structural observability which can be used for the network design of

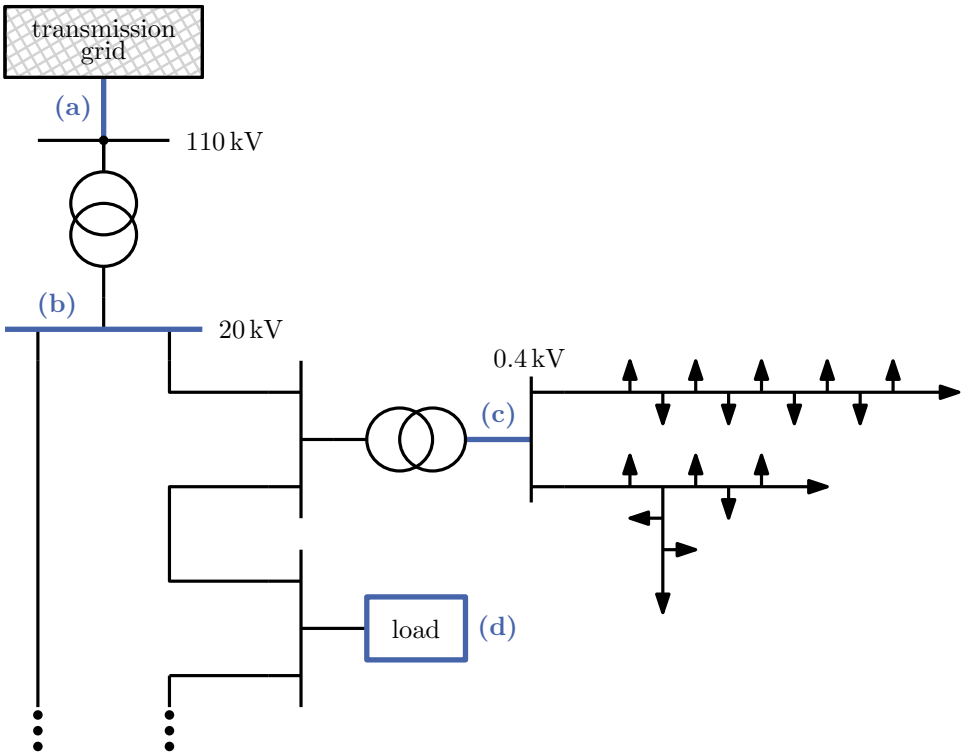

Figure 3.1: Rule of thumb sensor placement: Kouzelis and Katsavounis [KK15] propose to place sensors at the blue colored components of the electric distribution network, which are (a) the substations that are connected to the transmission grid, (b) the bus bars at the mid-point of the feeder, (c) the end-points of the feeder and (d) sensitive loads.

future smart grids. Their sensor placement procedure is independent of the physical parameter, as it only depends on the underlying network structure described by a structural adjacency matrix in $\{0, *\}^{(n \times n)}$, where n denotes the size of the network. The aim of their work is to find the minimum number of sensors to stabilize the steady-state estimation error (see Section 2.5). Alem and Benazzouz [AB14] also used a structural adjacency matrix for fault detection and isolation (FDI) in electric networks, based on generic observability. They introduce an algorithm which reconfigures the sensor positions in an existing network to make fault detection possible. This approach is based on the conversion of bond graph to digraph representation of LSSs.

As mentioned in the last paragraph, sensor placement in electric networks can be optimized with respect to the state estimation error. However, there exists no standard performance index for the evaluation of the impact of the sensor placement. Chen et al. [CLW+16] use the root-mean-square error (RMSE) which is the square root of the average of squared errors. Although they are able to formulate a linear objective function, their sensor placement model has non-linear and non-convex constraints. Li et al. [LSC13] present an optimization routine for Phasor Measurement Units (PMUs) using the joint accuracy-convergence metric ρ_*:

$$\rho_* = \sqrt{\beta/\omega} \tag{3.5}$$

This metric includes the numerical stability of the algorithm via ω as an upper bound for the algorithm's convergence and the estimation accuracy via β. Note that both of them depend on the PMU placement. The observability metric β can be calculated as follows:

$$\beta = \inf_{\mathbf{v}\in\mathbb{V}} \lambda_{min}\left[\tilde{\mathbf{F}}^{\intercal}(\mathbf{v})\tilde{\mathbf{F}}(\mathbf{v})\right] > 0, \tag{3.6}$$

where $\lambda_{min}[\cdot]$ is the minimum eigenvalue, $\mathbf{v}$ the vector containing the real and imaginary components of the complex voltage phasors for all vertices and $\tilde{\mathbf{F}}$ the Jacobian from the Gauss-Newton Algorithm.

Sensor placement in gas networks is not as far explored as the equivalent problem in the electric grid. There is a paper [vH15] in which the gas distribution network (GDN) is modeled with the steady-state Weymouth equation (see Equation 5.20). The sensor placement is formulated as an optimization problem minimizing the standard deviation (std) of the network flows

$$\min_{\mathbf{x}} \sum_{k=1}^{n} \mathrm{std}(\tilde{\mathbf{Q}}_k) \quad \text{s.t.} \tag{3.7}$$

$$1 \leq \max(\mathbf{x}) \leq n, \tag{3.8}$$

where the elements of the vector $\mathbf{x}$ for the sensor locations are integer and unique. The number of pipes in the network is denoted by n and $\tilde{\mathbf{Q}}_k$ is the vector of pipe flows in the network. They solved the sensor placement problem for the gas network of the city Texel using a greedy algorithm which needed several hours to complete.

There are neither known approaches for sensor placement in heat distribution networks (HDN) nor for MEDNs. Up to now, research in these networks focuses on power flow analysis [RWA09, GA07].

3.3 Summary

Chapter 3 summarizes the related work for this thesis. It is worth pointing out that there exists a research gap on observability and sensor placement for MEDNs. The main focus of former research was concentrated on electric power grids or single-domain solutions and cannot be applied on multi-carrier systems. Moreover, structural approaches are not suitable for a numerical observability criteria, as numerical observability only implies structural observability, but not the converse [BMBA93].

There is no general modeling approach available which considers the different domains in one setup and which can be used for a sensor placement optimization in MEDNs. However, a multi-carrier perspective is advantageous, since synergies of the different energy carriers can be taken into account. For example excessive electric energy from renewables can be stored easily in the gas network or CHP units can act as local micro power plants. In literature, there are no modeling approaches that consider the coupling of different energy networks and therefore this thesis contributes a MEDN model as well as an observability criterion in Chapter 5.

Chapter 4

Fundamentals

The fundamentals in Chapter 4 form the foundation of this thesis. This chapter can be divided into two parts, where the first one present the fundamentals of system theory and of electric network analysis and the second the fundamentals of energy-technical networks.

An essential part of this chapter is given in Section 4.1, where the term observability is defined. This is followed by the definition of the used system state variables in Section 4.2, which are the generalized variables effort and flow. Moreover, the nodal analysis from linear electric network analysis will be explained in Section 4.3, as it is necessary for the understanding of the generalized nodal analysis approach in Section 5.5.

In the second part of this chapter, the structure and monitoring of the different energy networks, viz. the electricity, gas and heat network, is presented. The main part of the information was provided by the network operators of Karlsruhe, which are the *Stadtwerke Karlsruhe* and *netzservice - Stadtwerke Karlsruhe*.

4.1 Observability

The importance of the concept of observability can be motivated by the advantage of an observable system as opposed to a non-observable system, which is the possibility to extrapolate from limited to complete knowledge of the system states.

The state of a system is the entity of all state variables (see Section 2.3). The system state variables that are used within this thesis will be presented in Subsection 4.2. In general, state variables can either be measurable or non-measurable and can be further divided into observable and non-observable. Observable state variables can be calculated or estimated, whereas non-observable states cannot be determined at all. An example for such a non-measurable, but observable state variable is the

velocity of a car, assumed that only the distance is measured. Then, it is possible to estimate the velocity by integrating the distance traveled. A further example is the charge state of a battery, which can only be estimated by the integration of the incoming and outgoing current.

In system theory the most popular observability criterion is the one for continuous state space models (see Section 2.3) introduced by Kalman in 1959 [Kal59]. He dealt with the problem of reconstructing unmeasurable state variables from the measurable ones in the minimum possible length of time. His definition of observability for state space models can be found for example in [Foe13, p.289].

Definition 4.1. A dynamic system (Equations 2.1 and 2.2) is called completely observable, if the arbitrary initial state vector $\mathbf{x}_0 := \mathbf{x}(t_0)$ can be determined using the known input vector $\mathbf{u}(t)$ and the measurement vector $\mathbf{y}(t)$ over a finite period of time with $t > t_0$.

The term "completely" in Definition 4.1 refers to the complete state vector. Only some specific states are determinable, if a system is partly observable. For static systems the concept of observability equals the question of computability, since the output only depends on the input $\mathbf{u}(t_S)$ at present time and not on all inputs with $t > t_0$ as it does for dynamic systems. This comes clear in Definition 4.1, if we replace "over a finite period of time with $t > t_0$" by "at a specific point in time $t = t_0$". The term observability is used for static systems in power engineering since the 1980's [KCD80, BMBA93, Cle90] and will be revived for the static network model in Chapter 5.

For state estimation the system's observability need to be checked in advance. Thus, an observability criterion is needed. According to Definition 4.1, the so called Kalman-Criterion 4.1 [Kal59] can be stated:

Criterion 4.1. A dynamic system (Equations 2.1 and 2.2) is completely observable if the observability matrix Q_B has full rank n.

An easy way to check Criterion 4.1 is to calculate the determinant of $\mathbf{Q}_B$. The system is observable, if it is not zero. Note that the given Criterion 4.1 can only be applied on state space models (see Equations 2.1 and 2.2). Other observability criteria for state space models are for example the Hautus-Criterion or the Gilbert-Criterion [Foe13, p.296]. Second can only by applied on dynamic systems with unique eigenvalues. Such a dynamic system is observable if the matrix $\mathbf{CV}$ has no column vector $\mathbf{e}_0$, where the matrix $\mathbf{V} = [\mathbf{v}_1, \ldots, \mathbf{v}_n]$ contains the eigenvectors of the system matrix $\mathbf{A}$. On the other hand, the Hautus-Criterion can also be applied on systems which have eigenvalues with an algebraic multiplicity ≥ 1. It declares that a dynamic system is observable if for every eigenvector $\mathbf{v}$ of $\mathbf{A}$ the product $\mathbf{Cv} \neq \mathbf{e}_0$.

4.2 System State Variables

The system state variables that are used in this thesis, are the generalized variables effort e and flow f. In the electric domain the generalized effort e represents a phase-to-ground voltage U and the generalized flow f the current I in the conductor. In the hydraulic domain the generalized effort e is the pressure p in the pipeline and the generalized flow f is the flow Q of the medium through the pipeline. The associated units for the electric and hydraulic domain are given in Table 4.1.

	electrical	hydraulic
effort e	voltage U in Volt (V)	pressure p in Pascal (bar)
flow f	current I in Ampere (A)	flow Q in (m^3/s)

Table 4.1: Generalized Variables in the style of Gawthrop and Bevan [GB07]. Gas and heat networks are both hydraulic networks.

The temperature in the heat network is not mentioned here, as it will not show up explicitly in the modeling approach. This is due to the fact that the pressure sensors are assumed to be equipped with additional temperature sensors, as temperature sensors are comparably cheap.

Feasible Flows

Flows are called *feasible* if they fulfill specific constraints [LMM+15]. In this work, a feasible flow has to meet the capacity constraint of its line:

$$-c(a_1) \leq f(u,v) \leq c(a_2) \quad \forall a = (u,v) \in A, \tag{4.1}$$

where $c : A \to \mathbb{R}$ represents the capacity function for each line $a \in A$. This ensures that the flows can be transported by the underlying physical system. In the electrical domain for example, the cables are dimensioned such that a maximum current can be transported. Excessive current flows would cause thermal overloads or in worst-case a cable fire. For the hydraulic domain, this constraint helps to keep friction losses within a reasonable limit and protects flow sensors from destruction.

Furthermore, a feasible flow has to fulfill the flow conservation (Equation 4.2), equivalent to Kirchhoff's Current Law:

$$\sum_{u \in V\,:\,(v,u) \in A} f^-(v,u) - \sum_{u \in V\,:\,(u,v) \in A} f^+(u,v) = \begin{cases} \tilde{f}(v) & \text{at vertices with disturbances} \\ 0 & \text{else.} \end{cases} \tag{4.2}$$

Feasible Efforts

For a secure operation of the network, there are some restrictions on the efforts, too. In the hydraulic domain, the pipelines have an associated maximum operating pressure (MOP) which results from their diameter and construction. For a secure network operation it is necessary that the pressure is smaller than the MOP, but not too low to ensure the transportation of the medium. A lower bound represents in any case the ambient pressure. Similar pressure rules apply for the heat network operation as well. For electric networks the feasible voltages are in the range of $\pm 10\%$ of the nominal voltage U_N to ensure the stability of the network's frequency [EN 50160]. We call an effort *feasible*, if $e_{\min,\chi} \leq e \leq e_{\max,\chi}$, where $e_{\min,\chi}$ and $e_{\max,\chi}$ are the lower and upper bound of the feasible effort for each energy carrier type $\chi \in \{el, g, h\}$.

4.3 Nodal Analysis

The nodal analysis, as well as the mesh analysis for planar networks [Doe11, p.35], is a technique to calculate all voltages and currents in a linear *electric* network [Doe11, p.38]. The nodal analysis combines Kirchoff's current law (see Equation 4.9) with Ohm's law (see Equation 4.3), whereas the mesh analysis combines Kirchoff's voltage law with Ohm's law (all voltages in a mesh sum up to zero). In case of a small network being radial or lightly meshed, both analysis types require a similar effort, since a similar number of equations needs to be deployed. For a meshed network, it becomes more and more difficult to determine a set of linear independent meshes, which is due to the fact, that this set is not unambiguous [Lei13, p.105]. Since this problem does not occur in the nodal analysis, the nodal analysis is more suitable for automated calculation. It is further developed towards a generalized nodal analysis in the modeling approach for MEDNs in Chapter 5, which is able to model electric, gas and heat networks all in one. Now, we present the Thévenin-Norton-Equivalent in Subsection 4.3.1 and in the following Subsection 4.3.2, the nodal analysis procedure.

4.3.1 Thévenin-Norton-Equivalent

We introduce the Thévenin-Norton-Equivalent, since it is necessary for the nodal analysis procedure in Subsection 4.3.2. It states that all voltage sources can be converted into current sources and vice versa. The Thévenin-Norton-Equivalent is depicted in Figure 4.1, where the circles are the symbols for sources and the rectangles can represent in general both, resistances or conductances. A horizontal

line inside a circle is the symbol for a current source, otherwise it is a voltage source. The conversion of current sources in an equivalent voltage source and vice versa is based on the reformulation of Ohm's law: the current $I \in \mathbb{R}$ through a conductor is directly proportional to the voltage $U \in \mathbb{R}$ across that conductor:

$$R^{el} = \frac{U}{I} \quad \Leftrightarrow \quad \frac{I}{U} = \frac{1}{R^{el}} := G^{el}. \tag{4.3}$$

Due to the proportionality between current I and voltage U, the circuit has a constant resistance $R^{el} \in \mathbb{R}_{\geq 0}$. The reciprocal value of R^{el} is called conductance $G^{el} \in \mathbb{R}_{\geq 0}$. The assignment of R^{el} or G^{el} to a specific arc in the network is denoted by $R^{el}(u, v)$ or $G^{el}(u, v)$ for the adjacent vertices u and v. The abbreviation for the respective carrier (here $\chi = el$) is superscripted:

$$G^{el}(u, v) = \frac{1}{R^{el}(u, v)} \tag{4.4}$$

The analogous definitions of the conductances for the gas and heat network will be given in Section 5.3.

4.3.2 Procedure

According to Dössel [Doe11, p.40], the following steps must be performed to determine the system of linear equations $\mathbf{I} = \mathcal{G}^{el}\mathbf{U}$ for an electrical network (see Equation 4.8), where $\mathbf{I} \in \mathbb{R}^{n_{V,el}}$ is the vector of all currents, $\mathbf{G}^{el} \in \mathbb{R}^{n_{V,el} \times n_{V,el}}$ is the conductance matrix, $\mathbf{U} \in \mathbb{R}^{n_{V,el}}$ is the vector of all voltages and $n_{V,el}$ is the number of vertices in the electric network.

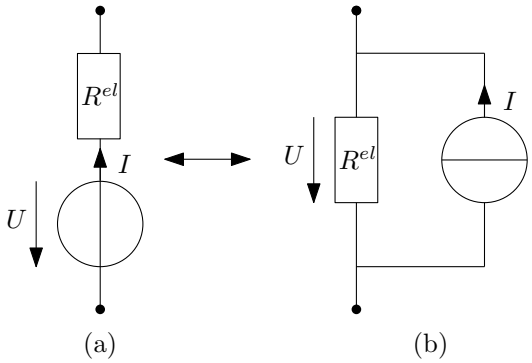

Figure 4.1: Thévenin-Norton-Equivalent: The rectangles denote the resistance R^{χ}, (a) is the Thévenin-Equivalent with a voltage source of U and (b) is the Norton-Equivalent with a current source of I.

For simplicity, we neglect the superscript $\chi = el$ for voltages U, currents I, resistances R and conductances G in this section.

1. Define a *reference vertex* which will be the zero potential. This is necessary for the solvability of the resulting system of equations (see Section 4.3.3) and can be explained logically: a voltage is defined as the difference between two electric potentials. Thus, at least one reference voltage is needed such that one knows to which potential the voltage refers.

2. Enumerate all leftover vertices with the potentials $U_1, U_2, U_3, \ldots, U_{n_{V,el}}$. These are the unknown potential variables which are aggregated into the vector of potentials $\mathbf{U} \in \mathbb{R}^{n_{V,el}}$:

$$\mathbf{U} = \begin{pmatrix} U_1 \\ U_2 \\ \vdots \\ U_{n_{V,el}} \end{pmatrix} = \left\{U_i\right\}_{i \in V^{el}} \tag{4.5}$$

3. Transform all voltage sources into current sources using the Thévenin-Norton-Equivalent. This is necessary to include the currents into Equation 4.9.

4. Transforming all resistances $R(u, v)$ into conductances $G(u, v)$ by Equation 4.4, as they will be needed for the statement of the conductance matrix $\mathcal{G}^{el}$ in the system of equations 4.8.

5. State the conductance matrix $\mathcal{G}^{el} \in \mathbb{R}^{n_{V,el} \times n_{V,el}}$,

$$\mathcal{G}^{el} = \begin{pmatrix} G(1,1) & -G(1,2) & \cdots & -G(1,n) \\ -G(2,1) & G(2,2) & \cdots & -G(2,n) \\ \vdots & \vdots & \ddots & \vdots \\ -G(n,1) & -G(n,2) & \cdots & G(n,n) \end{pmatrix}, \tag{4.6}$$

   where on the main diagonal there is, for each vertex, the sum of all conductances connected to that specific vertex.

$$G(v,v) = \sum_{u \in V^{el} \setminus \{v\}} G(u,v) \qquad \forall v \in V^{el} \tag{4.7}$$

   Above and below the main diagonal, there are the negative coupling conductances $G(u, v)$ with $u \neq v$ and $u, v \in V^{el}$. These are the conductances $G(u, v)$ between the vertex u and v, respectively. The conductance $G(u, v)$ is zero, if there is no arc (u, v) between u and v. Note that this structure will reappear in Equation 5.54 for the conductance matrix $\mathcal{G}$ of the MEDN.

6. State the set of linear equations:

$$\mathbf{I} = \mathcal{G}^{el} \cdot \mathbf{U}, \tag{4.8}$$

where the vector $\mathbf{I} \in \mathbb{R}^{n_{V,el}}$ contains the sum of currents at each vertex and is defined by,

$$\mathbf{I} = \begin{pmatrix} \sum_{u \in V^{el} \setminus \{1\}} I_{u,1} \\ \sum_{u \in V^{el} \setminus \{2\}} I_{u,2} \\ \vdots \\ \sum_{u \in V^{el} \setminus \{v\}} I_{u,v} \end{pmatrix} = \left\{ \sum_{u \in V^{el} \setminus \{v\}} I_{u,v} \right\}_{v \in V^{el}}. \tag{4.9}$$

By means of the signs, the direction of the actual current flow is defined. It gets a positive sign, if the current flows into a vertex. In Figure 4.2 the two currents $I_{1,2}$ and $I_{3,2}$ are flowing into vertex 2. Thus, they get a positive sign in Equation 4.10. On the other hand, the currents $I_{2,4}$ and $I_{2,5}$ are leaving vertex 2 and are consequently subtracted in the vertex balance equation (see Kirchhoff's Current Law in Equation 4.2).

$$0 = I_{1,2} + I_{3,2} - I_{2,4} - I_{2,5} \tag{4.10}$$

Note that the numbering in the currents' indices is done according to the positive flow direction and that the skew symmetric condition $I_{u,v} = -I_{v,u}$ holds for each current.

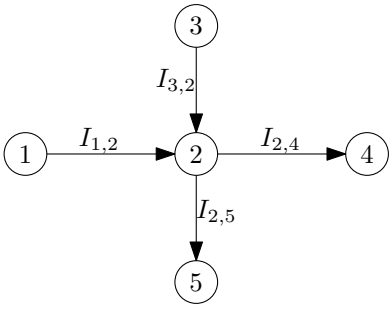

Figure 4.2: Sign convention for the current flows on arcs that are incident to vertex 2 which is connected to four other vertices 1, 3, 4 and 5.

4.3.3 Solvability of the Nodal Analysis

The set of linear equations from Equation 4.8 can be solved for $\mathbf{U}$ if $\mathcal{G}^{el}$ has full rank:

$$rk(\mathcal{G}^{el}) = n_{V,el}, \tag{4.11}$$

where $n_{V,el}$ is the number of vertices in the electric network. An alternative formulation to Equation 4.11 is given by $\det(\mathcal{G}^{el}) \neq 0$. The solvability of a set of linear equations will be important for the MEDN observability criterion in Chapter 5.6, since the modeling approach is done for a static network (see Section 5.2). Consequentially, the term observability and solvability coincide as it was explained using Definiton 4.1.

Here ends the first part of this chapter, where the fundamentals of system theory and of electric network analysis were presented. Next, the fundamentals of energy-technical networks, their structure and today's monitoring will be in focus.

4.4 Structure and Monitoring of Energy Networks

This section shows and explains the typical structure and monitoring of different energy networks. First, the electricity network is presented in Section 4.4.1, followed by the presentation of the gas network in Section 4.4.2. Last but not least, the heat network is presented in Section 4.4.3.

4.4.1 Electricity Network

In Figure 4.3 the basic structure of an electrical distribution network is depicted [Cue11, p.14], where the dots in the lower part indicate that the network continues in that certain direction. The electrical distribution network is supplied by the transmission grid at a transfer point. For example, there are three of these in Karlsruhe connecting the transmission grid (network operator: *TransnetBW*) and the local distribution network [net17]. In Figure 4.3, only one transfer point is depicted that has a voltage and current measurement at the substation. Additionally, there is a three-phase voltage and current measurement at the 110 kV and 20 kV busbars. Busbars serve as a central distributor of electrical energy since all the incoming and outgoing lines are connected to them. All blue-colored components in Figure 4.3 are measurements having telecommunications [net17, FLM+14, Jan]. This is necessary if the measurement should be available for the network operator at a central control station. The measurements that are colored black in Figure 4.3 can only be read out if an employee is in the specific substation and takes a

look on a meter or display. In the 20 kV ring, which is in open operation, about every fifth transformer station is equipped with telecommunications. And in the low-voltage grid there are only electricity meters that are read out once a year. There are hardly any smart meters in the electrical network of Karlsruhe up to this day [Sta14]. A smart meter is an intelligent electricity meter that can measure time series of the consumers consumptions and is able to exchange data with the network operator via Internet. Common time resolution for smart meters are hourly measurements down to intervals lasting only several minutes. One notices that there are more measurements with telecommunications on higher voltage levels available than on lower ones. In general, network operators only measure the least that is necessary for maintaining their operation [ATBS13]. The sensors in the electrical network were placed by using operating expertise and rules of thumbs.

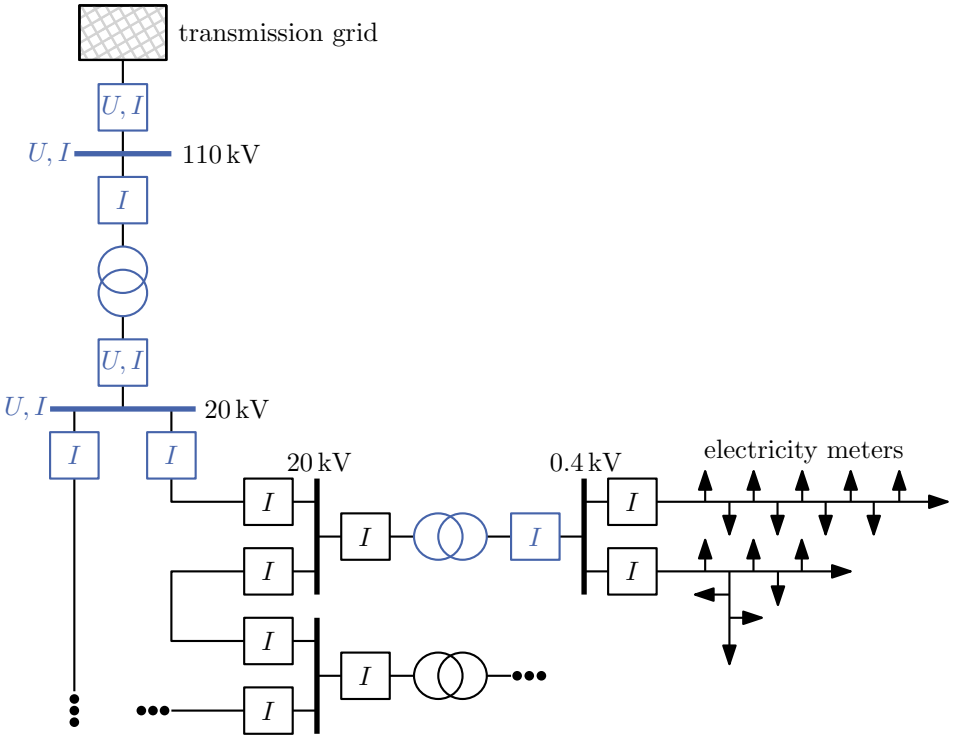

Figure 4.3: Electric distribution network structure: The rectangles denote substations and the label U or I indicate a voltage or current measurement, respectively. The fat lines that have an assigned voltage label (110 kV, 20 kV and 0.4 kV) are busbars. The symbol for a transformer consist of two overlapping circles.

4.4.2 Gas Network

Approximately 511.000 km of pipes are installed in the German gas network [Bun]. They transport natural gas, whose main component is methane CH_4 with a share of at least 75 % up to 99 % [BHK+14, MCKP02]. Since it is a burnable gas, it can be classified according to the Wobbe-Index into high calorific gas (H-gas) and low calorific gas (L-gas), where the Wobbe-Index is a measure for the energy density. In Karlsruhe for example, only H-gas is used in the gas network [Stad].

The gas network can be divided into the transportation and the distribution level. Within the second, further distinction is done according to the pressure levels in high-, medium- and low-pressure, respectively. Typical pressures and flow velocities in the gas transportation networks are $80 - 200$ bar and 10 m/s [Pfe15]. For the gas distribution network the nominal pressure is in between $0.04 - 16$ bar and the velocity can reach values up to 4 m/s [Pfe15]. Gas distribution networks are in general meshed which can be seen in the Figure 4.4.

In 2015, natural gas had a share of 21.1 % in the German primary energy consumption [Bun16, p.5]. This made gas the second most important energy carrier after oil (33.9 %). The main gas consumers in Germany are the industry with a share of 42 % and the households with a share of 38 %. The role of gas for the electricity generation in Germany trends downwards over the last years. In 2015, the share was 9.1 % (2014: 9.7 %)[Bun16, p.6].

In Figure 4.4 the basic structure of the medium gas distribution network of Karlsruhe is illustrated. An exemplary network segment of the low-pressure gas distribution network is unfortunately not available in this online version. The total length of all gas pipes in Karlsruhe for all pressure levels was 799.8 km in 2016 [Stae]. The gas network is not only supplying the 26 128 consumers [Stae] in the low pressure level but also major customers or gas power plants in the medium pressure level. The annual work of the gas consumption in the network of Karlsruhe amounts to 1 855 644 MW h [Stac]. There are three points where gas is fed in from the transmission grid, one from *transnetBW* and two from *OpenGrid Europe*, which are the names of the network operators, respectively. At those supply points there are measurements of flow, pressure and temperature available, since there is telecommunication technology [ALSS16, net17]. Gas can also be fed from Karlsruhe to a network in the south (*Stadtwerke Ettlingen*) and to one in the north (*Erdgas Südwest Netz GmbH*), where flow, pressure and temperature are measured at the exit points which are equipped with telecommunications as well [net17]. On the medium pressure level there are isolated measurements, but not on the low pressure level [STS17]. There, the consumption of the private consumers is only detected by gas meters which are read out once a year [CDF+15, TFL11]. The most common type in nearly all residential houses are diaphragm gas meters which measure the volume

flow by means of the gas displacement. In Figure 4.4 the yellow pipes are called PN 16 and have a maximum operating pressure (MOP) of 16 bar and the red ones are called PN 4 and have a MOP of at least 4 bar. Note that in normal operation, the pressure is below the MOP. In the exemplary network segment of Karlsruhe (see Chapter 6) the operation pressure is 13 bar for PN 16 and 3.2 bar for PN 4.

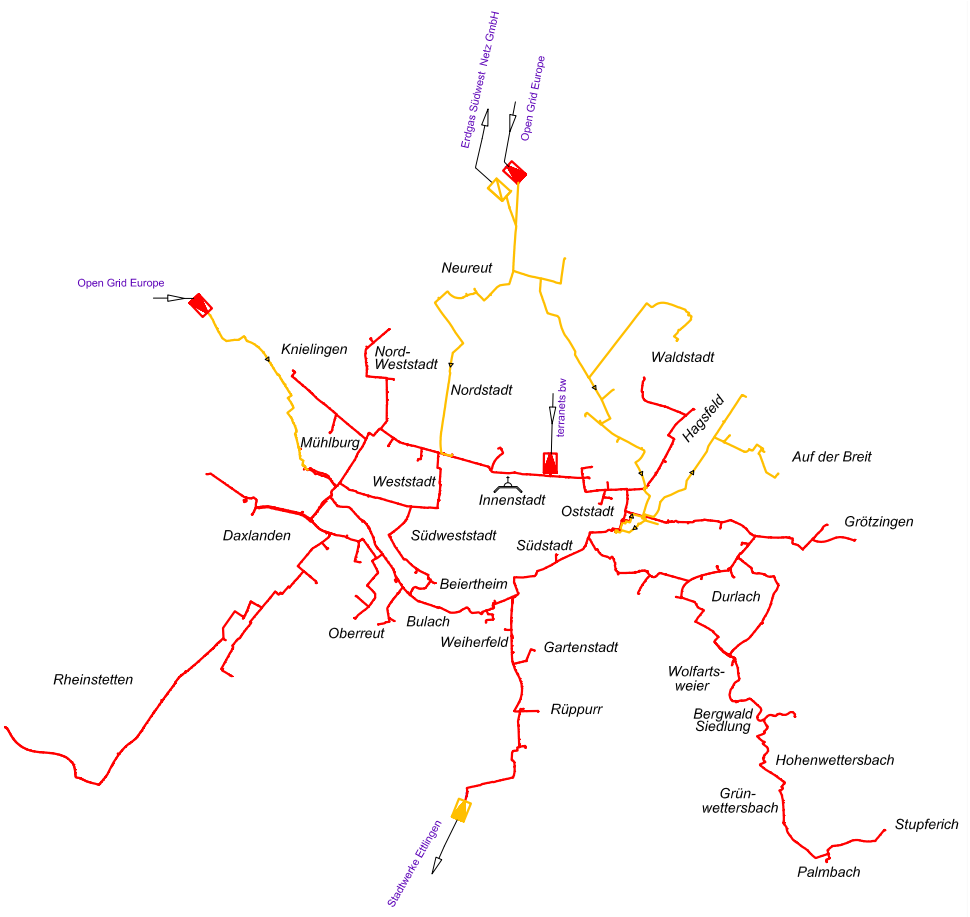

Figure 4.4: Medium pressure gas network of Karlsruhe [Stab]. The red rectangles denote the substations where gas is fed in from the transmission grid and the yellow ones denote the substations where gas is fed into other networks. The names of the adjacent network operators are given in purple and the names of the city districts in black font, respectively. There are two pipeline types in the network: PN 4 (red) and PN 16 (yellow).

4.4.3 Heat Network

Heat networks consist of pipelines for supply and return. Heat is transported in the form of hot water from the point of generation to the end consumer [LWJB16]. The heat distribution network in Karlsruhe contains 27.000 m^3 of water [Sta16]. To get a better feeling for this number, it can be compared to approximately twelve Olympic swimming pools. There are few thermal power plants that supply the local heat network, where the two biggest are a steam power plant at the Rhine and a heat power plant in the west of Karlsruhe. Their feed is monitored carefully by measurements of the water quality as well as of flow, pressure and temperature[Sta16]. In general, mainly the feed-in points are monitored in real-time [Ci15, Mah09, p.41]. The consumption of the consumers is aquired by thermal energy meters which are read out for the bill [HR 15]. The temperature control at the feed-in point is seasonal which means that it slowly adopts the water temperature in relation to the environmental temperature [UTE14]. Within the heat network, there are fifteen network points (key system points [PLC16]) at which pressures and temperatures are measured for the central control room [Sta16]. As it can be seen in Figure 4.5 the heat network is meshed and has only one network layer. We want to point out, that there are some analogies between the heat and the gas network which will be of use for their modeling. Both networks are meshed, planar and have a medium flowing through their pipelines.

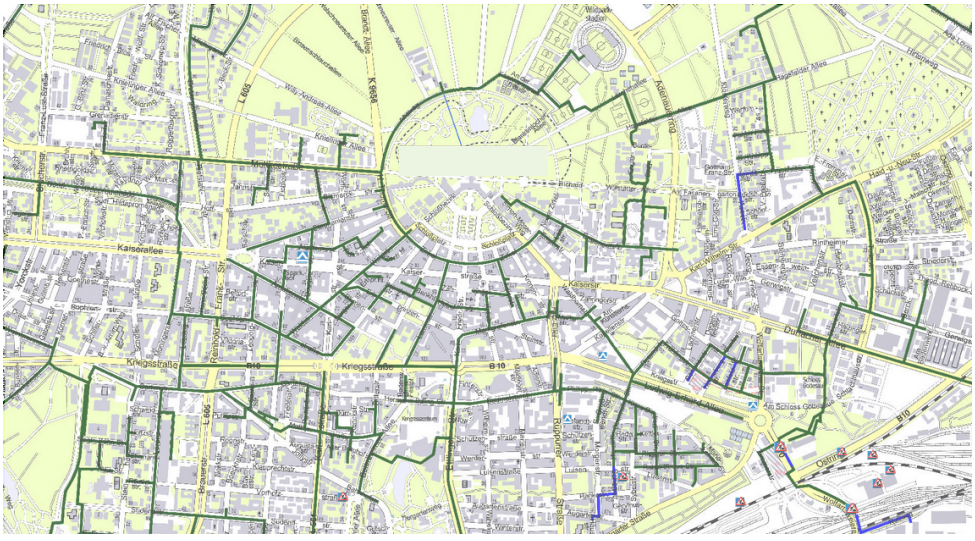

Figure 4.5: Heat distribution network of Karlsruhe [Staa]. The lines denote both supply and return. The green lines represent the existing network structure and in blue there are the planned pipelines which are in the construction stage.

Chapter 5

Modeling Approach

At the beginning of this chapter, the energy hub concept is presented in Section 5.1 and there is a discussion of the impracticality of power flow based modeling approaches for our task. We introduce the concept of a fundamental mesh in Section 5.3, by which the graph can be transferred into a closed mathematical representation. For this, we need to present the modeling approaches for single energy networks and the assumptions that we made therein (see Section 5.2). The MEDN is modeled as a directed graph $\mathcal{T}$, which includes three energy carriers and different types of energy converters. The modeling of $\mathcal{T}$ is presented in Section 5.4. The system of linear equations describing the MEDN is derived by using the generalized nodal analysis, which is explained in Section 5.5. For the resulting system of linear equations, the observability criterion is defined and discussed in Section 5.6. At the end of Chapter 5, the MEDN model is used to state an optimization problem for the sensor placement. The optimization results for an exemplary network of Karlsruhe are given in Chapter 6.

5.1 Energy Hub Concept

In literature, there currently exists only one widely-known modeling concept for MEDNs, which will be introduced in this section. It is called the *energy hub concept* and was characterized by the work of Martin Geidl [GA07, GA06, GA05a]. At the end of this section, we justify why this concept is not practicable for our task. The energy hub modeling concept can be used for the optimal power flow as well as the economic dispatch problem. First is concerned with calculating the best power flows between energy hubs and latter for the optimization of energy generation and conversion within a hub. The energy hub model includes energy conversion from one energy carrier into another and can also take account of energy storages. It is characterized through power flows and efficiencies only, where the number of considered energy carriers can be chosen arbitrarily.

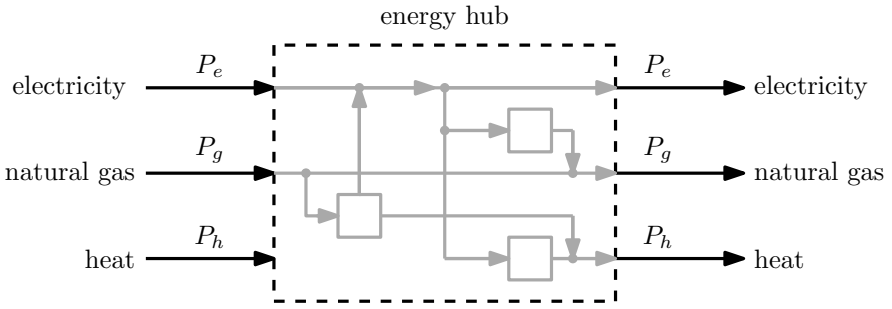

Figure 5.1: Basic energy hub structure in the style of [GA05b]. On the left-hand-side, there are the power inputs for the supply of the hub and on the right-hand-side, there are the power outputs for the loads, respectively. Inside the energy hub (dashed line) a P2G, a P2H and a CHP converter are illustrated as an example.

The basic hub structure is shown in Figure 5.1. On the left-hand-side, there are the three power inputs denoting the hub's supply with electricity, natural gas and district heat and on the right-hand-side, there are the power outputs to the loads. The inside of the hybrid energy hub is described by its coupling matrix $\mathbf{C}$ which maps the powers P_χ with $\chi = \{el, g, h\}$ from the in- to the output. This leads to a mathematical in- and output description $\mathbf{P}^+ = \mathbf{C} \cdot \mathbf{P}^-$. In this context, the term *hybrid* denotes the multiple energy carriers. For single-input single-output systems (SISO) the coupling factor C corresponds to the steady-state energy efficiency. Note that all entries of $\mathbf{P}^-$ and $\mathbf{P}^+$ must be greater or equal to zero for feasible power flows. Furthermore it is possible to include non-constant efficiencies $C = f(P^-)$. Power can flow bidirectionally between different energy hubs but only unidirectionally in their inside due to the energy conversion. Thus, an energy hub can be seen as a generalization of a multi-domain energy network node. An advantage of the hub definition is, that there are no restrictions to any size of the model. Moreover, this approach offers the flexibility to model a large variety of different systems, as for example power plants, industrial plants, big buildings and bounded geographical areas. An overview of in- and output systems that can be modeled with energy hubs is given in Table 5.1.

The energy hub concept is not suitable for our task, since its model is based on power flows. The system state of a MEDN modeled by energy hubs would only consist of power flows which does not match the given measurement structure of the underlying networks (see Sections 4.4.1, 4.4.2, 4.4.3). Hence, we will derive a suitable model based on generalized efforts and flows in the following chapter.

Input: \ Output:	SO	MO
SI	gas furnace: gas → heat	co-generation: gas → electricity, heat
MI	heat pump: heat, electricity → heat	reversible fuel cell systems: $4H + 0_2 \leftrightarrow$ electricity, heat

Table 5.1: Examples of different in- and output systems that can be modeled as an energy hub. By MI and MO we denote multiple-inputs and multiple-outputs, respectively, and SI and SO for single-input and single-ouput.

5.2 Network Line Modeling

The basic assumption for the network line modeling in this thesis will be, that the MEDN is in steady state. A system is said to be in steady state if the system's state variables are constant with respect to time $\partial \mathbf{x}(t)/\partial t = 0$. This implies that all dynamic processes have subsided. The opposite of this would be a transient state analysis which deals with dynamic effects as in possible error scenarios (lightning strike on an electric conductor) or converter control dynamics, for example. The terms *transient* und *steady* can be illustrated regarding the system of a water boiler filled with cold water. Initially, the system is in a steady state. It changes into the transient state, if it is turned on. When the water is warmed and it is only kept at this temperature, a steady state is reached again. Since we consider a MEDN in normal operation, it can be described by the static network model in Chapter 5. The following subsections will present the basic models for each of the single-carrier distribution networks. In this process, we also explain the assumptions made.

5.2.1 Electric Line Model

An exact line segment model for electric distribution networks is the three-phase Π line model [Ker02, p.126]. It is named after its shape, which can be seen in Figure 5.2. First, we present its mathematical description using a two-port network model (see Equation 5.1), which is a system with two in- and outputs by which it can be connected to other two-port networks. For the line model, the in- and outputs are the respective voltage and current vectors at the adjacent vertices u and v. Then we show, how the resistive model, which will be used in Section 5.5, emerges from the Π line model through further assumptions.

In the three-phase Π line model, all voltages $U \in \mathbb{R}$ are line-to-ground voltages and each line of the phase (a, b and c) has an impedance $z \in \mathbb{C}$ which consists of a resistance $R \in \mathbb{R}$ and an inductance $L \in \mathbb{R}$ ($z = R + jL$, where j denotes

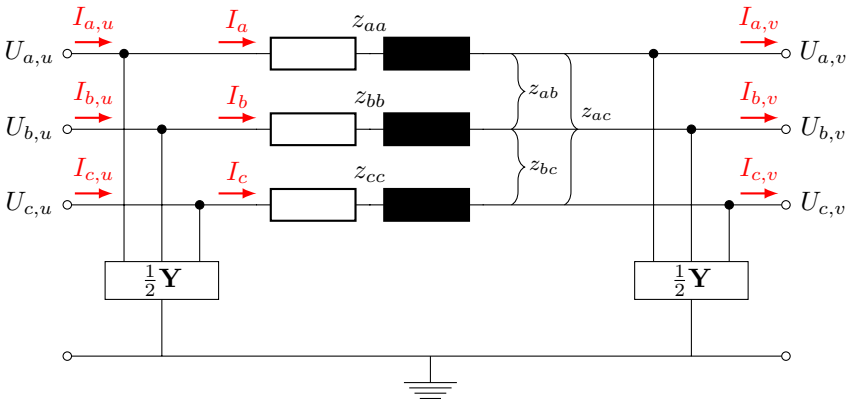

Figure 5.2: Three-phase Π line model in style of [Ker02, p.126], where z denotes the impedance of the line, $\mathbf{Y}$ denotes the capacity reactance and the small letters a, b and c denote the phases, respectively. All voltages are line-to-ground voltages. The vertex on the left side is called u and the one on the right v.

the imaginary unit). All impedances of the line segment are summed up in one impedance matrix $\mathbf{Z} \in \mathbb{R}^{(3\times3)}$. The susceptance matrix of the line $\mathbf{Y} \in \mathbb{R}^{(3\times3)}$ represents capacitive line properties and is divided in two parts (see Figure 5.2) to get a symmetric two-port network. For more details on this modeling decision we refer the reader to [Mie14, p.81]. A two-port network is characterized by Equation 5.1 where the voltages and currents between vertex u and v are linked by a two-port matrix $\mathbf{P}$. The elements of $\mathbf{P}$ are given by $\mathbf{p}_1, \mathbf{p}_2, \mathbf{p}_3$ and $\mathbf{p}_4$ in $\mathbb{R}^{(3\times3)}$.

$$\begin{bmatrix}\mathbf{U}\\ \mathbf{I}\end{bmatrix}_u = \begin{bmatrix}\mathbf{p}_1 & \mathbf{p}_2\\ \mathbf{p}_3 & \mathbf{p}_4\end{bmatrix}\begin{bmatrix}\mathbf{U}\\ \mathbf{I}\end{bmatrix}_v \tag{5.1}$$

In order to derive the two-port network model of the Π line model in form of Equation 5.1, we set up the vertex- and mesh equations 5.2 and 5.3:

$$\begin{bmatrix}I_a\\ I_b\\ I_c\end{bmatrix} = \begin{bmatrix}I_a\\ I_b\\ I_c\end{bmatrix}_v + \frac{1}{2}\cdot\begin{bmatrix}y_{aa} & y_{ab} & y_{ac}\\ y_{ba} & y_{bb} & y_{bc}\\ y_{ca} & y_{cb} & y_{cc}\end{bmatrix}\cdot\begin{bmatrix}U_a\\ U_b\\ U_c\end{bmatrix}_v, \tag{5.2}$$

$$\begin{bmatrix}U_a\\ U_b\\ U_c\end{bmatrix}_u = \begin{bmatrix}U_a\\ U_b\\ U_c\end{bmatrix}_v + \begin{bmatrix}z_{aa} & z_{ab} & z_{ac}\\ z_{ba} & z_{bb} & z_{bc}\\ z_{ca} & z_{cb} & z_{cc}\end{bmatrix}\cdot\begin{bmatrix}I_a\\ I_b\\ I_c\end{bmatrix}, \tag{5.3}$$

where $y_{(\cdot)}$ with $(\cdot) \in \{aa, bb, cc\}$ denotes the susceptance of the respective phase or with $(\cdot) \in \{ab, ac, ba, bc, ca, cb\}$ denotes the coupling susceptance between two phases.

Analogously $z_{(\cdot)}$ with $(\cdot) \in \{aa, bb, cc\}$ denotes the impedance of the respective phase or with $(\cdot) \in \{ab, ac, ba, bc, ca, cb\}$ denotes the coupling impedances between two phases. The Equations 5.2 and 5.3 can be summarized more briefly as

$$\mathbf{I} = \mathbf{I}_v + \frac{1}{2}\mathbf{Y}\mathbf{U}_v, \tag{5.4}$$

$$\mathbf{U}_u = \mathbf{U}_v + \mathbf{Z}, \tag{5.5}$$

where $\mathbf{I}$, $\mathbf{I}_u$ and $\mathbf{I}_v$ are current vectors in $\mathbb{R}^3$, where $\mathbf{U}_u$ and $\mathbf{U}_v$ are voltage vectors in $\mathbb{R}^3$ and where $\mathbf{Y}$, $\mathbf{Z}$ are the susceptance and impedance matrices in $\mathbb{R}^{(3\times3)}$, respectively. The transformations of the Equations 5.4 and 5.5 to the two-port network model form can be looked up by interested readers in [Ker02, pp.126ff]. For the different entries in $\mathbf{P}$ the reformulation yields:

$$\mathbf{p}_1 = \mathbf{1} + \frac{1}{2}\mathbf{Z}\mathbf{Y} \tag{5.6}$$

$$\mathbf{p}_2 = \mathbf{Z} \tag{5.7}$$

$$\mathbf{p}_3 = \mathbf{Y} + \frac{1}{4}\mathbf{Y}\mathbf{Z}\mathbf{Y} \tag{5.8}$$

$$\mathbf{p}_4 = \mathbf{1} + \frac{1}{2}\mathbf{Z}\mathbf{Y} \tag{5.9}$$

Since we do not want to model capacity effects of the line in this work, the susceptances are all assumed to be zero $\mathbf{Y} = \mathbf{0}$. Substituting this into the Equations 5.6 to 5.9 yields $\mathbf{p}_1 = \mathbf{1}$, $\mathbf{p}_2 = \mathbf{Z}$, $\mathbf{p}_3 = \mathbf{0}$ and $\mathbf{p}_4 = \mathbf{1}$. This is inserted in Equation 5.4 and 5.5 which results in $\mathbf{I}_u = \mathbf{I}_v$ and $\mathbf{U}_u = \mathbf{U}_v + \mathbf{Z}\mathbf{I}_v$.

Additionally, we assume that the network is symmetric [Cra12, p.26][Heu07, p.74]. Then, all impedances except for these on the main diagonal in $\mathbf{Z}$, are zero. The matrix $\mathbf{Z}$ can be rewritten for the symmetric case as follows:

$$\mathbf{Z} = \begin{bmatrix} z_{aa} & 0 & 0 \\ 0 & z_{bb} & 0 \\ 0 & 0 & z_{cc} \end{bmatrix} \tag{5.10}$$

It is obvious, that the three phases can now be regarded independently, since there are no coupling elements left. In [Str17, p.105], it is indicated, that the inductive part of the line segments is negligible small. Therefore, a purely resistive consideration of the line segment is made using the following matrix

$$\mathbf{Z} = \begin{bmatrix} R_{aa} & 0 & 0 \\ 0 & R_{bb} & 0 \\ 0 & 0 & R_{cc} \end{bmatrix} \tag{5.11}$$

for the line equations $\mathbf{I}_u = \mathbf{I}_v$ and $\mathbf{U}_u = \mathbf{U}_v + \mathbf{Z}\mathbf{I}_v$.

The DC resistance R of the line can be found in data sheets or can be determined by $R = \rho\frac{l}{A}$, where ρ denotes the density of the conductor, l its length and A its diameter [Flo05, p.32].

5.2.2 One-Dimensional Flows in Pipelines

This section provides the general differential equations for one-dimensional flows in hydraulic pipelines. In the gas network, the flowing medium is gas, whereas in the heat network, there is water in supply and return. Two basic assumption are made for the general differential equations for flow processes in pipelines [Lur08, p.4]. The first assumption is, that the medium is continuously filling the whole cross-section of the pipeline and the second, that flow parameters are the averaged physical parameters over the pipeline's cross-section. These assumption are necessary to state some differential equations in Section 5.2.2.

Variable	Explanation
α_k	constant depending on flow characteristic
$\alpha(x)$	slope of the pipeline axis to the horizontal $\alpha > 0$: ascending section
ρ	density of the medium
τ_W	shear stress of the pipe walls
d	diameter of the pipeline
e_{in}	internal energy of a unit mass
g	acceleration of gravity
i	hydraulic gradient
dM/dt	mass flow rate
p	pressure
$P(\rho)$	pressure function depending on ρ
q_n	heat flux going through the unit area of the pipeline surface per unit time
S	area of the pipeline's cross-section
t	time
v	(average) velocity in x-direction
x	position
$z(x)$	height of the pipeline axis above sea level

Table 5.2: Overview of the variables and parameters used in the differential equations for one-dimensional flows in pipelines (Equations 5.12, 5.13, 5.14 and 5.17) in Section 5.2.2.

The system of differential equations describing a one-dimensional flow in pipelines is extracted from [Lur08, p.29]. It consists of the continuity equation 5.12, the momentum equation 5.13, an equation for the mechanical energy balance (see Equation 5.14) and an equation for the total energy balance (see Equation 5.17). For one-dimensional flows, the parameters in the aforementioned equations only depend on the coordinate x and the time t. We recommend the first chapter of [Lur08], if there is interest in the explicit and detailed derivation of these equations. All variables and parameters that are used in the Equations 5.12 – 5.17 are listed in Table 5.2.

Continuity equation: The continuity differential equation represents the law of conservation for the transported medium's mass

$$\frac{\partial \rho S}{\partial t} + \frac{\partial \rho v S}{\partial x} = 0, \tag{5.12}$$

where ρ is the density of the medium, v the average velocity and S the area of the pipeline's cross-section. Equation 5.12 can be simplified to $\frac{\partial \rho v S}{\partial x} = 0$, where the mass flow rate $\dot{M}$ is constant along the pipeline [Lur08, p.8], if stationary flows are regarded ($\dot{M} = \rho v S = \text{const.}$). In case of an undeformable pipeline $S(x) = S_0$ with $S_0 = \text{const.}$, the product of density ρ and velocity v is constant, too. Moreover, for homogeneous, incompressible fluids the density of the medium is assumed to be constant [Lur08, p.8]. Consequentially, the

Momentum Equation: The momentum equation 5.13 describes the motion of the fluid according to Newton's second law ($F = ma$) [Lur08, p.9]:

$$\rho \left(\frac{\partial v}{\partial t} + v \frac{\partial v}{\partial x} \right) = -\frac{\partial p}{\partial x} - \frac{4}{d} \tau_W - \rho g \sin(\alpha(x)), \tag{5.13}$$

where τ_W denotes the shear stress of the pipe walls, $\alpha(x)$ for the slope of the pipeline axis to the horizontal and g for the acceleration due to gravity. The expression in brackets on the left side of Equation 5.13 is the total derivate of the velocity $\frac{dv}{dt} = \frac{\partial v}{\partial t} + v \frac{\partial v}{\partial x}$ and describes the particle acceleration [Lur08, p.10]. The product of the particle acceleration with the density of the medium equals to the sum of all forces acting on that medium. This is represented by the term on the right-hand-side, where the first term denotes pressure, the second friction and the latter one gravity forces.

Equation of Mechanical Energy Balance: The equation of mechanical energy balance in Equation 5.14 relates the change in kinetic energy (right-hand-side) to the sum of the work of all external (first term) and internal forces (second term) on fluid particles [Lur08, p.11]:

$$\frac{\partial}{\partial t}\left(\frac{\alpha_k v^2}{2}\right) + v \cdot \frac{\partial}{\partial x}\left(\frac{\alpha_k v^2}{2} + P(\rho) + gz\right) = vg \cdot i, \tag{5.14}$$

where $P(\rho)$ is a pressure function depending on ρ and i is the hydraulic gradient. The constant α_k in Equation 5.14 depends on the flow characteristics of the medium (laminar or turbulent flow) [Lur08, p.12]. It can be calculated using the difference between true velocity u and average velocity v, which is Δu.

$$\alpha_k = 1 + \frac{\overline{(\Delta u)^2}}{v^2} > 1, \tag{5.15}$$

where the term $\overline{(\Delta u)^2}$ denotes the root-mean-square value of Δu. A medium is called barotropic [Lur08, p.13], if the pressure only depends on the density. In case of a stationary flow, the first term in Equation 5.14 is zero. The rest of Equation 5.14 can then be reformulated in integral form yielding the Bernoulli equation for barotropic media [Lur08, p.13]:

$$\left(\frac{\alpha_k v^2}{2} + P(\rho) + gz\right)_{x_1} - \left(\frac{\alpha_k v^2}{2} + P(\rho) + gz\right)_{x_2} = -\int_{x_1}^{x_2} i dx, \tag{5.16}$$

where the medium is transported between the two fixed cross-sections x_1 and x_2.

Equation of Total Energy Balance: The equation of total energy balance is a consequence of the first law of thermodynamics, which makes sure that energy conservation is fulfilled [Lur08, p.22].

$$\frac{\partial}{\partial t}\left[\left(\frac{\alpha_k v^2}{2} + e_{in}\right)\rho S\right] + \frac{\partial}{\partial x}\left[\left(\frac{\alpha_k v^2}{2} + e_{in} + \frac{p}{\rho}\right)\rho v S\right] = \pi d \cdot q_n - \rho v g S \frac{dz}{dx} \tag{5.17}$$

In Equation 5.17, e_{in} denotes the internal energy of a unit mass, q_n is the heat flux going through the unit area of the pipeline's surface per unit time, $z(x)$ denotes the height of the pipeline axis above sea level and d denotes the pipeline's diameter [Lur08, p.23]. The term on the left-hand-side of Equation 5.17 represents the total energy of an arbitrary volume of the transported medium, the first term on the right-hand-side models the external inflow of heat and the second term the work of all external forces.

The four differential Equations 5.12, 5.13, 5.14 and 5.17 contain ten unknown functions $\rho, v, p, S, e_{in}, T, \tau_W, i, q_n$ and α_k. To solve the system of equations, additional relations are needed. These are called *closing relations* and can be obtained by performing a more detailed flow analysis. A list of possible relations is given in [Lur08, p.30]. In this section we presented the detailed differential equations for one-dimensional flows. However, for most calculations in gas and heat networks the approximate equations of the following sections can be used.

5.2.3 Gas Line Model

There are different approximate gas flow equations available that relate input and output pressure with the corresponding flow in between. A list of eleven equations, their limitations and applicability can be found in Chapter 2.2 in [Men05]. Here, only the *general flow equation* will be presented

$$Q = 1.1494 \cdot 10^{-3} \left(\frac{T_b}{P_b}\right) \left[\frac{\left({P_1}^2 - {P_2}^2\right)}{G T_f l Z f}\right]^{0.5} D^{2.5}, \tag{5.18}$$

where Q denotes the gas flow rate, T_b the base temperature, P_b the base pressure, P_1 and P_2 the up- and down stream pressures, G the gas gravity, T_f the average gas flowing temperature, l the length of the pipe segment, Z the gas compressibility factor and f the friction factor. For a better overview, all variables are listed with their SI-units in Table 5.3. The *general flow equation* 5.18 is used for steady-state isothermal flows [Men05, p.33], where *isothermal* means that the gas temperature T_f is assumed to be constant over the pipeline's length.

Variable	Explanation
D	pipe inside diameter, mm
f	friction factor, dimensionless
G	gas gravity, (for air: $G = 1$)
l	pipe segment length, km
P_1	upstream pressure, kPa
P_2	downstream pressure, kPa
P_b	base pressure, kPa
Q	gas flow rate, m^3/day
T_b	base temperature, K
T_f	average gas flowing temperature, K
Z	gas compressibility factor at T_f, dimensionless

Table 5.3: Overview of variables used in the general flow equation 5.18

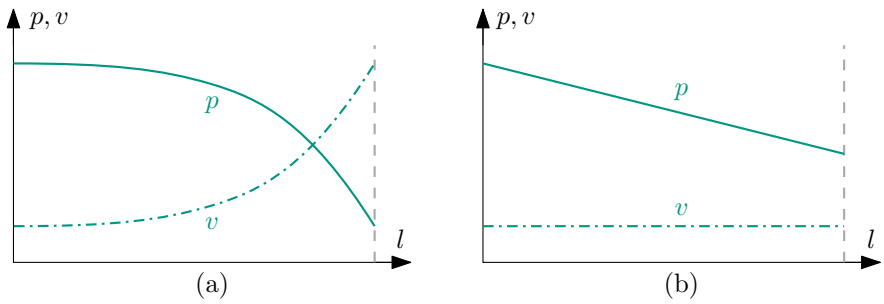

Figure 5.3: Pressure p and velocity v in pipelines of length l in style of [Cer04, p.131]. The graph on the left-hand-side (a) represents the space-varying gas conduction for high- and medium-pressure networks and the graph on the right-hand-side (b) the space constant conduction that applies for low-pressure networks.

Practice-Oriented Modeling

In practice-oriented pressure drop calculations one distinguishes between space varying conduction (case (a) in Figure 5.3) and space constant conduction (case (b) in Figure 5.3). For both cases it generally applies, that the longer the gas pipe, the greater is the pressure drop. Consequently, the density of the gas decreases if the same diameter of the pipe is assumed. Volume flow and the velocity of the flow behave contrary and increase, as it can be seen in Figure 5.3. The difference between (a) and (b) results from the assumption on the compressibility of the medium. On the left-hand-side the gas is assumed to be compressible and on the right-hand-side it is incompressible. The gas density is constant, if latter can be assumed. This holds in practice if the pressure drop is less than 5 % [Cer04, p.131]. For the low-pressure distribution this is generally true [Cer04, p.140] and the pressure drop can be calculated as follows [Cer04, p.148]:

$$\Delta p = R^g l \dot{V}_n^2, \tag{5.19}$$

where Δp denotes the pressure difference between the beginning and the end of the pipe, $\dot{V}$ denotes the volume flow, R^g the resistance and l the length of the pipe. For high- and medium-pressure networks, there is a nonlinear pressure drop

$$p_1^2 - p_2^2 = R^a l \dot{V}_n^2 \tag{5.20}$$

due to the change of density [Cer04, p.148], where p_1 and p_2 are the pressures at the beginning and the end of the pipe, respectively. The model of a gas pipeline for both cases is illustrated in Figure 5.4, where R^{pipe} must be replaced with the so-called R-values R^g or R^a from standard tables, respectively. In practice, the usage of Equation 5.19 delivers sufficient results for pressure drop calculations [Cer04, p.148].

5.2.4 Heat Line Model

Since flowing water can be modeled as incompressible homogeneous fluid [Lur08, p.15], the pressure drop can be calculated according to case (b) in Section 5.2.3 by

$$\Delta p = R^h l \dot{V}_n^2, \tag{5.21}$$

where R^h is the resistance of the heat pipeline. Note that temperature dependencies are already included by choosing a value for R^h from standard tables. The heat pipe model is given in Figure 5.4 by replacing R^{pipe} with R^h.

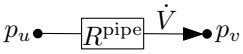

Figure 5.4: Model of a hydraulic pipeline which connects two vertices u and v, where there is a pressure p_u or p_v, respectively. The resistance of the pipeline is denoted by R^{pipe} and the flow by $\dot{V}$. The resistance for gas network lines is $R^{\text{pipe}} = R^g$ and for heat network lines $R^{\text{pipe}} = R^h$.

5.3 Fundamental Mesh

A fundamental mesh is shown in Figure 5.5. It can be used to model the connection of two vertices $u, v \in V_\chi$ with $\chi \in \{el, g, h\}$ of the graph $\mathcal{T}$. For a fundamental mesh, Ohm's law from Equation 4.3 is generalized to

$$f^\chi(u, v) = G^\chi(u, v)(e^\chi(v) - e^\chi(u)), \tag{5.22}$$

where $f^\chi(u, v) \in \mathbb{R}$, $G^\chi(u, v) \in \mathbb{R}_{\geq 0}$, $e^\chi(v) \in \mathbb{R}$ and $e^\chi(u) \in \mathbb{R}$ belong to the same energy carrier $\chi \in \{el,\ g,\ h\}$. For hydraulic networks, the flow $\dot{V}_n^2$ from Equation 5.19 for the gas network and from Equation 5.21 for the heat network, are substituted with the generalized flow $f^\chi(u, v)$. Note that within a mesh, only two of the three

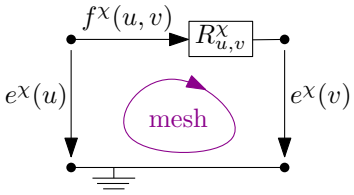

Figure 5.5: Fundamental mesh for an arbitrary energy carrier $\chi \in \{el, g, h\}$ between vertex u and v. The flow from vertex u to vertex v is $f^\chi(u, v)$ and the conductance on the arc (u, v) is given by $G^\chi(u, v)$.

measures can be linearly independent (see Equation 5.22). This will be of importance for the sensor placement problem in Section 5.7. The conductance $G^{\chi}(u,v)$ is defined as the reciprocal of the respective resistances $R^{\chi}(u,v)$,

$$G^{\chi}(u,v) = \begin{cases} 1/R^{el}(u,v), & \text{for electric networks, } \chi = el \\ 1/R^{g}(u,v), & \text{for gas networks, } \chi = g \\ 1/R^{h}(u,v), & \text{for heat networks, } \chi = h, \end{cases} \tag{5.23}$$

where $R^{g}(u,v)$ and $R^{h}(u,v)$ are the R-values of the gas and heat pipelines and $R^{el}(u,v)$ the resistance of the electric conductor. Since we assume that there are no storage effects in the gas and heat network in steady-state operation [Cer04, p.152], Kirchhoff's laws can be applied on hydraulic networks, too:

$$\sum_{u} f^{+} = \sum_{u} f^{-} \qquad \sum_{i,j \in \text{mesh}} (e_i - e_j) = 0 \tag{5.24}$$

The flow balance between the incoming f^{-} and outgoing flows f^{+} at a vertex u is given in the first equation, whereas the second states that the sum of all effort differences $e_i - e_j$ in a mesh is zero.

5.4 Modeling Multi-Energy Carrier Distribution Networks as Directed Graph

The MEDN is modeled as directed graph $\mathcal{T} = (V, A)$, which is composed of a vertex set V and an arc set A. The vertices in V represent substations, network branches or converters, whereas the arcs in A represent their interconnections by pipelines in the hydraulic, or by conductors in the electric networks. We model the graph as directed graph, since flows have a direction, too. However, the flow direction and the direction of the arc do not need to coincide for simplified notation.

Outflows in other network layers as well as conversion losses are modeled as disturbances [Foe13, p.1], since both are hardly predictable and cause a deviation of the states from their nominal values. Disturbances are modeled as flows on arcs $(u,v) \in A$ with $v \in V_T$ leaving vertices $u \in Z$, where Z is the set of vertices with disturbances and V_T is the set of sinks (see Section 5.4.1).

The different carriers will be distinguished by the index $\chi \in \{el, g, h\}$. Thereby, el denotes the electrical, g the gas and h the heat carrier. Although the modeling approach is capable of dealing with an arbitrary number of carrier types, we limit the number of considered carriers in this work to $|\{el, g, h\}| = 3$.

The vertex set V (see Equation 5.25) consists of the subsets $V_\chi \subset V$ for each carrier type χ, a set of converter vertices $V_C \subset V$ and a subset $V_T \subset V$ for the terminals (see Subsection 5.4.1). All subsets of V are necessarily disjoint (see Equation 5.26).

$$V = \{V_\chi, V_C, V_T\} \tag{5.25}$$

$$\emptyset = \bigcap_\chi V_\chi \cap V_C \cap V_T \tag{5.26}$$

The n_V vertices in the subsets V_χ are called *inner vertices* and have an associated generalized effort $e(v) \in \mathbb{R}$ for all $v \in V \setminus \{V_C, V_T\}$. All vertices, except from the terminals, are located within the system boundary. The *system environment* is defined as the area that is beyond the dashed line in Figure 5.6 (system boundary) containing only the terminals. The cardinalities of the different subsets are $|V_\chi| = n_V$, $|V_C| = n_{V_C}$ and $|V_T| = n_{V_T}$. Since the subsets for each carrier type in V_χ are disjoint, Equation 5.27 holds and the number of all vertices can be calculated according to Equation 5.28.

$$n_V = \sum_\chi n_{V,\chi} \tag{5.27}$$

$$|V| = n_V + n_{V_C} + n_{V_T} \tag{5.28}$$

The arc set A is composed of the necessarily disjoint sets $A_\chi = \{A_{el}, A_g, A_h\}$, A_C and A_T, where all edges are directed arbitrarily for simplicity.

$$A = \{A_\chi, A_C, A_T\} \tag{5.29}$$

$$\emptyset = \bigcap_\chi A_\chi \cap A_C \cap A_T \tag{5.30}$$

Arcs $a = (u, v)$ with $u, v \in A_\chi$ only connect vertices of the same carrier type χ. We do not allow that an arc connects vertices of different energy carriers. The coupling between the different energy networks is modeled by arcs $a_1 = (u, v) \in A_C$ and $a_2 = (v, w) \in A_C$ with $u, w \in V_\chi$ and $v \in V_C$, where the arcs a_1, a_2 are incident to a converter vertex v. Arcs $a = (u, v) \in A_T$ with $v \in V_T$ cross the system boundary. The subset A_T can be further divided in arcs $a = (u, v) \in A_{T,s}$ with $u \in V_T$ that connect to sources and in arcs $a = (v, w) \in A_{T,t}$ with $w \in V_T$ that connect to sinks. Every arc $a \in A$ has an associated generalized flow $f : A \to \mathbb{R}$ and each arc $a = (u, v) \in A_\chi$ has an associated conductance $G^\chi(u, v)$ (see Equation 5.23).

$$n_A = \sum_\chi n_{A,\chi} \tag{5.31}$$

$$|A| = n_A + n_{A_C} + n_{A_T} \tag{5.32}$$

The cardinalities of the different subsets are $|A_\chi| = n_A$, $|A_C| = n_{A_C}$ and $|A_T| = n_{A_T}$, respectively. Since the subsets V_χ are disjoint, Equation 5.31 holds and the number of all arcs can be calculated according to Equation 5.32.

The disturbances are modeled as flows $f(u, v) \in \mathbb{R}$ for all $\{(u, v) \in A_\chi | v \in V_T\}$ on an arc $a \in A_T$ leaving a vertex in $Z \subseteq V_\chi$. The number of disturbances is denoted by $|Z| = n_Z$ and depends on the underlying system structure, since a lower bound for n_Z is given by the number of converters n_C (for every converter, there is a disturbance at an incident vertex representing the conversion losses) and the upper bound by the number of vertices n_V (Equation 5.33).

$$0 \leq n_C \leq n_Z \leq n_V \tag{5.33}$$

$$|Z_\chi| = n_{Z,\chi} \leq n_{V,\chi} \tag{5.34}$$

Equation 5.34 ensures that there is only one disturbance at each vertex, as several disturbances at a vertex can not be held apart. For further explanation, we refer the reader to Figure 5.14.

In Figure 5.6, there is an example of a MEDN graph. For a better overview, converters (black rectangles) and transmission grids (shaded rectangles) are still modeled as black boxes. Of course, this is not the final model, since Figure 5.6 only illustrates the degree of abstraction we have reached so far. The different carriers χ can be distinguished by their colors: blue denotes the electricity network, green the gas and red the heat network. The number of vertices for the electric carrier

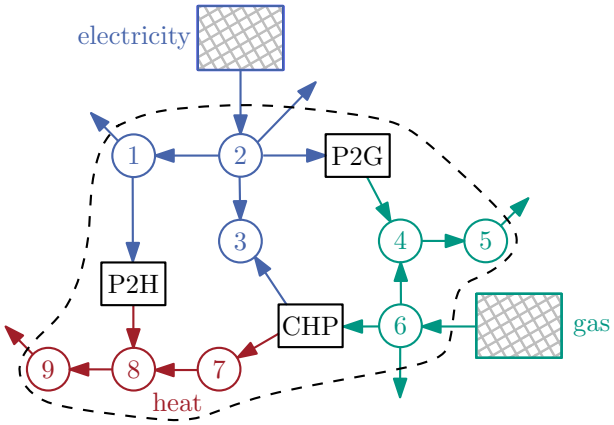

Figure 5.6: Graph with $n_V = 9$ inner vertices representing the multi-carrier distribution network. There are three energy carrier types $\chi \in \{el, g, h\}$, three energy converters (P2G, P2H and CHP), five disturbances and two injections from the gas and electricity transmission grid.

is $n_{V,el} = 3$, $n_{V,g} = 3$ for the gas carrier and $n_{V,h} = 3$ for the heat carrier. According to Equation 5.27, the number of inner vertices is $n_V = 9$. This MEDN has three different converters $n_C = 3$, which are a P2H, a P2G and a CHP unit. The number of arcs in the electric network is $n_{A,el} = 6$, in the gas network $n_{A,g} = 6$ and $n_{A,h} = 4$ in the heat network ($n_A = 16$, $n_{A_T} = 7$, $n_{A_C} = 7$). The arrows pointing into the system environment are the disturbances, of which there are $n_Z = 5$. Next, a closer look is taken on the modeling of terminals for the disturbances and the transmission grid in Subsection 5.4.1 and on the converter modeling in Subsection 5.4.2.

5.4.1 Terminals

In Equation 5.25, the set of terminals $V_T \subset V$ is introduced. It consists of one source vertex $V_{T,s}^{\chi}$ and one sink vertex $V_{T,t}^{\chi}$ for each energy carrier χ. All terminals are located in the system environment. On each arc $a = (u, v)$ with $a \in A_T$ and $u \in V_T$ connecting a source vertex to an inner vertex, a source flow $f_s^{\chi}(a)$ is defined. This source flow models the supply from superior network layers, by power plants or renewable energy sources, whereas sink flows model outflows in other network layers (e.g. energy consumption) or conversion losses. For each arc $a = (u, v)$ with $a \in A_T$ and $v \in V_T$ a sink flow is denoted by $f_t^{\chi}(a)$. The black boxes in Figure 5.6 represented the transportation levels. They can be further abstracted to source vertices, as it is depicted for example in Figure 5.7. The current flow I_e that is entering the vertex v, is modeled as an arc conducting the source flow f_s^{el}. Since the converters are modeled as dummy-vertices (see next Subsection 5.4.2), the conversion losses f_t^{el} are always assigned to the converter's input vertex v. At vertex u there is the outflow f_t^{h} which supplies the local consumers with heat.

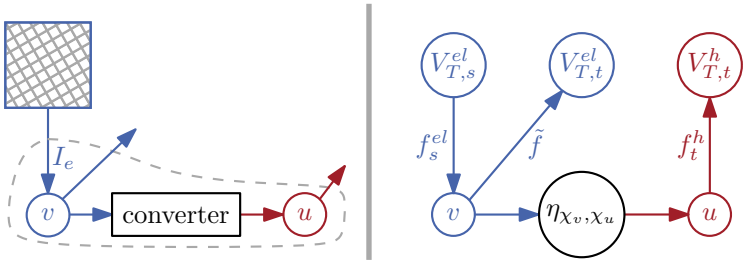

Figure 5.7: Definition of the source vertices $V_{T,s}^{\chi}$ and the sink vertices $V_{T,t}^{\chi}$, illustrated for an arbitrary network with two energy carrier types (electricity and heat), an injection from the electric transmission grid I_e and a converter vertex with an efficiency of η_{χ_v,χ_u}. Here and subsequently $\tilde{f}$ denote any kind of disturbance. In this particular example, $\tilde{f}$ sums up the conversion losses and the load at vertex v.

5.4.2 Modeling of Energy Converters

Energy converters are nonlinear dynamic systems [MSKH16]. They transform energy from one energy carrier χ_u into at least one other energy carrier χ_v and will be split up during the modeling process, if they transform energy into more than one energy network (e.g. combined heat and power in Figure 5.11). For the understanding of the energy converter modeling concept, we first take a look at the schematic diagram of a power flow-based model in Figure 5.8. The outgoing power-flow $P^+_{\chi_v}$ can be calculated by the knowledge of the incoming power flow $P^-_{\chi_u}$ and the unit-less converter efficiency η:

$$P^+_{\chi_v} = \eta \cdot P^-_{\chi_u} \tag{5.35}$$

Since power can be expressed by the product of effort e_χ and flow f_χ, we transform Equation 5.35 to a flow based in- and output description of a converter

$$f^+_{\chi_v} \quad = \quad \eta \cdot \frac{e^-_{\chi_u}}{e^+_{\chi_v}} \cdot f^-_{\chi_u}, \tag{5.36}$$

where we define an "efficiency" η_{χ_u,χ_v}, that has a unit for conversion purposes given by the fraction of the units from the efforts $e^-_{\chi_u}$ and $e^+_{\chi_v}$:

$$\eta_{\chi_u,\chi_v} := \eta \cdot \frac{e^-_{\chi_u}}{e^+_{\chi_v}} \approx \eta \cdot \frac{e^-_{\chi_u,\mathrm{nom}}}{e^+_{\chi_v,\mathrm{nom}}} \tag{5.37}$$

The efforts $e^-_{\chi_u}$ and $e^+_{\chi_v}$ in Equation 5.37 are approximated by their nominal network values $e^-_{\chi_u,\mathrm{nom}}$ and $e^+_{\chi_v,\mathrm{nom}}$. For the electricity grid for example, this value is the nominal system voltage. In general, it would have been possible to strike another path and use

$$e^+_{\chi_v} = \eta \cdot \frac{f^-_{\chi_u}}{f^+_{\chi_v}} \cdot e^-_{\chi_u} \tag{5.38}$$

instead of Equation 5.36. The decision was against the effort based description, as it would lead to two efforts at one vertex.

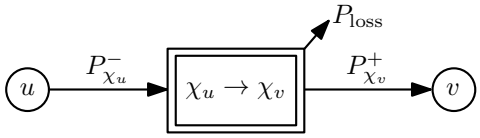

Figure 5.8: Schematic diagram of a nonlinear power flow based model of an energy converter between the vertices u and v transforming from energy carrier χ_u to χ_v. The incoming power flow is denoted by $P^-_{\chi_u}$ and the outgoing power flow by $P^+_{\chi_v}$. The conversion losses are P_{loss}.

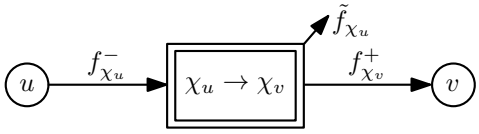

Figure 5.9: Schematic diagram of a nonlinear dynamic model of an energy converter, which transforms energy from χ_u to χ_v. The incoming flow is denoted by $f^-_{\chi_u}$, the outgoing flow by $f^+_{\chi_v}$ and the conversion losses by $\tilde{f}_{\chi_v}$.

The single-carrier-output energy converter scheme (conversion from χ_u to χ_v) is depicted in Figure 5.9. There is a flow $f^-_{\chi_u}$ as input, a flow $f^+_{\chi_v}$ as output; conversion losses are denoted by $\tilde{f}_{\chi_u}$. The MEDN is modeled in steady state operation (see Section 5.2). Hence, the converter are characterized by a nonlinear static system model. Linearization leads to a constant efficiency $\{\eta_{\chi_u,\chi_v} \in \mathbb{R} \mid 0 \leq \eta_{\chi_u,\chi_v} \leq 1\}$ that depends in general on the actual operating point. However, it should be considered to model converters dynamically for future work, as efficiencies depend on the input flow $\eta(f^-_{\chi_u,\chi_v})$.

The converter modeling fulfills the law of energy conservation. This can be seen in Equation 5.39, where the first term denotes the effective share and the latter one the conversion losses.

$$f^-_{\chi_u} = \eta_{\chi_u,\chi_v} \cdot f^-_{\chi_u} + (1 - \eta_{\chi_u,\chi_v}) \cdot f^-_{\chi_u} \tag{5.39}$$

$$\tilde{f}_{\chi_u} = (1 - \eta_{\chi_u,\chi_v}) \cdot f^-_{\chi_u} \tag{5.40}$$

The conversion losses $\tilde{f}_{\chi_u}$ will be joined with the disturbance $\tilde{f}$ at vertex u. The *converter equation* 5.41 will be used in the generalized nodal analysis in Section 5.5 for the coupling of the different networks in the system of equations.

$$f^+_{\chi_v} = \eta_{\chi_u,\chi_v} \cdot f^-_{\chi_u} \tag{5.41}$$

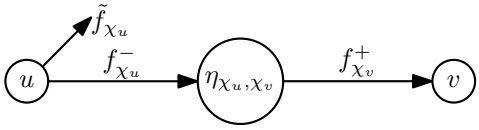

Figure 5.10: Graph representation of the energy converter model: The dummy vertex for the converter's efficiency η_{χ_u,χ_v} is between the vertices u and v. The conversion losses $\tilde{f}_{\chi_u}$ go off from vertex u.

Energy converters, such as CHP units, that transform energy carrier χ_u into two other energy carriers χ_v and χ_w, are modeled in a particular way (see Figure 5.11). The input flow $f^-_{\chi_u}$ is first split up into two new input flows $f^-_{\chi_u,\chi_v}$ and $f^-_{\chi_u,\chi_w}$

$$f^-_{\chi_u} = f^-_{\chi_u,\chi_v} + f^-_{\chi_u,\chi_w}, \tag{5.42}$$

$$\text{split ratio} = \frac{f^-_{\chi_u,\chi_v}}{f^-_{\chi_u,\chi_w}}, \tag{5.43}$$

where the split ratio $\in (0,1)$ will be chosen according to the operating point of the converter. The next steps are entirely analogous to Equation 5.39 from the single-carrier-output energy converter. The two input flows $f^-_{\chi_u,\chi_v}$ and $f^-_{\chi_u,\chi_w}$ are split up again according to their efficiencies η_{χ_u,χ_v} and η_{χ_u,χ_w} to

$$f^-_{\chi_u,\chi_v} = \eta_{\chi_u,\chi_v} \cdot f^-_{\chi_u,\chi_v} + (1-\eta_{\chi_u,\chi_v}) \cdot f^-_{\chi_u,\chi_v} \tag{5.44}$$

$$f^-_{\chi_u,\chi_w} = \eta_{\chi_u,\chi_w} \cdot f^-_{\chi_u,\chi_w} + (1-\eta_{\chi_u,\chi_w}) \cdot f^-_{\chi_u,\chi_w} \tag{5.45}$$

$$\tilde{f}_{\chi_u} = (1-\eta_{\chi_u,\chi_v}) \cdot f^-_{\chi_u,\chi_v} + (1-\eta_{\chi_u,\chi_w}) \cdot f^-_{\chi_u,\chi_w}, \tag{5.46}$$

where Equation 5.46 adds up the energy conversion losses from both single-carrier-output converters to $\tilde{f}_{\chi_u}$. The converter equations 5.47 and 5.48 will be used in the generalized nodal analysis in Section 5.5 to include this type of energy converter as two single-carrier-output converters.

$$f^+_{\chi_v} = \eta_{\chi_u,\chi_v} \cdot f^-_{\chi_u,\chi_v} \tag{5.47}$$

$$f^+_{\chi_w} = \eta_{\chi_u,\chi_w} \cdot f^-_{\chi_u,\chi_w} \tag{5.48}$$

In Figure 5.12 the completed MEDN-graph $\mathcal{T}$ for the example from Figure 5.6 is shown. The legend of colors is the same as before: blue denotes the electricity network, green the gas network and red the heat network. The MEDN-graph $\mathcal{T}$ contains

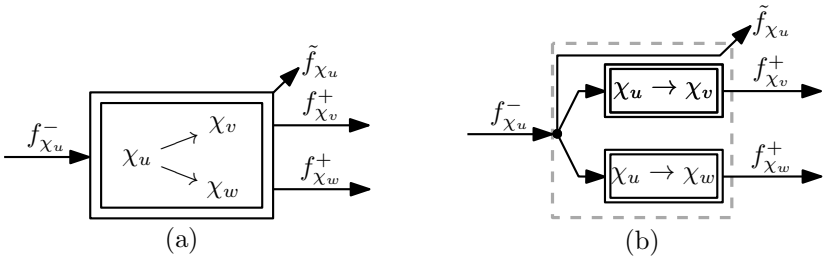

Figure 5.11: Model for energy converters that transform energy from χ_u into two other energy carriers χ_v and χ_w. In (a) the black-box model of a converter with two energy carriers as outputs is shown and (b) the converter model consisting of two single-carrier-output energy converters is depicted.

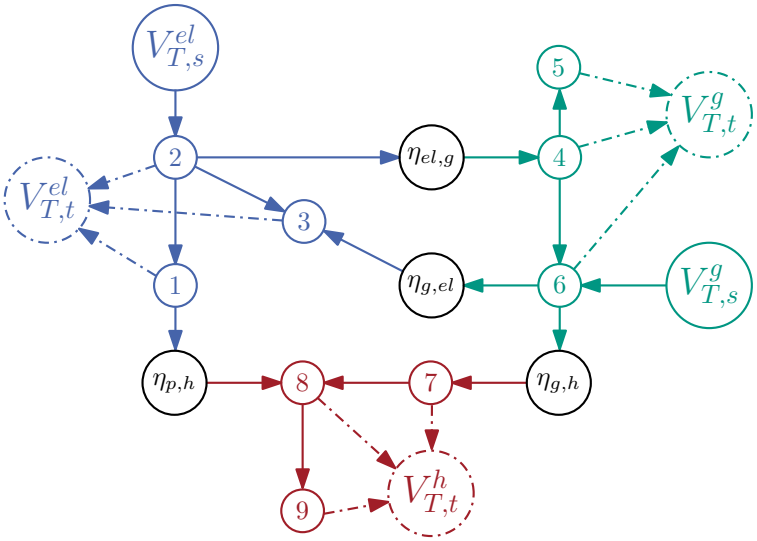

Figure 5.12: Modeling of the exemplary graph from Figure 5.6, where the blue parts denote the electricity network, the green parts the gas network and the red parts the heat network. The converter vertices are drawn in black and contain the respective converter efficiency η_{χ_u,χ_v}.

all source vertices $V^{\chi}_{T,s}$ and sink vertices $V^{\chi}_{T,t}$ as well as the dummy vertices for the converters η_{χ_u,χ_v}. For the sake of clarity, the sink vertices $V^{\chi}_{T,t}$ and the corresponding outflows $f^{\chi}_t(a)$ into the environment are drawn with dash-dotted lines. In the next section, this graph is used to derive a system of equations in the generalized nodal analysis which will be of use for the observability criterion for MEDNs.

5.5 Generalized Nodal Analysis

In this section, the system of equations with disturbances $\mathbf{k} = \mathcal{N}\mathbf{u}$ (see Equation 5.62) describing the MEDN is deployed, where $\mathcal{N}$ is a matrix that denotes the MEDN and $\mathbf{u}$ and $\mathbf{k}$ are vectors that contain the unknown and known generalized variables, respectively. The basic idea behind the generalized nodal analysis (GNA) is illustrated in Equation 5.49.

$$\mathbf{f}^{\chi} = \mathcal{G}^{\chi}\mathbf{e}^{\chi}\ \forall\chi \xrightarrow{\text{coupling}} \mathbf{k} = \mathcal{N}\mathbf{u} \tag{5.49}$$

First, the principles of the nodal analysis from Section 4.3 are applied on each network. Based upon the definition of the conductances G^{χ} in Equation 5.23, conductance matrices $\mathcal{G}^{\chi}$ for each network will be deployed (see Section 5.5.1) so that each

network can be described by a system of equations $\mathbf{f}^\chi = \mathcal{G}^\chi \mathbf{e}^\chi$. Next, the couplings of the different energy carriers are taken into account which results in the system of equations $\mathbf{k} = \mathcal{N}\mathbf{u}$. The following list provides an overview of the procedure of the GNA, which is described in detail in the following subsections.

1. We perform a nodal analysis $\mathbf{f}^\chi = \mathcal{G}^\chi \mathbf{e}^\chi$ for all energy carriers χ in Subsection 5.5.1 and combine the results in a system of equations $\mathbf{f} = \mathcal{G}\mathbf{e}$, where $\mathbf{f}$, $\mathbf{e} \in \mathbb{R}^{n_V}$ and $\mathcal{G} \in \mathbb{R}^{n_V \times n_V}$. An alternative procedure is given too, since it is also possible to deploy the conductance matrix $\mathcal{G}$ directly from the graph $\mathcal{T}$.

2. We rearrange $\mathbf{f} = \mathcal{G}\mathbf{e}$ in Subsection 5.5.2 such that all unknown variables $\mathbf{u}$ are on the right side of the system of equations.

3. In Subsection 5.5.3, we add the converter equations 5.41, 5.47 and 5.48 to the system of equations to obtain $\mathbf{k} = \mathcal{N}\mathbf{u}$.

The previous steps illustrate the procedure of the GNA. Later, it is no longer necessary to perform each step individually. The fastest way is to deploy $\mathcal{G}$ from the graph $\mathcal{T}$ and set up Equation 5.62 directly.

5.5.1 Step 1: Stating the Conductance Matrix

The system of equations $\mathbf{f} = \mathcal{G}\mathbf{e}$ can be stated using the principles of the nodal analysis from Section 4.3 analogically for MEDNs. Let $\mathbf{e} \in \mathbb{R}^{n_V}$ denote the vector which contains the effort of each vertex $v \in V_\chi$ and let $\mathbf{f} \in \mathbb{R}^{n_V}$ denote the vector which assigns all terminal and converter flows to their incident vertices. Then, $\mathbf{f}$ can be calculated by

$$\mathbf{f} = \mathbf{f}_S + \mathbf{f}_Z + \mathbf{f}_C^- + \mathbf{f}_C^+, \tag{5.50}$$

where $\mathbf{f}_S \in \mathbb{R}^{n_V}$ assigns all flows from source vertices to the supplied vertex v_e by

$$\mathbf{f}_S = \left\{ \sum_{\substack{(u,v)\in A^\chi \\ u \in V_T}} f^\chi(u,v) \right\}_{v \in V_\chi}, \tag{5.51}$$

where $\mathbf{f}_Z \in \mathbb{R}^{n_V}$ denotes the flows into the sink vertices (disturbances) leaving each vertex v_e,

$$\mathbf{f}_Z = \left\{ \sum_{\substack{(v,u)\in A^\chi \\ u \in V_T}} f^\chi(v,u) \right\}_{v \in V_\chi} \tag{5.52}$$

and where the converter in- and outflows $\mathbf{f}_C^- \in \mathbb{R}^{n_V}$ and $\mathbf{f}_C^+ \in \mathbb{R}^{n_V}$ can be assigned to the vertices which they enter or leave, respectively.

$$\mathbf{f}_C^- = \left\{ \sum_{\substack{(u,v)\in A^\chi \\ v\in V_C}} f^\chi(u,v) \right\}_{u\in V_\chi}, \quad \mathbf{f}_C^+ = \left\{ \sum_{\substack{(v,w)\in A^\chi \\ v\in V_C}} f^\chi(v,w) \right\}_{w\in V_\chi} \tag{5.53}$$

The conductance matrix $\mathcal{G} \in \mathbb{R}^{(n_V \times n_V)}$ for all energy carriers $\chi \in \{el, g, h\}$ of the MEDN can be stated as

$$\mathcal{G} = \begin{bmatrix} G^\chi_{1,1} & -G^\chi_{1,2} & \cdots & -G^\chi_{1,n_V} \\ -G^\chi_{2,1} & G^\chi_{2,2} & \cdots & -G^\chi_{2,n_V} \\ \vdots & \vdots & \ddots & \vdots \\ -G^\chi_{n_V,1} & -G^\chi_{n_V,2} & \cdots & G^\chi_{n_V,n_V} \end{bmatrix}, \tag{5.54}$$

where the elements on the main diagonal of the symmetric matrix $\mathcal{G}^\chi$ are calculated according to

$$G^\chi_{v,v} = \sum_{u\in V_\chi \setminus \{v\}} G^\chi_{u,v} \qquad \forall v \in V_\chi. \tag{5.55}$$

The matrix $\mathcal{G}$ is of block diagonal form, if the numbering of the vertices is done domain-wise. Therein the different energy carriers are separated according to $\mathbf{f}^\chi = \mathcal{G}^\chi \mathbf{e}^\chi$ for all χ

$$\begin{bmatrix} \mathbf{f}^{el} \\ \mathbf{f}^{g} \\ \mathbf{f}^{h} \end{bmatrix} = \begin{bmatrix} \mathcal{G}^{el} & \mathbf{0} & \mathbf{0} \\ \mathbf{0} & \mathcal{G}^{g} & \mathbf{0} \\ \mathbf{0} & \mathbf{0} & \mathcal{G}^{h} \end{bmatrix} \begin{bmatrix} \mathbf{e}^{el} \\ \mathbf{e}^{g} \\ \mathbf{e}^{h} \end{bmatrix}, \tag{5.56}$$

where $\mathcal{G}^\chi \in \mathbb{R}^{(n_{V,\chi} \times n_{V,\chi})}$ is the conductance matrix of each single-carrier network χ, $\mathbf{e}^\chi$ are the efforts and $\mathbf{f}^\chi$ contains the terminal and converter flows in each network. The advantage of this numbering is obvious for the deployment of large networks by hand. It is easier to set up the smaller matrices $\mathcal{G}^\chi$ first, instead of the more complex matrix $\mathcal{G}$. To obtain this block diagonal form, all inner vertices in the electric network are numbered from 1 to $n_{V,e}$, the inner vertices in the gas network from $n_{V,e}+1$ to $n_{V,e}+n_{V,g}$ and the inner vertices in the heat network from $n_{V,e}+n_{V,g}+1$ to $n_V = n_{V,e}+n_{V,g}+n_{V,h}$.

Derivation of $\mathcal{G}$ from Graph $\mathcal{T}$

The conductance matrix $\mathcal{G} \in \mathbb{R}^{n_V \times n_V}$ for all energy carrier types χ can also be deployed directly by means of a reduced graph $\mathcal{T}^\star := \mathcal{T}_{V\setminus\{V_C,V_T\}}$. This reduced graph $\mathcal{T}^\star$ only contains the inner vertices. We have reduced the MEDN graph $\mathcal{T}$ from the exemplary graph from Figure 5.12 to reduced form, which can be seen in

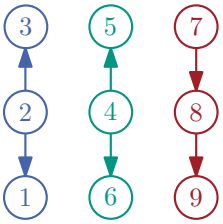

Figure 5.13: Reduced Graph $\mathcal{T}^\star$ from the exemplary graph in Figure 5.12. The reduced graph is not a connected graph anymore. It consists of three connected subgraphs for each energy carrier.

Figure 5.13. For $\mathcal{T}^\star$ the sparse incidence matrix $\mathcal{B}(\mathcal{T}^\star) \in \mathbb{R}^{n_V \times n_A}$ and the sparse incidence conductance matrix $\mathcal{B}_{\text{cond}}(\mathcal{T}^\star) \in \mathbb{R}^{n_A \times n_V}$ can be stated. The incidence matrices containing the conductances $\mathcal{B}_{\text{cond}}(\mathcal{T}^\star)$ can be stated row-by-row, where each row corresponds to an arc $a = (u, v) \in A_\chi$ (arc is pointing from u to v). Write down

$$\begin{cases} G^\chi(u,v), & \text{in column } u \\ -G^\chi(u,v), & \text{in column } v \\ 0, & \text{in every other column} \end{cases} \tag{5.57}$$

for each row of the incidence conductance matrix $\mathcal{B}_{\text{cond}}(\mathcal{T}^\star)$. For the derivation of $\mathcal{T}^\star$ the procedure is analogically done by writing for each row

$$\begin{cases} 1, & \text{in column } u \\ -1, & \text{in column } v \\ 0, & \text{in every other column.} \end{cases} \tag{5.58}$$

The conductance matrix $\mathcal{G}$ can be calculated directly by $\mathcal{G} = \mathcal{B}(\mathcal{T}^\star)^\intercal \mathcal{B}_{\text{cond}}(\mathcal{T}^\star)$.

5.5.2 Step 2: Solving for the Unknown Variables

The system of equations $\mathbf{f} = \mathcal{G}\mathbf{e}$ will now be transformed such that all unknown variables $[\mathbf{e}, \mathbf{f_C}, \tilde{\mathbf{f}}]^\intercal := \mathbf{u} \in \mathbb{R}^{(n_V + 2n_C + n_Z)}$ are on the right and all known variables $\mathbf{f}_S$ are on the left side of the system of equations. This results in

$$\mathbf{f}_S = \begin{bmatrix} \mathcal{G} & \mathbf{c_o} & \mathbf{Z}_{\tilde{\mathbf{f}}} \end{bmatrix} \begin{bmatrix} \mathbf{e} \\ \mathbf{f_C} \\ \tilde{\mathbf{f}} \end{bmatrix}, \tag{5.59}$$

where $\mathbf{c}_o \in \{0, \pm 1\}^{n_V \times 2n_Z}$ is a matrix in which the converter inflows $\mathbf{f}_C^-$ are denoted with a "+1" entry and the converter ouflows $\mathbf{f}_C^+$ with a "−1" entry at the specific row denoting the incident vertex in V_χ. The matrix that allocates the disturbances $\tilde{\mathbf{f}}$ to the vertices, which they are leaving, is denoted by $\mathbf{Z}_{\tilde{f}} \in \{0, -1\}^{n_V \times n_Z}$. The vector $\mathbf{f_C}$ contains the variables for the unknown converter in- and outflows:

$$\mathbf{f_C} = \begin{Bmatrix} f^\chi(u,v) \\ f^\chi(v,w) \end{Bmatrix}_{(u,v)\wedge(v,w)\in A | v \in V_C} \tag{5.60}$$

Note that $\mathbf{f_C} \neq \mathbf{f}_C^+ + \mathbf{f}_C^-$.

5.5.3 Step 3: Adding the Converter Equations

In the last step, the converter equations from Section 5.4.2 are added to the system of equations 5.59. The converter equations 5.41, 5.47 and 5.48 are rearranged for convenience such that the entries of the efficiencies in $\mathcal{N}$ are non-negative.

$$0 = \eta_{\chi_u,\chi_v} \cdot f^-_{\chi_u}(u) - f^+_{\chi_v}(v) \tag{5.61}$$

For every P2G and P2H converter in the MEDN, there is one equation and for every CHP unit, there are two equations added to the system of equations 5.59. The coefficients of the converter flows in Equation 5.61 are η_{χ_u,χ_v} and -1. Both are the only non-zero entries of the matrix $\mathbf{c}_u \in \mathbb{R}^{n_C \times 2n_C}$. This leads to the system of equations describing the MEDN

$$\mathbf{k} = \mathcal{N}\mathbf{u}, \tag{5.62}$$

$$\begin{bmatrix} \mathbf{f}_S \\ \mathbf{0} \end{bmatrix} = \begin{bmatrix} \mathcal{G} & \mathbf{c}_o & \mathbf{Z}_{\tilde{f}} \\ \mathbf{0} & \mathbf{c}_u & \mathbf{0} \end{bmatrix} \begin{bmatrix} \mathbf{e} \\ \mathbf{f}_c \\ \tilde{\mathbf{f}} \end{bmatrix}, \tag{5.63}$$

where $\mathbf{k} \in \mathbb{R}^{(n_V+n_C)}$ is the vector containing all known flows, $\tilde{\mathbf{f}} \in \mathbb{R}^{nz}$ contains the variables for unknown disturbances and $\mathcal{N} \in \mathbb{R}^{(n_V+n_C)\times(n_V+2n_C+n_Z)}$ is the network matrix of the MEDN . The structure of the network matrix $\mathcal{N}$ is shown exemplary by Equation 5.5.3, where the dashed lines separate the different sub-matrices $\mathcal{G}, \mathbf{c}_o, \mathbf{c}_u, \mathbf{Z}_{\tilde{f}}$.

$$\mathcal{N} = \left[\begin{array}{cc|cccc|cccc} & & \vdots & \cdots & \vdots & \cdots & \vdots & \cdots & \vdots \\ & & 0 & \cdots & 0 & \cdots & 0 & \cdots & 0 \\ & & 1 & \cdots & 0 & \cdots & -1 & 0 & 0 \\ & & 0 & \cdots & 0 & \cdots & 0 & \cdots & 0 \\ \mathcal{G} & & \vdots & \cdots & \vdots & \cdots & \vdots & \cdots & \vdots \\ & & 0 & \cdots & 0 & \cdots & 0 & \cdots & 0 \\ & & 0 & \cdots & -1 & \cdots & 0 & 0 & -1 \\ & & 0 & \cdots & 0 & \cdots & 0 & \cdots & 0 \\ & & \vdots & \cdots & \vdots & \cdots & \vdots & \cdots & \vdots \\ \hline & & \eta_{\chi_u,\chi_v} & \cdots & -1 & \cdots & & & \\ \mathbf{0} & & 0 & \cdots & 0 & \cdots & & \mathbf{0} & \\ & & \vdots & \cdots & \vdots & \cdots & & & \end{array}\right] \tag{5.64}$$

The system of equations (5.62) has to be known at the start of the optimization. In each optimization step, Equation 5.62 needs to be adapted according to the measurement structure, that was proposed by the optimizer. To denote the iteration, an index (o) with $o \in \mathbb{N}$ is introduced.

$$\mathbf{k}^{(o)} = \mathcal{N}^{(o)}\mathbf{u}^{(o)} \tag{5.65}$$

In order to obtain the network matrix $\mathcal{N}^{(o)}$, the following two steps are carried out by a *network generation algorithm* (see Algorihtm 4):

1. The column i in $\mathcal{N}$ will be deleted, if an effort e_i is measured.
2. All conductances $G(u, v)$ are replaced by zeros in the conductance matrix $\mathcal{G}$, which is a sub-matrix of $\mathcal{N}$, if a flow on an edge $a = (u, v) \in A_\chi$ is measured.

The pseudo code of the *network generation algorithm* can be found in Appendix B.1.

5.6 Observability for Multi-Carrier Energy Distribution Networks

In the last section, we derived a static network model for MEDNs which will be used as the cornerstone for the following observability criterion 5.1. Unlike dynamic models, static systems have no *memory*. This means, that the system's behavior only depends on the recent input but not additionally on all foregone ones, as it

does for dynamic systems. Thus, the term observability for static network models can be put on the same level as computability (see Section 4.1). The MEDN is observable if and only if it is computable. This leads to the following definition of observability:

Definition 5.1. The multi-carrier energy network $\mathcal{N}$ (MEDN) is said to be observable if all unknown efforts and flows can be calculated only by the knowledge of the graph $\mathcal{T}$, the conductances $\mathcal{G}$, the measurements $\mathcal{M}$ and the input network data $\mathcal{D}$.

The network data $\mathcal{D}$ contains information on converter types, efficiencies and positions in the MEDN (see Table A.1 in Appendix). Consequently, the MEDN is a network $\mathcal{N}$

$$\mathcal{N} = \{\mathcal{T}, \mathcal{G}, \mathcal{M}, \mathcal{D}\}, \tag{5.66}$$

where the inputs are a MEDN graph $\mathcal{T}$, a conductances matrix $\mathcal{G}$, measurements $\mathcal{M}$ ($|\mathcal{M}| = n_M$) and network data $\mathcal{D}$ of the energy converters.

5.6.1 Observability Criterion

For a network $\mathcal{N} = \{\mathcal{T}, \mathcal{G}, \mathcal{M}, \mathcal{D}\}$, where the source flows $\mathbf{f}_S$ are known, we state the following observability criterion, based on network $\mathcal{N}^{(o)} \in \mathbb{R}^{(n_V+n_C)\times(n_V+2n_C+n_Z)}$ in the recent iteration (o):

Criterion 5.1. For observability the n_M measurements must contain:
C1) at least one effort as reference (necessary)
C2) at least $n_Z + n_C$ linear independent measurements (necessary)
C3) $rk(\mathcal{N}^{(o)}) = n_Z + n_C$ (necessary and sufficient)

Note that C1) and C2) are necessary criteria, whereas C3) is necessary and sufficient. Furthermore C2) is a relaxation of C3).

We assume that source flows f_s^χ are known, so that we are able to distinguish source f_s^χ from sink flows f_t^χ at injection vertices, which are vertices that are supplied by source flows f_s^χ. This assumption is evident, since the present monitoring of the different energy networks in Chapter 4 showed, that the supply is monitored for all energy networks. In theory, the source flows f_s^χ could be treated as unknown flows too, as it is done for the sink flows f_t^χ. But, if both flows f_s^χ and f_t^χ at a *injection vertex* are unknown, it is not possible to calculate each. This is a fact, as it is never possible to determine more than one unknown variable by an equation. We illustrate this correlation using the scheme of an injection vertex in Figure 5.14. The reason for the incomputability is the nodal balance at the injection vertex i. The measurements of f_s^χ and f_t^χ are only included in the i-th vertex equation and not in a mesh equation. By a vertex equation, only one unknown variable could be

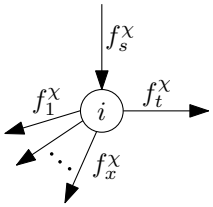

Figure 5.14: Illustration of the nodal balance at an injection vertex, where f_t^χ represent the source flow, f_t^χ is a sink flow and $f_1^\chi, \ldots, f_x^\chi$ on arcs in A_χ are network flows. The energy carrier χ is arbitrary, as this relation holds for each injection vertex connected to a source in every energy network.

determined, either f_s^χ or f_t^χ. It is only possible to solve for the sum of $f_s^\chi + f_t^\chi$, if both are unknown. In comparison to f_s^χ and f_t^χ, the flows $f_1^\chi, \ldots, f_x^\chi$ on arcs in A_χ are included in a vertex and x respective mesh equations. Thus, it is possible to calculate $x + 1$ variables, assuming that all necessary measurements for the mesh equations are available.

5.6.2 Discussion

In general, it is not possible to calculate all efforts in a network by the knowledge of all flows. This can be shown for the matrix $\mathcal{G}$ in Equation 5.54 from the generalized nodal analysis (see Section 5.5) which would then be singular. A proof of this can be found in Appendix B.2. Thus, at least one reference effort for each energy network is needed for observability which is ensured by condition C1) in Criterion 5.1.

	known	unknown		upper and
		im-	measurable	lower bounds
disturbances	0	n_Z	0	$n_C \leq n_Z \leq n_V$
injections	e	0	0	e
converter in-	0	0	p	$p = n_C$
and outflows	0	0	q	$p \leq q \leq 2p$
flows for all $a \in A_\chi$	0	0	n_A	$n_V - 3 \leq n_A \leq 2\binom{n_V}{2}$
efforts for all $v \in V_\chi$	3	0	$n_V - 3$	n_V
Σ	$e + 3$	n_Z	$p + q + n_A + n_V - 3$	

Table 5.4: Overview over the known and unknown variables as it was assumed for the MEDN in this work ($\chi \in \{el, g, h\}$). The number of source flows is e, the number of converter inflows is p and the number of converter outflows is q.

The form of the observability criterion is strongly influenced by the underlying system model. This should be considered in further work. For a new and more precise MEDN system model, a reformulation of the criterion could be needed, if a dynamic coupling of the different energy carriers should be taken into account. With a dynamic MEDN model, it could be possible, that expenses for certain sensors could be saved up, since one can use past values for the state estimation as well.

For reasons of clarity, we have listed all the known and unknown variables of the MEDN in Table 5.4. The upper and lower bounds of the respective variables are given in the rightmost column, if they exist. The boundaries for n_Z were already explained in Section 5.4. There are at least as much converter outflows q as there are converter inflows p, but not more than $2p$, if all converters were CHP units with two outflows. The lower bound on n_A is given by the number of arcs of three radial graphs for each energy network (see Figure 5.13) and the upper bound by the number of arcs in a complete graph (see G.7 in Section 2.5).

5.7 Sensor Placement Problem

In this section, the sensor placement problem is stated as an optimization problem which is a mixed-integer linear program (MILP). The observabiltiy criterion for MEDNs from Section 5.6 is applied in the constraints. It remains to prove that this optimization problem is NP-hard, which is assumed so far. The term optimal sensor placement can also refer to a minimization of the estimation error. However, in this work the optimal sensor placement yields observability at the cheapest costs.

Sensor Types: Two sensor type sets are defined as follows:

- Sensor types at vertices for each carrier χ: $S_{V,\chi}$
- Sensor types on arcs for each carrier χ: $S_{A,\chi}$

It is assumed that a type of sensor belongs to only one energy carrier type, since they are developed for the usage in one network. Anyway, it is possible that they measure more than one quantity (combined sensor). In the set $S_{V,\chi}$ there is a dummy sensor S_{dummy} to model the fixed costs (e.g. telecommunications, installation, ...) using the sensor cost functions below.

Specific Sensor Costs: The sensor cost functions relate every sensor type to their specific costs for a specific energy carrier χ:

$$\mathrm{SSC}_{V,\chi} \quad : \quad S_{V,\chi} \longrightarrow \mathbb{R}_{\geq 0} \tag{5.67}$$

$$\mathrm{SSC}_{A,\chi} \quad : \quad S_{A,\chi} \longrightarrow \mathbb{R}_{\geq 0} \tag{5.68}$$

For Equations 5.67 and 5.68 it is assumed that the specific costs for a sensor type is constant for an energy carrier χ. This means for example, that a pressure sensor for the heat network always costs the same, but a gas pressure sensor can have different costs. The costs for a dummy sensor correspond to the fixed costs $c_{V,\chi,\mathrm{fix}}$, which are different for each energy network.

$$\mathrm{SSC}_{V,\chi}(S_{\mathrm{dummy},\chi}) = c_{V,\chi,\mathrm{fix}} \tag{5.69}$$

In Equation 5.70 it can be seen, that the fix costs $c_{V,\chi,\mathrm{fix}}$ compromise of the costs for telecommunications $c_{V,\chi,\mathrm{tele}}$, the costs for a control cabinet $c_{V,\chi,\mathrm{cab}}$ and the costs for installation $c_{V,\chi,\mathrm{inst}}$ for a specific energy carrier χ.

$$c_{V,\chi,\mathrm{fix}} = c_{V,\chi,\mathrm{tele}} + c_{V,\chi,\mathrm{cab}} + c_{V,\chi,\mathrm{inst}} \tag{5.70}$$

For the objective function in Equation 5.80, the vector $\mathbf{SSC}_{V,\chi}$ and $\mathbf{SSC}_{A,\chi}$ are defined. They contain all specific sensor costs of each energy carrier χ and have the dimension $(|S_{V,\chi}|, 1)$ or $(|S_{A,\chi}|, 1)$, respectively.

$$\mathbf{SSC}_{V,\chi} = \begin{bmatrix} c_{V,\chi,1} \\ \vdots \\ c_{V,\chi,(|S_{V,\chi}|-1)} \\ c_{V,\chi,\mathrm{fix}} \end{bmatrix} \tag{5.71}$$

$$\mathbf{SSC}_{A,\chi} = \begin{bmatrix} c_{A,\chi,1} \\ \vdots \\ c_{A,\chi,|S_{A,\chi}|} \end{bmatrix} \tag{5.72}$$

Here, $c_{V,\chi,1}, \ldots, c_{V,\chi,(|S_{V,\chi}|-1)}$ are the specific sensor costs for each sensor type in $S_{V,\chi}$, $c_{V,\chi,\mathrm{fix}}$ are the costs of the dummy sensor and $c_{A,\chi,1}, \ldots, c_{A,\chi,|S_{A,\chi}|}$ are the specific sensor cost for each sensor type in $S_{A,\chi}$.

Sensor Placement Function: Whether a sensor is placed or not, is a binary decision:

$$\begin{cases} 1, & \text{a sensor is placed} \\ 0, & \text{no sensor is placed} \end{cases} \tag{5.73}$$

Thus, two binary decision-functions μ and ν are introduced. These functions map the set of sensor types and the set of vertices V or the set of arcs A, respectively, to zeros or ones.

- Sensor placement on a vertex belonging to energy carrier χ:

$$\mu : V_\chi \times S_{V,\chi} \longrightarrow \{0,1\} \tag{5.74}$$

- Sensor placement on an arc belonging to energy carrier χ:

$$\nu : A_\chi \times S_{A,\chi} \longrightarrow \{0,1\} \tag{5.75}$$

For the implementation of the objective function in Equation 5.80 the sensor matrices $\mathbf{M}_\chi \in \{0,1\}^{n_{V,\chi} \times |S_{V,\chi}|}$ and $\mathbf{N}_\chi \in \{0,1\}^{n_{A,\chi} \times |S_{A,\chi}|}$ are used. The columns of the sensor matrices denote the sensor type and the rows the vertex number in case of $\mathbf{M}_\chi$, or the arc number in case of $\mathbf{N}_\chi$. The last column is the dummy vertex column. Only if the elements $1, \ldots, (|S_{V,\chi}| - 1)$ in a row are zero, the last element in this row is allowed to be zero, too. This will be considered later on in the telecommunication constraints of the optimization problem.

Sensor Cost Functions: The sensor cost functions return the overall costs for all sensors in one energy network.

$$\mathrm{SCF}_{V,\chi} \colon V_\chi \times S_{V,\chi} \times \mathbb{R}_{\geq 0} \to \mathbb{R}_{\geq 0} \qquad \forall \chi \tag{5.76}$$

$$\mathrm{SCF}_{A,\chi} \colon A_\chi \times S_{A,\chi} \times \mathbb{R}_{\geq 0} \to \mathbb{R}_{\geq 0} \qquad \forall \chi \tag{5.77}$$

The calculation of the sensor costs for each carrier type χ can be done by using the vectors $\mathbf{SSC}_{V,\chi}$ and $\mathbf{SSC}_{A,\chi}$ (see Equation 5.71 and 5.72) as well as the matrices $\mathbf{M}_\chi$ and $\mathbf{N}_\chi$. To get a scalar value as a result, a multiplication with the identity vector $\mathbf{e_1}$ of respective size is needed.

$$\mathrm{SCF}_{V,\chi} = \mathbf{e_1}^\intercal \cdot \mathbf{M}_\chi \cdot \mathbf{SSC}_{V,\chi} \tag{5.78}$$

$$\mathrm{SCF}_{A,\chi} = \mathbf{e_1}^\intercal \cdot \mathbf{N}_\chi \cdot \mathbf{SSC}_{A,\chi} \tag{5.79}$$

Optimization Problem

The objective function for the cost optimal sensor placement is given in Equation 5.80. Therein, the sensor cost functions for each energy carrier are summed up to the total sensor costs. This objective minimizes the total costs by the variation of the optimization variables μ and ν.

$$\underset{\mu,\nu}{\text{minimize}} \quad J = \sum_{\forall \chi} \left(\text{SCF}_{V,\chi} + \text{SCF}_{A,\chi} \right) \quad \text{w.r.t.} \tag{5.80}$$

- Telecommunication constraints:

  A1) At least one of the incident vertices needs a dummy sensor $s_{d,\chi} \in S_{V,\chi}$, if a flow on an arc $a = (u, v) \in A_\chi$ is measured by $s_a \in S_{A,\chi}$: if $\nu(a, s_a) = 1$ then $\mu(u, s_{d,\chi}) = 1 \vee \mu(v, s_{d,\chi}) = 1$.

  A2) A vertex $u \in V_\chi$ needs a dummy sensor $s_{d,\chi} \in S_{V,\chi}$, if there is a measurement $s_u \in S_{V,\chi}$ at vertex u: if $\mu(u, s_u) = 1$ then $\mu(u, s_{d,\chi}) = 1$.

- Avoidance of redundant measurements:

  B1) For all $a = (u, v) \in A_\chi$ there are only two independent measurements in a fundamental mesh: $\nu(a, s_a) + \mu(u, s_u) + \mu(v, s_v) \leq 2$, where $s_a \in S_{A,\chi}$ and $s_u, s_v \in S_{V,\chi}$ denote arbitrary sensors.

  B2) For all arcs $a_1, a_2 \in A_C$ only one flow $f^-_{\chi_u}(u)$ or $f^+_{\chi_v}(v)$ at a converter needs to be measured by $s_{a1}, s_{a2} \in S_{A,\chi}$, since they linearly depend on each other: $\nu(a_1, s_{a_1}) + \nu(a_2, s_{a_2}) \leq 1$.

- $\mathcal{N}$ is observable:

  C1) At least one effort in each domain needs to be measured as reference, else the matrix $\mathcal{N}$ would be singular:
  $\sum_{s \in S_{V,el}} \sum_{u \in V_{el}} \mu(u, s) \geq 1$, $\sum_{s \in S_{V,g}} \sum_{v \in V_g} \mu(v, s) \geq 1$ and $\sum_{s \in S_{V,h}} \sum_{w \in V_h} \mu(w, s) \geq 1$

  C2) At least $n_Z + n_C$ linear independent measurements are necessary:
  $\sum_{u \in V_\chi} \sum_{s \in S_V} \mu(u, s) + \sum_{a \in A} \sum_{s \in S_A} \nu(a, s) \geq n_Z + n_C$

  C3) Matrix $\mathcal{N}$ needs a full rank $\text{rk}(\mathcal{N}^{(\mathbf{o})}) = n_Z + n_C$ for observability. Then, the system of equations 5.62 is invertible for the unknown variables $\mathbf{u}$.

With this sensor placement problem formulation two different optimization tasks can be treated, where the following key question can be asked:

- How can the existing sensors and telecommunications be completed reasonably?
- How would be the greenfield approach if there were no initial sensors given?

In the next chapter, the modeling approach is performed on an academic example (see Section 6.2) and on a greenfield approach for a real network of Karlsruhe (see Section 6.3).

Chapter 6

Case Studies

In this chapter, we present the implementation of the sensor placement optimization problem from Section 5.7, which is first illustrated for an academic minimal example in Section 6.2 and then for a case study of a subnetwork of Karlsruhe (Germany) in Section 6.3. We describe the problems that have arisen during the implementation of the rank constraint and how they were solved. At the end of this chapter, a closer look is taken on the complexity of the problem and the optimization results will be discussed.

6.1 Implementation of the Optimization Problem

The sensor placement optimization problem (see Section 5.7) for a given network was implemented in `C++` for Microsoft Visual Studio and Gurobi. Gurobi is one of the most powerful commercial optimization solvers with a free academical license, which can handle linear (LP), quadratic (QP), quadratically constrained (QCP), mixed integer linear (MILP), mixed integer quadratic (MIQP) and mixed integer quadratically constrained programs (MIQCP). Gurobi does not only support `C++`, but also other modeling languages like `C`, MATLAB, Java and Python.

An advantage of Gurobi is the possibility to use precast software elements such as a variety of constraint types. In the following, we will present the constraints that we have used for the implementation, which are linear, indicator and lazy constraints. Subsequently, we show how the Gurobi model is initialized and how the constraints are added to the model in the pseudo-code of the Algorithm 1.

Linear Constraints: Linear constraints are restrictions on the objective function, which can be illustrated as n-dimensional straight lines

$$\mathbf{a}^\intercal \mathbf{x} \leq b, \tag{6.1}$$

where n is the size of the vectors, $\mathbf{x} \in \mathbb{R}^n$ contains the optimization variables, $\mathbf{a} \in \mathbb{R}^n$ the corresponding coefficients and $b \in \mathbb{R}$ the upper bound for the weighted sum of all optimization variables. The sensor placement problem has four different types of constraints that are modeled as linear constraints (see Section 5.7). We avoid linear dependent measurements at converters and in fundamental meshes by the Constraints B1) and B2). Moreover, the necessary constraints for observability, Constraint C1) for the reference and Constraint C2) for the number of measurements, are linear constraints, too. The linear Constraint C2) is added to the model in row 7 of Algorithm 1.

Indicator Constraints: An indicator constraint is an if-then condition. A linear constraint like the one in Equation 6.1 must be true, if the binary indicator variable y is assigned a binary variable $f \in \{0, 1\}$.

$$y = f \longrightarrow \mathbf{a}^\intercal \mathbf{x} \leq b \tag{6.2}$$

It is left to the programmer whether the constraint should be active if the indicator variable is set to zero or one. In this work, we used the indicator constraints for the telecommunication Constraints A1) and A2) from Section 5.7, where the indicator variable is the binary variable from the sensor placement on vertices or edges, respectively. The indicator variable is set to true, if an effort or flow is measured. Then, the activated linear constraint ensures the placement of telecommunications. The Constraint A2) is added to the model in row 5 of Algorithm 1.

With the two aforementioned constraint types, all sensor placement constraints can be modeled, with the exception of the rank Constraint C3). For the rank constraint there is no explicit method available yet, that adds them to the model. Thus, a solution was worked out that uses lazy constraints and a solver callback.

Algorithm 1: Initialization of the Gurobi model. The indicator constraint A2) and the linear constraint C2) are added to the model.

Input: Network $\mathcal{N}$, specific sensor costs $\mathbf{SSC}_{V,\chi}$ and $\mathbf{SSC}_{A,\chi}$
Output: Gurobi model model with constraints

```
1 env = new GRBEnv();                    /* initialization of the Gurobi environment */
2 GRBModel model = GRBModel(*env);  /* create the Gurobi optimization model */
3 ...
  // Constraint A2):  if sensor at i ∈ V_χ then place a dummy sensor s_{d,χ}(i)
4 for int i = 0; i < n_V; i++ do
5   model.addGenConstrIndicator(μ(i) == 1, true, ..., s_{d,χ}(i) == 1);
6 ...
  // Constraint C2):  Number of measurements
7 model.addConstr(Σ_{i∈V_χ} μ(i) + Σ_{(u,v)∈A_χ} ν(u,v) ≥ n_Z + n_C, "Measurements");
```

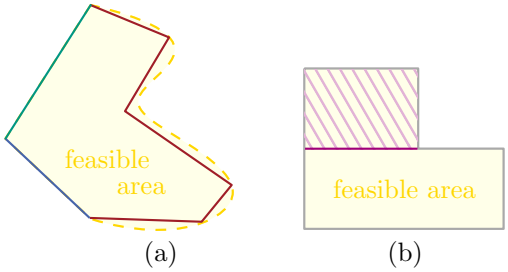

Figure 6.1: Lazy constraints (a) vs. user cuts (b): In the picture on the left (a), the boundary of the gold-dashed feasible area is approximated by a set of lazy constraints (red lines). The picture on the right (b) shows how another feasible area is restricted by a user cut (purple horizontal line), which cuts off the hatched area.

Lazy Constraints and the Solver Callback: Lazy Constraints are linear constraints (see Equation 6.1) that are added to the model during the optimization. Unlike user cuts, they do not restrict the set of all constraints, but instead extend an incomplete set of constraints until the feasible area has been completely or approximately set [IBM]. The difference between user cuts and lazy constraints is depicted in Figure 6.1. On the left-hand side, the linear constraints in green and blue do not capture the whole feasible area. By adding the lazy constraints (red lines) an approximation of the feasible area is given. On the right side, the boundary of the feasible area is known. The user's cut further restricts the hatched area by an additional constraint (purple line).

Lazy constraints are used if the set of constraints is not known at the beginning of the optimization or if the set of constraints is too large to state it in advance. Lazy constraints are usually added to a model within a solver callback. Such a *solver callback* is a method that enables the programmer to modify the set of constraints during the optimization process. This is done for example in the sub-tour elimination of the traveling salesman problem, where it is not possible to forbid all sub-tours at the beginning of the optimization. The unwanted sub-tours are banned during optimization by lazy constraints of the form:

$$\sum_{\substack{i,j \in S \\ i \neq j}} b_{ij} \leq |S| - 1, \quad \forall S \subset V,\ S \neq \emptyset, \tag{6.3}$$

where S denotes the set of cities visited in the sub-tour, which is a subset of all cities V and b_{ij} denotes the binary decision whether to take a route between the cities i and j. For example in Figure 6.2(a), the lazy constraint in Equation 6.3 will ensure that in the next iteration only $|4| - 1 = 3$ out of 4 cities from a sub-tour are visited in a row.

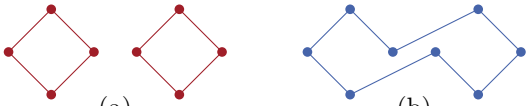

(a) (b)

Figure 6.2: Sub-tour elimination for the traveling salesman problem: On the left side (a), there is a solution with two sub-tours, where the traveled distance is shorter than the traveled distance of the correct solution (b).

The analogy to our problem is that we want to ban all non-observable sensor placements, since we are not able to state the rank constraint C3) from Section 5.7 directly in Gurobi. This can be done by

$$\sum_{i \in \mathcal{B}} |b_i - b_i^\star| \neq 0, \tag{6.4}$$

where $b_i^\star$ denotes the i-th binary optimization variable from the non-observable sensor placement, b_i the i-th binary optimization variable and $\mathcal{B}$ the set of all binary optimization variables. The power set of $\mathcal{B}$ corresponds to the set of all possible sensor placements, including both feasible and infeasible solutions. Equation 6.4 ensures that the non-observable sensor placement cannot be a feasible solution for the reduced optimization problem anymore, because the difference summed up for all binaries would then equal zero. The constraint in Equation 6.4 must be reformulated to the standard form for the implementation in Gurobi, which is done in the following:

$$1 \leq \sum_{i \in \mathcal{B}:\, b_i^\star = 0} b_i + \sum_{i \in \mathcal{B}:\, b_i^\star = 1} (1 - b_i) \tag{6.5}$$

$$1 \leq \sum_{i \in \mathcal{B}:\, b_i^\star = 0} b_i - \sum_{i \in \mathcal{B}:\, b_i^\star = 1} b_i + \sum_{i \in \mathcal{B}:\, b_i^\star = 1} 1. \tag{6.6}$$

Here, the absolute value of the difference between b_i and $b_i^\star$ was dissolved first. The last sum over all ones in Equation 6.6 denotes the number of measurements n_M. Inserting n_M for the sum leads to

$$\sum_{i \in \mathcal{B}:\, b_i^\star = 1} b_i - \sum_{i \in \mathcal{B}:\, b_i^\star = 0} b_i \leq n_M - 1, \tag{6.7}$$

where the first term denotes the sum of all binary variables for sensors that are set by the optimizer and the second term denotes the sum of all binary variables for sensors that are not set, respectively. The difference of both sums must be less than or equal to the number of measurements minus one.

Algorithm 2: Pseudo-code of the callback class definition: the callback method checks whether a solution is feasible with respect to the rank constraint and adds a lazy constraint, if the solution is infeasible.

Input: Network $\mathcal{N}$, $\mathbf{M}$ and $\mathbf{N}$ in the current iteration (o), conductance matrix $\mathcal{G}$, number of variables v in the vector of unkowns $\mathbf{u}$ and the network size n_V
Output: Gurobi model model with lazy constraints

```
1 class INFEASIBLE_RANK_ELIMINATION: public GRBCALLBACK
2 ...
3 protected:
4 CALLBACK
  // check for solution:
5 if where == GRB_CB_MIPSOL then
      // determine N^(o) and check rank (see Algortihm 4):
6     obsv = NETWORK_GENERATION_ALGORTIHM (N^(o), M,N, G, v, u, n_V);
7     if obsv == 0 then
          // forbid non-observable sensor placement:
8         addLazy (sum_{i∈B: b_i^⋆=1} b_i − sum_{i∈B: b_i^⋆=0} b_i ≤ n_M − 1)
```

In a first step of the implementation, we define a kind class of Gurobi's abstract solver callback class `GRBCallback`, which is show in Algorithm 2. By checking, if the value of the protected variable `where` equals `GRB_CB_MIPSOL`, it can be figured out whether the solver has found a solution for the reduced optimization problem without the rank constraint. In case it has found a solution, the callback method calls the network generation algorithm (see Algorithm 4), which determines the network matrix for the current iteration $\mathcal{N}^{(o)}$ and checks its rank. The matrix is not of full rank, if the sensor placement from the recent iteration is non-observable. Thus, the network generation algorithm returns one, for observable sensor placements and zero for non-observable ones. For latter, the lazy constraint is added to the model using the rearranged form from Equation 6.7.

6.2 Academic Example

The first exemplary network in Figure 6.3 is of academic character, since it only has six vertices, a combined heat and power converter and three energy carrier types. The vertices 1 and 2 belong to the gas, 3 and 6 to the electric and 4 and 5 to the heat domain. There are three disturbances at the inner vertices 2, 3 and 4. The combined heat and power converter is fed by vertex 2 and is modeled as two single energy carrier output converters as described in Section 5.4.2. The respective in- ($f^g_{2,3}$ and $f^g_{2,4}$) and outflows ($f^{el}_{2,3}$ and $f^h_{2,4}$) of the converters are described by the

converter Equations 5.47 and 5.48, which yields

$$f^{el}_{2,3} = \eta_{G2P} \cdot f^{g}_{2,3} \tag{6.8}$$
$$f^{h}_{2,4} = \eta_{G2H} \cdot f^{g}_{2,4}, \tag{6.9}$$

where η_{G2P} and η_{G2H} are the efficiencies of the combined heat and power unit for the gas-to-power (G2P) and gas-to-heat (G2H) part. In the following, we will show how the system of equations $\mathbf{f} = \mathcal{G}\mathbf{e}$ can be derived. Usually, this procedure is abbreviated as described in Section 5.5. The first step will be the set up of the nodal and mesh equations from the network in Figure 6.3. Next, the mesh equations are used to replace the flows within the network in the nodal equations. After this, the converter equations are added to the system of equations, which is then rearranged to the form $\mathbf{k} = \mathcal{N}\mathbf{u}$. First, we state the nodal equations in the order of their nodal numbering from vertex 1 to vertex 6:

$$0 = f^{g}_{S,1} - f^{g}_{1,2} \tag{6.10}$$
$$0 = f^{g}_{1,2} - f^{g}_{2,4} - f^{g}_{2,3} - \tilde{f}^{g}_{2,t} \tag{6.11}$$
$$0 = f^{el}_{2,3} - f^{el}_{3,6} - \tilde{f}^{el}_{3,t} \tag{6.12}$$
$$0 = f^{h}_{2,4} - f^{h}_{4,5} - \tilde{f}^{h}_{4,t} \tag{6.13}$$
$$0 = f^{h}_{4,5} + f^{h}_{S,5} \tag{6.14}$$
$$0 = f^{el}_{3,6} + f^{el}_{S,6}, \tag{6.15}$$

where $f^{el}_{S,6}$, $f^{g}_{S,1}$ and $f^{h}_{S,5}$ denote the source flows, $\tilde{f}^{g}_{2,t}$, $\tilde{f}^{el}_{3,t}$ and $\tilde{f}^{h}_{4,t}$ denote the disturbances and $f^{g}_{1,2}$, $f^{el}_{3,6}$ and $f^{h}_{4,5}$ are the remaining flows within the network.

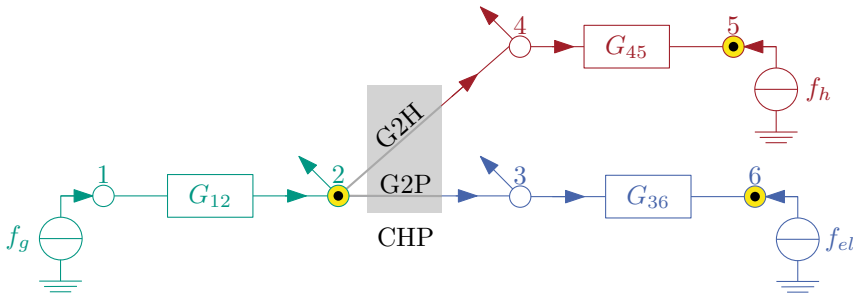

Figure 6.3: Exemplary network of academic character with two vertices for each energy carrier. There is a CHP unit between the vertices 2, 3 and 4 modeled as two single energy carrier output converters G2P and G2H. There are three disturbances at the vertices 2, 3 and 4. The optimizer proposed to place effort measurements at the yellow filled vertices and dummy sensors for telecommunication at vertices that are marked with a black dot.

There are three fundamental meshes in the network which can be described by:

$$(e_2^g - e_1^g) \cdot G_{1,2}^g = f_{1,2}^g \tag{6.16}$$
$$(e_6^{el} - e_3^{el}) \cdot G_{3,6}^{el} = f_{3,6}^{el} \tag{6.17}$$
$$(e_5^h - e_4^h) \cdot G_{4,5}^h = f_{4,5}^h, \tag{6.18}$$

where e_1^g, e_2^g, e_3^{el}, e_4^h, e_5^h and e_6^{el} are the efforts at the respective vertex and $G_{1,2}^g$, $G_{3,6}^{el}$ and $G_{4,5}^h$ are the conductances that are associated to the arc that connects the vertices in a mesh.

The first mesh Equation 6.16 includes the vertices 1 and 2, the second mesh Equation 6.17 the vertices 3 and 6 and the third mesh Equation 6.18 the vertices 4 and 5. By replacing the flows $f_{1,2}^g$, $f_{3,6}^{el}$ and $f_{4,5}^h$ of the nodal equations by the mesh equations and rearranging for the left-over flows, the following system of equations can be stated:

$$\begin{bmatrix} -f_{S,1}^g \\ \tilde{f}_{2,t}^g \\ \tilde{f}_{3,t}^{el} \\ \tilde{f}_{4,t}^h \\ -f_{S,5}^h \\ -f_{S,6}^{el} \end{bmatrix} = \begin{bmatrix} G_{1,2}^g & -G_{1,2}^g & 0 & 0 & 0 & 0 \\ -G_{1,2}^g & G_{1,2}^g & 0 & 0 & 0 & 0 \\ 0 & 0 & G_{3,6}^{el} & 0 & 0 & -G_{3,6}^{el} \\ 0 & 0 & 0 & G_{4,5}^h & -G_{4,5}^h & 0 \\ 0 & 0 & 0 & -G_{4,5}^h & G_{4,5}^h & 0 \\ 0 & 0 & -G_{3,6}^{el} & 0 & 0 & G_{3,6}^{el} \end{bmatrix} \begin{bmatrix} e_1^g \\ e_2^g \\ e_3^{el} \\ e_4^h \\ e_5^h \\ e_6^{el} \end{bmatrix} \tag{6.19}$$

Here, the first vector is denoted by $\mathbf{f}$, the matrix by $\mathcal{G}$ and the vector on the right by $\mathbf{e}$. In a next step, the converter equations 5.47 and 5.48 are added to the system of equations 6.19. This increases the number of equations for the thirteen unknown variables e_1^g, e_2^g, e_3^{el}, e_4^h, e_5^h, e_6^{el}, $f_{2,3}^g$, $f_{2,4}^g$, $f_{2,3}^{el}$, $f_{2,4}^h$, $\tilde{f}_{2,t}^g$, $\tilde{f}_{3,t}^{el}$, $\tilde{f}_{4,t}^h$ to eight. The unknown variables can be written in the vector $\mathbf{u}$ when Equation 6.19 is reformulated to $\mathbf{k} = \mathcal{N}\mathbf{u}$. The resulting system of equations can be looked up in Figure A.1 in Appendix A.1.

The model was solved with the values given in the Listing in Appendix A.1. Since we do not have a list of the sensor costs for different networks, we have worked with fictitious prices, which only reflect the ratio of the prizes among each other. The fixed costs for the telecommunications were assumed to be ten times higher than the costs of the respective flow or effort sensors. The efficiencies of the converter parts η_{G2P} and η_{G2H} were roughly estimated in the range of usual values. Visual Studio solved this optimization problem very fast in less than 5 seconds. The Gurobi solver proposed an observable placement of three effort sensors at the vertices 2, 5 and 6 as well as three dummy sensors for telecommunication at the vertices 2, 5 and 6, which results in overall costs of 33. In Figure 6.3, the effort sensor positions are marked yellow and telecommunication is indicated by black dots.

6.3 Subnetwork of Karlsruhe

The *netzservice Stadtwerke Karlsruhe* has provided network plans of a subnetwork of Karlsruhe. We modeled a street in the suburb, called Waldstadt (see Figure 4.4 for city map) in which there is a gas-fired heat and power plant (see yellow area on the left side of Figure 6.4; geographical coordinates: 49° 02′ 29.8″N 8° 27′ 01.5″E). This plant was modeled by a G2P and a G2H converter. Additionally, two more conceptional converters, a P2G and P2H converter, were assumed in the yellow area on the right hand side of Figure 6.4. For the derivation of the graph from the network plans, we have assigned vertices at all major branches in the gas and heat network respectively and in the electric network, every substation of the 20 kV-ring is modeled by a vertex. The network interfaces with the environment were modeled as terminal vertices and are given as non-filled circles in Figure 6.4. Overall, there are $n_{V,el} = 5$ vertices in the electric network of the graph (blue), $n_{V,g} = 13$ vertices in the gas network of the graph (green) , $n_{V,h} = 14$ vertices in the heat network of the graph (red), $n_C = 4$ converters and $n_Z = 19$ vertices with disturbances. In order to find the assignment of the disturbances to the individual vertices, the reader is referred to the matrix $\mathbf{Z}_{\tilde{f}}$ in Figure A.4 in Appendix A. Due to the complexity of the subnetwork,

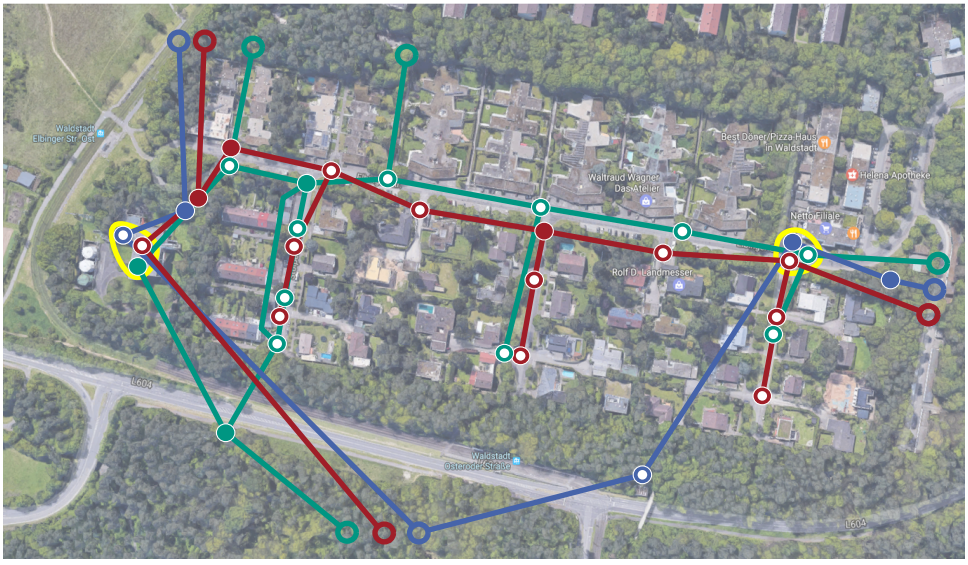

Figure 6.4: Map and graph of the MEDN subnetwork of Karlsruhe, where the blue parts of the graph denote the electric network ($n_{V,el} = 5$), the green ones the gas network ($n_{V,g} = 13$) and the red ones the heat network ($n_{V,h} = 14$). There are four converters ($n_C = 4$), two in each of the yellow areas. The white dots indicate the locations of effort measurements and telecommunication proposed by the solver.

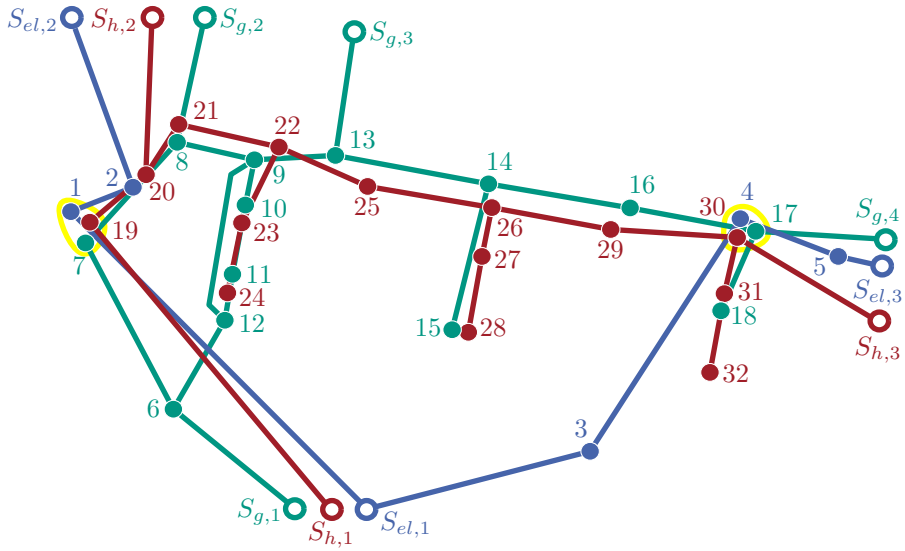

Figure 6.5: Numbering of the vertices for the MEDN graph from Figure 6.4, where the terminal vertices are denoted by $S_{\chi,<\text{number}>}$ with $\chi \in \{el, g, h\}$.

the derivation of the system of equations 5.62 cannot be illustrated here, since the dimension of the network matrix $\mathcal{N}$ is $(32+4) \times (32+2 \cdot 4+19) = 36 \times 59$. However, all sub-matrices of $\mathcal{N}$ and their values are given in Appendix A. These are the values for the optimization in Listing A.2, the matrices $\mathcal{G}_{el}$, $\mathcal{G}_g$ and $\mathcal{G}_h$ in Figure A.2 as well as c_o and c_u in Figure A.3. The vertex numbering of the graph is shown in Figure 6.5. The row numbers of c_o and $Z_{\tilde{f}}$ refer to the vertex number. This is also valid for the matrix $\mathcal{G}$ if $\mathcal{G}_{el}$, $\mathcal{G}_g$ and $\mathcal{G}_h$ from Figure A.2 are set up according to Equation 5.56.

Algorithm 3: Optimization result for the subnetwork of Karlsruhe using the given values from Listing B.2

Input: Network $\mathcal{N}$, specific sensor costs $\mathbf{SSC}_{V,\chi}$ and $\mathbf{SSC}_{A,\chi}$
Output: Gurobi model `model` with lazy constraints

```
// feasible sensor placement (network is observable)
// effort measurements at the following vertices:
1 1 + 3 + 8 + 10 + 11 + 12 + 13 + 14 + 15 + 16 + 17 + 18 + 19 + 22 + 23 + 24 +
  25 + 27 + 28 + 29 + 30 + 31 + 32
// necessary telecommunications at the following vertices:
2 1 + 3 + 8 + 10 + 11 + 12 + 13 + 14 + 15 + 16 + 17 + 18 + 19 + 22 + 23 + 24 +
  25 + 27 + 28 + 29 + 30 + 31 + 32
// overall sensor costs:
3 253
```

The Gurobi solver found the first feasible solution within 15 minutes (see Algorithm 3). It cannot be guaranteed that it is the optimal solution, because the optimization problem is non-convex. We stopped the solver after fourteen hours, as there has no better solution been found. Since there are no flow measurements, the locations of the dummy sensors for telecommunications are at the vertices with effort measurements (see rows 1 and 2 in Algorithm 3 or white dots in Figure 6.4).

6.4 Discussion

First of all, it needs to be mentioned that the implementation of the sensor placement does not solve the system of Equations 5.62 for the unknown variables. Thus, it is likely that it saves computation time in comparison to approaches were all states are calculated.

It can be seen in the optimization results of the exemplary networks, that the solver tends to place only effort measurements. The reason for this is due to the generalized nodal analysis procedure, where the network flows are only included indirectly in the network matrix $\mathcal{N}$ via the entries of the respective conductances. Since a flow is defined on an arc $a = (u, v)$ that always connects two vertices, we have for each flow exactly four entries $\pm G_{u,v}$ in the matrix $\mathcal{N}$. The entries are removed (see Algorithm 4), if a flow is known, which means that it is measured. For lightly meshed networks the zero entries often lead to zero rows in the system of equations. Both considered networks in this thesis where lightly meshed which can be seen by looking at the graph structure of the MEDN in Figure A.5. We recommend to examine a strongly meshed network as the next example.

Complexity of the Problem: The rank Constraint C3) from Section 5.7 on the network matrix $\mathcal{N}^{(o)}$ is assumed to be non-convex and therefore we assume that it is generally NP-hard to solve the sensor placement problem (similar to the problem in [SGS11, p.1]). Since the rank constraint is necessary and sufficient for observability, the other observability Constraints C1) and C2) as well as the Constraints B1) and B2) that forbid independent measurements, could be left out of the set of constraints. This is only reasonable if the used solver (unlike Gurobi) is able to deal with the rank constraint. We decided to add these necessary constraints to relax the rank constraint and help the solver to find a fast solution, which is then checked for observability.

The task to choose n_M sensor positions in the MEDN is basically a problem of combinatorial analysis called *variation without repetition*. If n_M sensors have to be located on $n_V + n_A$ possible sensor positions, the number of possible combinations is

$$\binom{n_V + n_A}{n_M} = \frac{(n_V + n_A)!}{(n_V + n_A - n_M)!}, \tag{6.20}$$

where so far, it has not been considered that there are different types of sensors. The possibility to place n different types of sensors at a vertex would increase the number of possibilities by the potency n.

In the first academic experiment, there were $n_V = 6$ nodes and $n_A = 7$ arcs. With Equation 6.20 this results in 1716 possible combinations. To check every sensor placements for the network's observability would be possible, but very costly regarding the computational effort. For larger networks like the subnetwork of Karlsruhe with $n_V = 32$ nodes and $n_A = 39$ edges, where $n_M = n_Z + n_C = 19 + 4$ sensors should be placed, this results in

$$\binom{32 + 39}{23} = 6.8 \cdot 10^{40} \text{ (68 duodecillion)} \tag{6.21}$$

possible sensor placements. It can easily be seen that for large networks the check of all possible sensor placements for observability is an impossible task as it is to state all non-observable sensor placements before the optimization. Thus, the usage of lazy constraints is justified.

Chapter 7

Conclusion

In this thesis, the sensor placement problem for multi-carrier energy distribution networks (MEDNs) has been developed as an economic optimization problem, which guarantees observability. The solution to an instance of the problem determines sensor types and locations in the network so that it is observable at minimal cost. A multi-carrier perspective was pursued, since it is advantageous to take into account synergies for energy storage or decentralized generation.

First, an approach for a graph-theoretical modeling of MEDNs was presented. In the directed MEDN-graph, there were different subsets of vertices and arcs for the respective energy carrier or converter type. For this graph, the generalized nodal analysis, which yields a closed mathematical representation of the network in form of a system of equations, was derived. Using this system of equations the observability criterion for MEDNs was defined. A MEDN is said to be observable if the unknown network states can be calculated, only with the values of certain measurements. This criterion was embedded as a rank constraint in the sensor placement problem next to the constraints for the placement of telecommunications. The optimization problem is a mixed-integer linear program which minimizes the overall sensor costs in the network. Since the rank constraint is assumed to be convex, the problem is supposed to be NP-hard.

The sensor placement problem was implemented in C++ for Microsoft Visual Studio and Gurobi. First, the modeling approach was shown for a small academic example of six vertices. Then, the sensor placement problem was solved for a subnetwork of Karlsruhe (Germany) with 32 vertices and four converters. In both cases, the optimization quickly found cost-effective sensor placements which ensured the observability of the network.

An advantage of the formulation of the sensor placement problem is, that it could be also used for future MEDN modeling approaches that propose other observability criteria. We stated the possibility to include different sensor types and sensors from various manufacturers in the optimization process. For future work, we suggest

adding minimization of the estimation error to the objective function of the sensor placement problem, so that there is a trade-off between choosing a cheap sensor and a sensor with low noise.

Other possible extensions of the objective should be investigated as well. For example, rank maximization of the network matrix could be part of the objective without stating the required number of measurements as a constraint. Then the different parts of the multi-criteria objective could be weighted in such a way that the reliability of the sensor placement is guaranteed. For networks with sensor redundancy, it should be investigated whether the removal of a sensor leads to two emerging sub-networks that are still observable.

In addition, a list of the specific sensor costs should be requested from the network operator so that the optimization can use more realistic values. Until now, it is not considered that there could be a cost reduction for the telecommunications if network vertices representing different energy carriers are located at the same spot. Furthermore, the dynamic processes of subsystems like P2G, P2H or CHP units should be examined carefully, so that more precise energy converter models could be added to the MEDN modeling approach. For this, the converter efficiencies need to be treated non-constant.

Further work should be done about the algorithmic examination of the optimization model. It should be proved that the problem is NP-hard and that the rank constraint is non-convex. For faster and more efficient algorithms the focus could lay on finding a convex approximation of the rank constraint. Algorithmic analogies from the simultaneous feedback vertex set [ALMS15], column generation for large integer-problems [BJN$^+$98], rank-constrained semi-definite programs [Nal16, Dat05, Sec. 4.5] and the multi-commodity problem could be of interest for this.

Appendix A

Data

The MEDN was defined as network $\mathcal{N} = \{\mathcal{T}, \mathcal{G}, \mathcal{M}, \mathcal{D}\}$ in Section 5.6. The network data $\mathcal{D}$ can be implemented as a list which contains the positions of the converters in the MEDN, information on converter types (energy carrier type at in- and output) and the respective efficiencies.

incident vertices			energy carrier at			efficiencies		split ratio
input	outputs		input	outputs		$\eta_{u,v}$	$\eta_{u,w}$	(Eq. 5.43)
$u \in V_\chi$	$v \in V_\chi$	$w \in V_\chi$	χ_u	χ_v	χ_w	$[0,1]$	$[0,1]$	$(0,1)$
$\vdots$	$\vdots$	$\vdots$	$\vdots$	$\vdots$	$\vdots$	$\vdots$	$\vdots$	$\vdots$

Table A.1: Implementation of the network data $\mathcal{D}$ as list.

A.1 Academic Example

```
// specific sensor costs for measuring efforts in the
int const SSC_e_el = 1; // electric,
int const SSC_e_g = 1;  // gas and
int const SSC_e_h = 1;  // heat network
// specific sensor costs for measuring flows in the
int const SSC_f_el = 1; // electric,
int const SSC_f_g = 1;  // gas and
int const SSC_f_h = 1;  // heat network
// fixed costs for telecommunication in the
int const fix_el = 10;  // electric,
int const fix_g = 10;   // gas and
int const fix_h = 10;   // heat network

const int n_V_el = 2;  // number of vertices in the electric,
const int n_V_g = 2;   // gas and
const int n_V_h = 2;   // heat network
const int n_Z = 3;     // number of disturbances
const int n_V = n_V_el + n_V_g + n_V_h; // number of inner vertices
const int n_C = 2;     // the combined heat and power converter
    accounts for two converters, since it is modeled by two single
    energy carrier output converters.

const double eta_G2P = 0.5;  // efficiency of the gas-2-power part
const double eta_G2H = 0.9;  // efficiency of the gas-2-heat part

// arbitrary values for conductances > 0
const int G_el = 10; // conductance for electric lines
const int G_g = 20;  // conductance for gas pipelines
const int G_h = 50;  // conductance for heat pipelines
```

Listing A.1: Variables and their values which were used in the academic example from Section 6.2.

A.2 Subnetwork of Karlsruhe

```
// specific sensor costs for measuring efforts in the
int const SSC_e_el = 1; // electric,
int const SSC_e_g = 1;  // gas and
int const SSC_e_h = 1;  // heat network
// specific sensor costs for measuring flows in the
int const SSC_f_el = 1; // electric,
int const SSC_f_g = 1;  // gas and
int const SSC_f_h = 1;  // heat network
// fixed costs for telecommunication in the
int const fix_el = 10;  // electric,
int const fix_g = 10;   // gas and
int const fix_h = 10;   // heat network

const int n_V_el = 5;  // number of vertices in the electric,
const int n_V_g = 13;   // gas and
const int n_V_h = 14;   // heat network
const int n_Z = 19;     // number of disturbances
const int n_V = n_V_el + n_V_g + n_V_h; // number of inner vertices
const int n_C = 4;      // the gas-fired heat and power plant accounts
    for two converters, since it is modeled by two single energy
    carrier output converters.

const double eta_G2P = 0.5;  // efficiency of the gas-2-power converter
const double eta_G2H = 0.9;  // efficiency of the gas-2-heat converter
const double eta_P2H = 0.95; // efficiency of the power-2-heat
    converter
const double eta_P2G = 0.4;  // efficiency of the power-2-gas converter

// arbitrary values for conductances > 0
const int G_el = 10; // conductance for electric conductors
const int G_g = 20;  // conductance for gas pipelines
const int G_h = 50;  // conductance for heat pipelines
```

Listing A.2: Variables and their values which were used for the optimization of the sensor placement in the subnetwork of Karlsruhe from Section 6.3.

$$
\begin{bmatrix} -f^g_{S,1} \\ 0 \\ 0 \\ 0 \\ -f^h_{S,5} \\ -f^{el}_{S,6} \\ 0 \\ 0 \end{bmatrix} =
\begin{bmatrix}
\mathcal{G}^g_{1,2} & -\mathcal{G}^g_{1,2} & 0 & 0 & 0 & 0 & 0 & 0 & 0 & 0 & 0 & 0 & 0 \\
-\mathcal{G}^g_{1,2} & \mathcal{G}^g_{1,2} & 0 & 0 & 0 & 0 & 0 & 1 & 0 & 1 & -1 & 0 & 0 \\
0 & 0 & \mathcal{G}^{el}_{3,6} & 0 & 0 & -\mathcal{G}^{el}_{3,6} & -1 & 0 & 0 & 0 & 0 & -1 & 0 \\
0 & 0 & 0 & \mathcal{G}^h_{4,5} & -\mathcal{G}^h_{4,5} & 0 & 0 & 0 & -1 & 0 & 0 & 0 & -1 \\
0 & 0 & 0 & -\mathcal{G}^h_{4,5} & \mathcal{G}^h_{4,5} & 0 & 0 & 0 & 0 & 0 & 0 & 0 & 0 \\
0 & 0 & -\mathcal{G}^{el}_{3,6} & 0 & 0 & \mathcal{G}^{el}_{3,6} & 0 & 0 & 0 & 0 & 0 & 0 & 0 \\
0 & 0 & 0 & 0 & 0 & 0 & -1 & \eta_{G2P} & 0 & 0 & 0 & 0 & 0 \\
0 & 0 & 0 & 0 & 0 & 0 & 0 & 0 & -1 & \eta_{G2H} & 0 & 0 & 0
\end{bmatrix}
\begin{bmatrix} e^g_1 \\ e^g_2 \\ e^{el}_3 \\ e^h_4 \\ e^h_5 \\ e^{el}_6 \\ f^{el}_{2,3} \\ f^g_{2,3} \\ f^h_{2,4} \\ f^g_{2,4} \\ \tilde{f}^g_{2,t} \\ \tilde{f}^{el}_{3,t} \\ \tilde{f}^h_{4,t} \end{bmatrix}
$$

Figure A.1: System of equations $\mathbf{k} = \mathcal{N}\mathbf{u}$ for the academic example with six vertices and a CHP unit (see Section 6.2).

$$
\mathbf{G}_{el} = \begin{bmatrix}
G_{1,2} & -G_{1,2} & 0 & 0 & 0 \\
-G_{1,2} & G_{1,2} & 0 & 0 & 0 \\
0 & 0 & G_{3,4} & -G_{3,4} & 0 \\
0 & 0 & -G_{3,4} & G_{3,4}+G_{4,5} & -G_{4,5} \\
0 & 0 & 0 & -G_{4,5} & G_{4,5}
\end{bmatrix}
$$

$$
\mathbf{G}_g = \begin{bmatrix}
G_{6,12}+G_{6,7} & -G_{6,7} & 0 & 0 & 0 & 0 & 0 & 0 & -G_{6,12} & 0 & 0 & 0 & 0 & 0 & 0 & 0 \\
-G_{6,7} & G_{6,7}+G_{7,8} & -G_{7,8} & 0 & 0 & 0 & 0 & 0 & 0 & 0 & 0 & 0 & 0 & 0 & 0 & 0 \\
0 & -G_{7,8} & G_{7,8}+G_{8,9} & -G_{8,9} & 0 & 0 & 0 & 0 & 0 & 0 & 0 & 0 & 0 & 0 & 0 & 0 \\
0 & 0 & -G_{8,9} & G_{8,9}+G_{9,12}+G_{9,10}+G_{9,13} & -G_{9,10} & 0 & 0 & 0 & 0 & -G_{9,13} & 0 & 0 & 0 & 0 & 0 & 0 \\
0 & 0 & 0 & -G_{9,10} & G_{9,10}+G_{10,11} & -G_{10,11} & 0 & 0 & -G_{9,12} & 0 & 0 & 0 & 0 & 0 & 0 & 0 \\
0 & 0 & 0 & 0 & -G_{10,11} & G_{10,11}+G_{11,12} & -G_{11,12} & 0 & 0 & 0 & 0 & 0 & 0 & 0 & 0 & 0 \\
-G_{6,12} & 0 & 0 & -G_{9,12} & 0 & -G_{11,12} & G_{11,12}+G_{6,12}+G_{9,12} & 0 & 0 & G_{9,13}+G_{13,14} & 0 & 0 & 0 & 0 & 0 & 0 \\
0 & 0 & 0 & -G_{9,13} & 0 & 0 & 0 & 0 & 0 & -G_{13,14} & 0 & 0 & 0 & 0 & 0 & 0 \\
0 & 0 & 0 & 0 & 0 & 0 & 0 & 0 & 0 & 0 & G_{13,14}+G_{14,15}+G_{14,16} & -G_{14,15} & -G_{14,16} & 0 & 0 & 0 \\
0 & 0 & 0 & 0 & 0 & 0 & 0 & 0 & 0 & 0 & -G_{14,15} & G_{14,15} & 0 & -G_{16,17} & 0 & 0 \\
0 & 0 & 0 & 0 & 0 & 0 & 0 & 0 & 0 & 0 & -G_{14,16} & 0 & G_{14,16}+G_{16,17} & -G_{16,17} & -G_{17,18} & -G_{17,18} \\
0 & 0 & 0 & 0 & 0 & 0 & 0 & 0 & 0 & 0 & 0 & 0 & -G_{16,17} & G_{16,17}+G_{17,18} & -G_{17,18} & G_{17,18}
\end{bmatrix}
$$

$$
\mathbf{G}_h = \begin{bmatrix}
G_{19,20} & -G_{19,20} & 0 & 0 & 0 & 0 & 0 & 0 & 0 & 0 & 0 & 0 & 0 & 0 & 0 & 0 \\
-G_{19,20} & G_{19,20}+G_{20,21} & -G_{20,21} & 0 & 0 & 0 & 0 & 0 & 0 & 0 & 0 & 0 & 0 & 0 & 0 & 0 \\
0 & -G_{20,21} & G_{20,21}+G_{21,22} & -G_{21,22} & 0 & 0 & 0 & 0 & 0 & 0 & 0 & 0 & 0 & 0 & 0 & 0 \\
0 & 0 & -G_{21,22} & G_{21,22}+G_{22,23}+G_{22,25} & -G_{22,23} & 0 & -G_{22,25} & 0 & 0 & 0 & 0 & 0 & 0 & 0 & 0 & 0 \\
0 & 0 & 0 & -G_{22,23} & G_{22,23}+G_{23,24} & -G_{23,24} & 0 & 0 & 0 & 0 & 0 & 0 & 0 & 0 & 0 & 0 \\
0 & 0 & 0 & 0 & -G_{23,24} & G_{23,24} & 0 & 0 & 0 & 0 & 0 & 0 & 0 & 0 & 0 & 0 \\
0 & 0 & 0 & -G_{22,25} & 0 & 0 & G_{22,25}+G_{25,26} & -G_{25,26} & 0 & 0 & 0 & 0 & 0 & 0 & 0 & 0 \\
0 & 0 & 0 & 0 & 0 & 0 & -G_{25,26} & G_{25,26}+G_{26,27}+G_{26,29} & -G_{26,27} & 0 & 0 & 0 & 0 & 0 & 0 & 0 \\
0 & 0 & 0 & 0 & 0 & 0 & 0 & -G_{26,27} & G_{26,27}+G_{27,28} & -G_{27,28} & 0 & 0 & 0 & 0 & 0 & 0 \\
0 & 0 & 0 & 0 & 0 & 0 & 0 & 0 & -G_{27,28} & G_{27,28} & 0 & 0 & 0 & 0 & 0 & 0 \\
0 & 0 & 0 & 0 & 0 & 0 & 0 & -G_{26,29} & 0 & 0 & G_{26,29}+G_{29,30} & -G_{29,30} & 0 & 0 & 0 & 0 \\
0 & 0 & 0 & 0 & 0 & 0 & 0 & 0 & 0 & 0 & -G_{29,30} & G_{29,30}+G_{30,31} & -G_{30,31} & 0 & 0 & 0 \\
0 & 0 & 0 & 0 & 0 & 0 & 0 & 0 & 0 & 0 & 0 & -G_{30,31} & G_{30,31}+G_{31,32} & -G_{31,32} & -G_{31,32} & 0 \\
0 & 0 & 0 & 0 & 0 & 0 & 0 & 0 & 0 & 0 & 0 & 0 & -G_{31,32} & G_{31,32} & G_{31,32} & 0
\end{bmatrix}
$$

Figure A.2: Conductance matrices $\mathcal{G}_{el}$, $\mathcal{G}_g$ and $\mathcal{G}_h$ for the subnetwork of Karlsruhe from Section 6.3.

$$\mathbf{c}_o = \begin{bmatrix}
0 & -1 & 0 & 0 & 0 & 0 & 0 & 0 \\
0 & 0 & 0 & 0 & 0 & 0 & 0 & 0 \\
0 & 0 & 0 & 0 & 0 & 0 & 0 & 0 \\
0 & 0 & 0 & 0 & 0 & 0 & 0 & 0 \\
0 & 0 & 0 & 0 & -1 & 0 & -1 & 0 \\
0 & 0 & 0 & 0 & 0 & 0 & 0 & 0 \\
-1 & 0 & -1 & 0 & 0 & 0 & 0 & 0 \\
0 & 0 & 0 & 0 & 0 & 0 & 0 & 0 \\
0 & 0 & 0 & 0 & 0 & 0 & 0 & 0 \\
0 & 0 & 0 & 0 & 0 & 0 & 0 & 0 \\
0 & 0 & 0 & 0 & 0 & 0 & 0 & 0 \\
0 & 0 & 0 & 0 & 0 & 0 & 0 & 0 \\
0 & 0 & 0 & 0 & 0 & 0 & 0 & 0 \\
0 & 0 & 0 & 0 & 0 & 0 & 0 & 0 \\
0 & 0 & 0 & 0 & 0 & 0 & 0 & 0 \\
0 & 0 & 0 & 0 & 0 & 0 & 0 & 0 \\
0 & 0 & 0 & 0 & 0 & 0 & 0 & -1 \\
0 & 0 & 0 & 0 & 0 & 0 & 0 & 0 \\
0 & 0 & 0 & -1 & 0 & 0 & 0 & 0 \\
0 & 0 & 0 & 0 & 0 & 0 & 0 & 0 \\
0 & 0 & 0 & 0 & 0 & 0 & 0 & 0 \\
0 & 0 & 0 & 0 & 0 & 0 & 0 & 0 \\
0 & 0 & 0 & 0 & 0 & 0 & 0 & 0 \\
0 & 0 & 0 & 0 & 0 & 0 & 0 & 0 \\
0 & 0 & 0 & 0 & 0 & 0 & 0 & 0 \\
0 & 0 & 0 & 0 & 0 & 0 & 0 & 0 \\
0 & 0 & 0 & 0 & 0 & 0 & 0 & 0 \\
0 & 0 & 0 & 0 & 0 & 0 & 0 & 0 \\
0 & 0 & 0 & 0 & 0 & 0 & 0 & 0 \\
0 & 0 & 0 & 0 & 0 & -1 & 0 & 0 \\
0 & 0 & 0 & 0 & 0 & 0 & 0 & 0 \\
0 & 0 & 0 & 0 & 0 & 0 & 0 & 0
\end{bmatrix}$$

$$\mathbf{c}_u = \begin{bmatrix}
\eta_{G2P} & -1 & 0 & 0 & 0 & 0 & 0 & 0 \\
0 & 0 & \eta_{G2H} & -1 & 0 & 0 & 0 & 0 \\
0 & 0 & 0 & 0 & \eta_{P2H} & -1 & 0 & 0 \\
0 & 0 & 0 & 0 & 0 & 0 & \eta_{P2G} & -1
\end{bmatrix}$$

Figure A.3: Converter matrices c_o and c_u for the subnetwork of Karlsruhe from Section 6.3.

$$
\mathbf{Z}_{\tilde{f}} = \begin{bmatrix}
0 & 0 & 0 & 0 & 0 & 0 & 0 & 0 & 0 & 0 & 0 & 0 & 0 & 0 & 0 & 0 & 0 & 0 & 0 \\
0 & 0 & 0 & 0 & 0 & 0 & 0 & 0 & 0 & 0 & 0 & 0 & 0 & 0 & 0 & 0 & 0 & 0 & 0 \\
0 & 0 & 0 & 0 & 0 & 0 & 0 & 0 & 0 & 0 & 0 & 0 & 0 & 0 & 0 & 0 & 0 & 0 & 0 \\
-1 & 0 & 0 & 0 & 0 & 0 & 0 & 0 & 0 & 0 & 0 & 0 & 0 & 0 & 0 & 0 & 0 & 0 & 0 \\
0 & 0 & 0 & 0 & 0 & 0 & 0 & 0 & 0 & 0 & 0 & 0 & 0 & 0 & 0 & 0 & 0 & 0 & 0 \\
0 & 0 & 0 & 0 & 0 & 0 & 0 & 0 & 0 & 0 & 0 & 0 & 0 & 0 & 0 & 0 & 0 & 0 & 0 \\
0 & -1 & 0 & 0 & 0 & 0 & 0 & 0 & 0 & 0 & 0 & 0 & 0 & 0 & 0 & 0 & 0 & 0 & 0 \\
0 & 0 & 0 & 0 & 0 & 0 & 0 & 0 & 0 & 0 & 0 & 0 & 0 & 0 & 0 & 0 & 0 & 0 & 0 \\
0 & 0 & -1 & 0 & 0 & 0 & 0 & 0 & 0 & 0 & 0 & 0 & 0 & 0 & 0 & 0 & 0 & 0 & 0 \\
0 & 0 & 0 & -1 & 0 & 0 & 0 & 0 & 0 & 0 & 0 & 0 & 0 & 0 & 0 & 0 & 0 & 0 & 0 \\
0 & 0 & 0 & 0 & -1 & 0 & 0 & 0 & 0 & 0 & 0 & 0 & 0 & 0 & 0 & 0 & 0 & 0 & 0 \\
0 & 0 & 0 & 0 & 0 & -1 & 0 & 0 & 0 & 0 & 0 & 0 & 0 & 0 & 0 & 0 & 0 & 0 & 0 \\
0 & 0 & 0 & 0 & 0 & 0 & 0 & 0 & 0 & 0 & 0 & 0 & 0 & 0 & 0 & 0 & 0 & 0 & 0 \\
0 & 0 & 0 & 0 & 0 & 0 & -1 & 0 & 0 & 0 & 0 & 0 & 0 & 0 & 0 & 0 & 0 & 0 & 0 \\
0 & 0 & 0 & 0 & 0 & 0 & 0 & -1 & 0 & 0 & 0 & 0 & 0 & 0 & 0 & 0 & 0 & 0 & 0 \\
0 & 0 & 0 & 0 & 0 & 0 & 0 & 0 & -1 & 0 & 0 & 0 & 0 & 0 & 0 & 0 & 0 & 0 & 0 \\
0 & 0 & 0 & 0 & 0 & 0 & 0 & 0 & 0 & 0 & 0 & 0 & 0 & 0 & 0 & 0 & 0 & 0 & 0 \\
0 & 0 & 0 & 0 & 0 & 0 & 0 & 0 & 0 & -1 & 0 & 0 & 0 & 0 & 0 & 0 & 0 & 0 & 0 \\
0 & 0 & 0 & 0 & 0 & 0 & 0 & 0 & 0 & 0 & 0 & 0 & 0 & 0 & 0 & 0 & 0 & 0 & 0 \\
0 & 0 & 0 & 0 & 0 & 0 & 0 & 0 & 0 & 0 & 0 & 0 & 0 & 0 & 0 & 0 & 0 & 0 & 0 \\
0 & 0 & 0 & 0 & 0 & 0 & 0 & 0 & 0 & 0 & 0 & 0 & 0 & 0 & 0 & 0 & 0 & 0 & 0 \\
0 & 0 & 0 & 0 & 0 & 0 & 0 & 0 & 0 & 0 & -1 & 0 & 0 & 0 & 0 & 0 & 0 & 0 & 0 \\
0 & 0 & 0 & 0 & 0 & 0 & 0 & 0 & 0 & 0 & 0 & -1 & 0 & 0 & 0 & 0 & 0 & 0 & 0 \\
0 & 0 & 0 & 0 & 0 & 0 & 0 & 0 & 0 & 0 & 0 & 0 & -1 & 0 & 0 & 0 & 0 & 0 & 0 \\
0 & 0 & 0 & 0 & 0 & 0 & 0 & 0 & 0 & 0 & 0 & 0 & 0 & -1 & 0 & 0 & 0 & 0 & 0 \\
0 & 0 & 0 & 0 & 0 & 0 & 0 & 0 & 0 & 0 & 0 & 0 & 0 & 0 & 0 & 0 & 0 & 0 & 0 \\
0 & 0 & 0 & 0 & 0 & 0 & 0 & 0 & 0 & 0 & 0 & 0 & 0 & 0 & -1 & 0 & 0 & 0 & 0 \\
0 & 0 & 0 & 0 & 0 & 0 & 0 & 0 & 0 & 0 & 0 & 0 & 0 & 0 & 0 & -1 & 0 & 0 & 0 \\
0 & 0 & 0 & 0 & 0 & 0 & 0 & 0 & 0 & 0 & 0 & 0 & 0 & 0 & 0 & 0 & -1 & 0 & 0 \\
0 & 0 & 0 & 0 & 0 & 0 & 0 & 0 & 0 & 0 & 0 & 0 & 0 & 0 & 0 & 0 & 0 & 0 & 0 \\
0 & 0 & 0 & 0 & 0 & 0 & 0 & 0 & 0 & 0 & 0 & 0 & 0 & 0 & 0 & 0 & 0 & -1 & 0 \\
0 & 0 & 0 & 0 & 0 & 0 & 0 & 0 & 0 & 0 & 0 & 0 & 0 & 0 & 0 & 0 & 0 & 0 & -1
\end{bmatrix}
$$

Figure A.4: Matrix for the location of disturbances to the respective vertices for the subnetwork of Karlsruhe from Section 6.3.

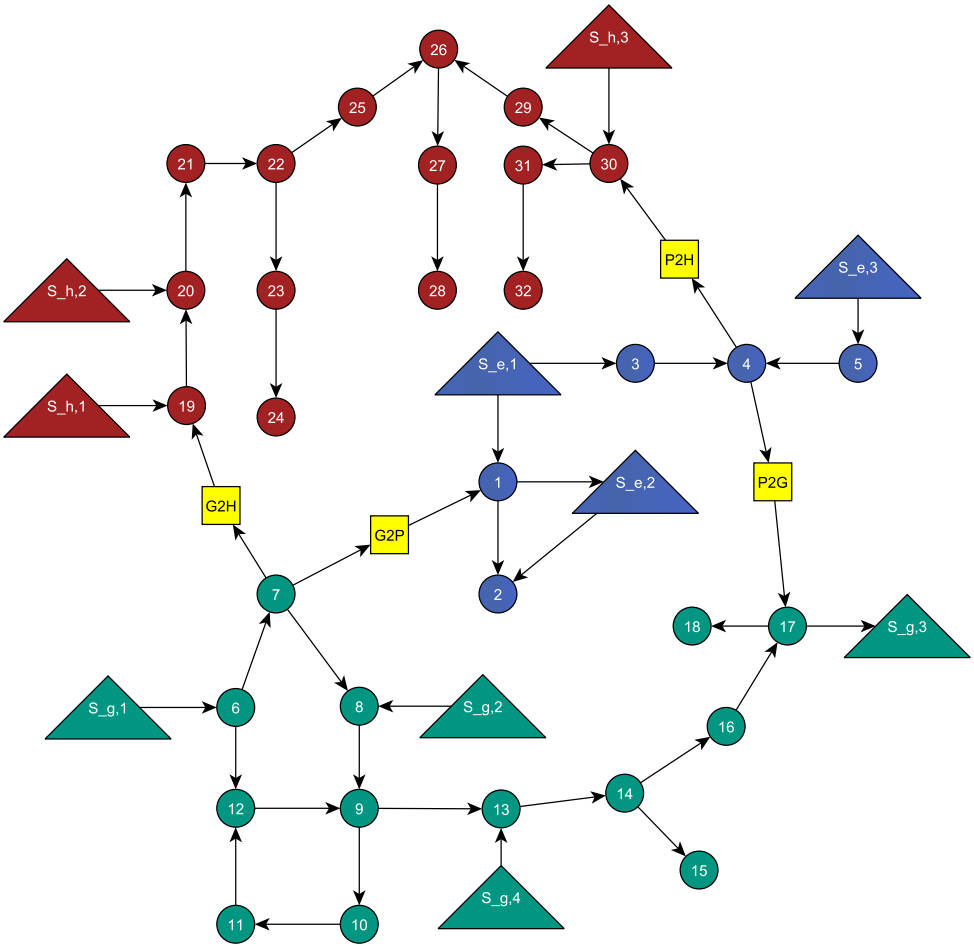

Figure A.5: Topological graph for the subnetwork of Karlsruhe from Section 6.3, where the blue parts of the graph denote the electric network ($n_{V,el} = 5$), the green parts the gas network ($n_{V,g} = 13$) and the red parts the heat network ($n_{V,h} = 14$).

Appendix B

Others

In Appendix B.1, the network generation algorithm is presented. It is used in Algorithm 2 and was mentioned first in Subsection 5.5.3. This function generates $\mathcal{N}^{(o)}$ and checks for observability. In Appendix B.2, there is the proof of noninvertibility of $\mathcal{G}$.

B.1 Pseudo Code: Generation of $\mathcal{N}^{(o)}$

Algorithm 4: Network generation algorithm: This function generates $\mathcal{N}^{(o)}$ and checks for observability.

Input: Network $\mathcal{N}$, sensor placement $\mathbf{M}$ and $\mathbf{N}$ in the current iteration (o), conductance matrix $\mathcal{G}$, number of variables v in the vector of unkowns $\mathbf{u}$, the network size n_V

Output: returns 1 if network is observable and 0 if not

```
   // Manipulation of 𝒩 to generate 𝒩^(o)
 1 for int i = 0; i < n_V; i++ do
 2     if M(i,1) == 1 then
 3         delete column i from 𝒩^(o)
 4         v=v-1
 5     for int j = 0; i < i; j++ do
 6         if N(i,j) == 1 then
               // remove entries of G(i,j) in 𝒩 by
 7             𝒩^(o)(i,i) = 𝒩^(o)(i,i) − G(i,j)
               𝒩^(o)(i,j) = 𝒩^(o)(i,j) + G(i,j)
               𝒩^(o)(j,i) = 𝒩^(o)(j,i) + G(i,j)
               𝒩^(o)(j,j) = 𝒩^(o)(j,j) − G(i,j)
   // Check network matrix 𝒩^(o) for full rank
 8 if rank(𝒩^(o)) == v then
 9     return 1 ;
10 else
11     return 0 ;
```

B.2 Proof: $\mathcal{G}$ is not Invertible

The conductance matrix for all energy carriers χ is denoted by $\mathcal{G} \in \mathbb{R}^{(n_V \times n_V)}$ and can be stated as

$$\mathcal{G} = \begin{bmatrix} G^{\chi}_{1,1} & -G^{\chi}_{1,2} & \cdots & -G^{\chi}_{1,n_V} \\ -G^{\chi}_{2,1} & G^{\chi}_{2,2} & \cdots & -G^{\chi}_{2,n_V} \\ \vdots & \vdots & \ddots & \vdots \\ -G^{\chi}_{n_V,1} & -G^{\chi}_{n_V,2} & \cdots & G^{\chi}_{n_V,n_V} \end{bmatrix}, \tag{B.1}$$

where the elements on the main diagonal of the symmetric matrix $\mathcal{G}^{\chi}$ are calculated according to

$$G^{\chi}_{v,v} = \sum_{u \in V_{\chi} \setminus \{v\}} G^{\chi}_{u,v} \qquad \forall v \in V_{\chi}. \tag{B.2}$$

Lemma: The matrix $\mathcal{G} \in \mathbb{R}^{(n_V \times n_V)}$ is not invertible.

Given: Conductance matrix $\mathcal{G} \in \mathbb{R}^{(n_V \times n_V)}$ and an arbitrary matrix of same size $\mathbf{H} \in \mathbb{R}^{(n_V \times n_V)}$ for which we claim $\mathbf{H} \neq \mathbf{0}$ with (1) $\mathcal{G}\mathbf{H} = \mathbf{0}$ and (2) $\mathbf{H}\mathcal{G} = \mathbf{0}$.

Proof by Contradiction: We want to show that $\mathcal{G}$ is invertible. Then there exists $\mathcal{G}^{-1}$ with $\mathcal{G}\mathcal{G}^{-1} = \mathcal{G}^{-1}\mathcal{G} = \mathbf{1}$.

(1) $\mathbf{H} = \mathbf{1H} = \mathcal{G}^{-1}\mathcal{G}\mathbf{H} = \mathcal{G}^{-1}(\mathcal{G}\mathbf{H}) = \mathbf{0}$ this is in contradiction to the assumption $\mathbf{H} \neq \mathbf{0}$

(2) $\mathbf{H} = \mathbf{H1} = \mathbf{H}\mathcal{G}\mathcal{G}^{-1} = (\mathbf{H}G)\mathcal{G}^{-1} = \mathbf{0}$ this is in contradiction to the assumption $\mathbf{H} \neq \mathbf{0}$

$\Rightarrow \mathcal{G}$ is not invertible.

An example for a matrix $\mathbf{H}$ that fulfills the assumptions of the proof, is a matrix that has only ones as entries.

Bibliography

[AB14] Alem, S. and Benazzouz, D.: *Bond Graph to Digraph Conversion: A Sensor Placement Optimization for Fault Detection and Isolation by a Structural Approach.* Sadhana, 39(5):1151–1164, 2014.

[ALMS15] Agrawal, A., Lokshtanov, D., Mouawad, A. and Saurabh, S.: *Simultaneous Feedback Vertex Set: A Parameterized Perspective.* CoRR, abs/1510.01557, 2015.

[ALSS16] Abbatantuono, G., Lamonaca, S., Scala, M. L. and Stecchi, U.: *Monitoring and Emergency Control of Natural Gas Distribution Urban Networks.* In *IEEE Workshop on Environmental, Energy, and Structural Monitoring Systems (EESMS)*, pages 1–6, June 2016.

[ATBS13] Abdel-Majeed, A., Tenbohlen, S., Braun, M. and Schöllhorn, D.: *Platzierung von Messstationen zur Zustandsschätzung in Niederspannungsnetzen (engl.: Measurement Placement for Low Voltage State Estimation).* In *Internationaler ETG-Kongress*, 2013.

[BHH+99] Bakken, B., Haugsted, A., Hornnes, K., Vist, S., Gustavsen, B. and Roynstrand, J.: *Simulation and Optimization of Systems with Multiple Energy Carriers.* Technical Report, SINTEF Energy Research, Trondheim, Norway, 1999.

[BHK+14] Brandt, A. R., Heath, G. A., Kort, E. A., O'Sullivan, F., Pétron, G., Jordaan, S. M., Tans, P., Wilcox, J., Gopstein, A. M., Arent, D., Wofsy, S., Brown, N. J., Bradley, R., Stucky, G. D., Eardley, D. and Harriss, R.: *Methane Leaks from North American Natural Gas Systems.* Science, 343(6172):733–735, 2014.

[BHM07] Boukhobza, T., Hamelin, F. and Martinez-Martinez, S.: *State and Input Observability for Structured Linear Systems: A Graph-Theoretic Approach.* Automatica, 43(7):1204 – 1210, 2007.

[BJN+98] Barnhart, C., Johnson, E., Nemhauser, G., Savelsbergh, M. and Vance, P.: *Branch-and-Price: Column Generation for Solving Huge Integer Programs.* Operations research, 46:316–329, 1998.

[BMBA93] Baldwin, T.L., Mili, L., Boisen, M. B. and Adapa, R.: *Power System Observability with Minimal Phasor Measurement Placement.* IEEE Transactions on Power Systems, 8(2):707–715, May 1993.

[Bun] Bundesministerium für Wirtschaft und Energie: *Erdgasversorgung in Deutschland (engl.: Natural Gas Supply in Germany).* [Online; accessed 01-02-2017].

[Bun16] Bundesministerium für Wirtschaft und Energie: *Versorgungssicherheit bei Erdgas (engl.: Supply Reliability of Natural Gas).* Monitoring-Bericht nach Paragraph 51 EnWG, July 2016. [Online; accessed 01-02-2017].

[CDF+15] Celenza, L., Dell'Isola, M., Ficco, G., Vigo, P., Bertoli, E., Incerti, L. and Zocchi, T.: *Critical Aspects of New Domestic Static Gas Meter.* In *XVIII AISEM Annual Conference*, pages 1–4, February 2015.

[Cer04] Cerbe, G.: *Grundlagen der Gastechnik (engl.: Basics of Gas Technology).* HANSER, 2004. ISBN 3-446-22803-9.

[Ci15] Cyber Lightning and industrial internet consortium: *District Heating Network Monitoring, Control and Optimization with CyberVille IoE Application Platform*, May 2015. [Online; accessed 27-05-2017].

[Cle90] Clements, K. A.: *Observability Methods and Optimal Meter Placement.* International Journal of Electrical Power & Energy Systems, 12(2):88–93, 1990.

[CLW+16] Chen, X., Lin, J., Wan, C., Song, Y., You, S., Zong, Y., Guo, W. and Li, Y.: *Optimal Meter Placement for Distribution Network State Estimation: A Circuit Representation Based MILP Approach.* IEEE Transactions on Power Systems, 31(6):4357–4370, 2016.

[Cra12] Crastan, V.: *Elektrische Energieversorgung 1 (engl.: Electric Energy Supply)*, volume 3. Springer Vieweg, 2012.

[Cue11] Cuenin, Y.: *Simulation eines elektrischen Netzes mit DIgSILENT PowerFactory (engl.: Simulation of an Electrical Network with DIgSILENT PowerFactory).* Master's thesis, Fachhochschule Südwestfalen, January 2011.

[Dat05] Dattorro, J.: *Convex Optimization & Euclidean Distance Geometry.* Meboo Publishing USA, 2005.

[Die06] Diestel, R.: *Graph Theory.* Electronic library of mathematics. Springer, 2006.

[Doe11] Doessel, O.: *Vorlesungsskript zur Vorlesung Lineare Elektrische Netze (engl.: Script for the Lecture on Linear Electrical Networks).* KIT, 2011.

[FBL+15] Ferdowsi, M., Benigni, A., Löwen, A., Zargar, B., Monti, A. and Ponci, F.: *A Scalable Data-Driven Monitoring Approach for Distribution Systems.* IEEE Transactions on Instrumentation and Measurement, 64(5):1292–1305, May 2015.

[FLM+14] Ferdowsi, M., Löwen, A., McKeever, P., Monti, A., Ponci, F. and Benigni, A.: *New Monitoring Approach for Distribution Systems.* In *2014 IEEE International Instrumentation and Measurement Technology Conference (I2MTC) Proceedings*, pages 1506–1511, May 2014.

[Flo05] Flosdorff, Hilgarth: *Elektrische Energieverteilung (engl.: Electrical Energy Distribution)*, volume 9. Teubner, 2005.

[Foe13] Foellinger, O.: *Regelungstechnik (engl.: Control Engineering)*, volume 11. VDE-Verlag, 2013.

[GA05a] Geidl, M. and Andersson, G.: *A Modeling and Optimization Approach for Multiple Energy Carrier Power Flow.* In *Power Tech, IEEE Russia*, 2005.

[GA05b] Geidl, M. and Andersson, G.: *Optimal Power Dispatch and Conversion in Systems with Multiple Energy Carriers.* In *Proceedings of 15th Power Systems Computation Conference (PSCC)*, 2005.

[GA06] Geidl, M. and Andersson, G.: *Operational and Structural Optimization of Multi-Carrier Energy Systems.* European Transactions on Electrical Power, 16(5):463–477, 2006.

[GA07] Geidl, M. and Andersson, G.: *Optimal Power Flow of Multiple Energy Carriers.* IEEE Transactions on Power Systems, 22(1):145–155, 2007.

[GB07] Gawthrop, P. J. and Bevan, G. P.: *Bond-Graph Modeling.* IEEE Control Systems, 27(2):24–45, April 2007.

[GJ79] Garey, M. R. and Johnson, D. S.: *Computers and Intractability; A Guide to the Theory of NP-completeness.* W. H. Freeman & Co., 1979.

[Gur] Gurobi Optimization, Inc.: *Gurobi Optimizer Reference Manual.* [Online; accessed 03-03-2017].

[HCF+07] Hajimiragha, A., Canizares, C., Fowler, M., Geidl, M. and Andersson, G.: *Optimal Energy Flow of Integrated Energy Systems with Hydrogen Economy Considerations.* In *Bulk Power System Dynamics and Control-VII. Revitalizing Operational Reliability, iREP Symposium*, pages 1–11. IEEE, 2007.

[Heu07] Heuck, Dettmann, Schulz: *Elektrisch Energieversorgung (engl.: Electric Power Supply)*, volume 7. vieweg, 2007.

[HMM+09] Handschin, E., Mahlke, D., Martin, A., Rehtanz, C., Waniek, D. and Zelmer, A.: *Kostenoptimierte Planung gekoppelter Strom-,*

Gas- und Wärmenetze (engl.: Cost-Optimized Planning of Coupled Electricity, Gas and Heating Networks). Innovative Modellierung und Optimierung von Energiesystemen, III.:9–38, 2009.

[HR 15] HR Energiemanagement GmbH: *Stationäre und Mobile Wärmemengenmessung mit Ultraschall und Datenauswertung mit Loxone (engl.: Stationary and Mobile Heat Quantity Measurement with Ultrasound and Data Analysis with Loxone)*, Oktober 2015. [Online; accessed 27-05-2017].

[IBM] IBM Knowledge Center: *Differences Between User Cuts and Lazy Constraints.* [Online, accessed 10-04-2017].

[IIP08] Ibrahim, H., Ilinca, A. and Perron, J.: *Energy Storage Systems - Characteristics and Comparisons.* Renewable and Sustainable Energy Reviews, 12(5):1221–1250, 2008.

[Jan] Janitza: *Messtechnik für Verteilnetze – Messen über drei Ebenen (engl.: Measuring Technology for Distribution Networks - Measuring Over Three Levels).* [Online; accessed 27-05-2017].

[Kal59] Kalman, R.: *On the General Theory of Control Systems.* IRE Transactions on Automatic Control, 4(3):481–492, 1959.

[Kar72] Karp, R.: *Complexity of Computer Computations: Proceedings of a Symposium on the Complexity of Computer Computations*, chapter Reducibility among Combinatorial Problems, pages 85–103. Springer, 1972.

[KCD80] Krumpholz, G. R., Clements, K. A. and Davis, P. W.: *Power System Observability: A Practical Algorithm Using Network Topology.* IEEE Transactions on Power Apparatus and Systems, PAS-99(4):1534–1542, July 1980.

[KD11] Khan, U. and Doostmohammadian, M.: *A Sensor Placement and Network Design Paradigm for Future Smart Grids.* In *Computational Advances in Multi-Sensor Adaptive Processing (CAMSAP), 2011 4th IEEE International Workshop on*, pages 137–140, 2011.

[Ker02] Kersting, W.: *Distribution System Modeling and Analysis.* CRC Press, 2002.

[KK15] Kouzelis, K. and Katsavounis, K.: *Enhancing the Observability of Traditional Distribution Grids by Strategic Meter Allocation.* In *IEEE PowerTech Eindhoven*, 2015.

[Klu14] Kluwe, M.: *Vorlesungsskript zur Vorlesung Regelung linearer Mehrgrößensysteme (engl.: Script for the Lecture of Linear Multi-Variable Systems).* Institut für Regelungs- und Steuerungssysteme, KIT, 2014.

[Lei13] Leibfried, T.: *Elektroenergiesysteme - Manuskript zur Vorlesung (engl.: Electroenergy Systems - Manuscript for the Lecture).* Institut für Elektroenergiesysteme und Hochspannungstechnik, KIT, 2013.

[LMM+15] Leibfried, T., Mchedlidze, T., Meyer-Hübner, N., Nöllenburg, M., Rutter, I., Sanders, P., Wagner, D. and Wegner, F.: *Operating Power Grids with Few Flow Control Buses.* In *Proceedings of the 2015 ACM Sixth International Conference on Future Energy Systems, e-Energy 2015, Bangalore, India, July 14-17, 2015*, pages 289–294, 2015.

[LSC13] Li, X., Scaglione, A. and Chang, T.: *Optimal Sensor Placement for Hybrid State Estimation in Smart Grid.* In *2013 IEEE International Conference on Acoustics, Speech and Signal Processing*, pages 5253–5257, 2013.

[Lur08] Lurie, M.: *Modeling of Oil Product and Gas Pipeline Transportation.* Wiley-VCH Verlag GmbH & Co. KGaA, 2008.

[LWJB16] Liu, X., Wu, J., Jenkins, N. and Bagdanavicius, A.: *Combined Analysis of Electricity and Heat Networks.* Applied Energy, 162:1238–1250, 2016.

[Mah09] Maheshwar Kiran Ati, U.: *Heat Exchanger Network Design, Monitoring and Optimization.* Master's thesis, Mc Master University, August 2009.

[MCKP02] Min, B. H., Chung, J. T., Kim, H. Y. and Park, S.: *Effects of Gas Composition on the Performance and Emissions of Compressed Natural Gas Engines.* KSME International Journal, 16(2):219–226, 2002.

[Men05] Menon, E.: *Gas Pipeline Hydraulics.* CRC Press, 2005.

[Mie14] Mieth, C.: *Modellierung von radialen Verteilnetzen und Verifikation anhand von Benchmark-Systemen, (engl.: Modeling of Radial Distribution Networks and Verification using Benchmark Systems).* Bachelor thesis, Karlsruhe Institute of Technology, 2014.

[Mon99] Monticelli, A.: *State Estimation in Electric Power Systems : a Generalized Approach.* Kluwer, 1999.

[MSKH16] Maurer, J., Sauter, P. S., Kluwe, M. and Hohmann, S.: *Optimal Energy Management of Low Level Multi-Carrier Distribution Grids.* In *2016 IEEE International Conference on Power System Technology (POWERCON)*, pages 1–6, September 2016.

[MW85a] Monticelli, A. and Wu, F.: *Network Observability: Identification of Observable Islands and Measurement Placement.* IEEE Power Engineering Review, 5(5):32–32, May 1985.

[MW85b] Monticelli, A. and Wu, F.: *Network Observability: Theory.* IEEE Power Engineering Review, PER-5(5):32–33, May 1985.

[Nal16] Naldi, S.: *Solving Rank-Constrained Semidefinite Programs in Exact Arithmetic.* CoRR, abs/1602.00431, 2016.

[net17] netzservice Stadtwerke Karlsruhe: *Interview on Gas and Electricity Networks of Karlsruhe with Employees*, contacted in 2017.

[Pfe15] Pfeifer, M.: *Allgemeine Einührung in die netzbasierte Energieversorgung in Deutschland (engl.: An Introduction to Networked-Based Energy Supply in Germany).* Technical Report, Institute of Control Systems, 2015.

[PLC16] PLC technologies: *Control and Monitoring of a Heat Distribution Network*, 2016. [Online; accessed 27-05-2017].

[RHS14] Reissig, G., Hartung, C. and Svaricek, F.: *Strong Structural Controllability and Observability of Linear Time-Varying Systems.* IEEE Transactions on Automatic Control, 59(11):3087–3092, 2014.

[RWA09] Rees, M., Wu, J. and Awad, B.: *Steady State Flow Analysis for Integrated Urban Heat and Power Distribution Networks.* In *44th International Universities Power Engineering Conference (UPEC)*, 2009.

[SGS11] Shalev-Shwartz, S., Gonen, A. and Shamir, O.: *Large-Scale Convex Minimization with a Low-Rank Constraint.* In *Proceedings of the 28th International Conference on Machine Learning*, pages 329–336, 2011.

[Staa] Stadtwerke Karlsruhe: *Fernwärmenetzplan Karlsruhe Innenstadt (engl.: District Heating Plan Karlsruhe).* [Online; accessed 27-05-2017].

[Stab] Stadtwerke Karlsruhe Netzservice: *Das örtliche Gas-Verteilnetz (engl.: Local Gas Distribution Network).* Downloadcenter. [Online; accessed 27-02-2017].

[Stac] Stadtwerke Karlsruhe Netzservice: *Energiestrukturdaten des Gasnetzes (engl.: Energy Structure Data of the Gas Network).* [Online; accessed 27-05-2017].

[Stad] Stadtwerke Karlsruhe Netzservice: *Gasnetzbeschreibung (engl.: Description of the Gas Network).* [Online; accessed 27-05-2017].

[Stae] Stadtwerke Karlsruhe Netzservice: *Netzstrukturdaten des Gasnetzes (engl.: Structure Data of the Gas Network).* [Online; accessed 27-05-2017].

[Sta14] Stadtwerke Karlsruhe: *Stadtwerke und EnBW wollen intelligente Messsysteme voranbringen (engl.: Stadtwerke and EnBW Want to Advance Intelligent Measuring Systems)*, April 2014. [Online; accessed 27-05-2017].

[Sta16] Stadtwerke Karlsruhe: *Telephone Interview with Employee on the Heat Network of Karlsruhe*, contacted in November 2016.

[Str17] Strehle, F.: *Modeling of Multi-Carrier Energy Distribution Systems with Port-Hamiltonian Systems.* Master's thesis, Karlsruhe Institute of Technology, 2017.

[STS17] STS global.sensor.excellence: *Gas Distribution Grid Monitoring by Continuous Pressure Measurement*, January 2017. [Online; accessed 27-05-2017].

[SW70] Schweppe, F. C. and Wildes, J.: *Power System Static-State Estimation, Part I: Exact Model.* IEEE Transactions on Power Apparatus and Systems, PAS-89(1):120–125, January 1970.

[TFL11] Tewolde, M., Fritch, J. C. and Longtin, J. P.: *High-Resolution Meter Reading Technique for Appliance Gas Usage Monitoring for the Smart Grid.* In *8th International Conference Expo on Emerging Technologies for a Smarter World*, pages 1–6, November 2011.

[UTE14] UTEC, Ingenieurbüro für Entwicklung und Anwendung umweltfreundlicher Technik GmbH: *Endbericht Optimierung von Wärmenetzen an Biogasanlagen (engl.: Final Report on Optimization of Heat Networks Connected to Biogas Plants)*, Oktober 2014. [Online, accessed 22-05-2017].

[vH15] van Westering, W. and Hellendoorn, H.: *Optimal Sensor Placement Using Gas Distribution Network Models: A Case Study.* In *IEEE 12th International Conference on Networking, Sensing and Control*, pages 321–326, April 2015.

[WL98] Wagner, D. and Liebers, A.: *Grundlagen: Begriffe zu Graphen (engl.: Fundamentals on Graphs)*, September 1998. [Online, accessed 28-11-2016].